5-2019

Photochemical Control of Homogeneous Olefin Polymerization Catalysts

Jordan Michael Kaiser
University of Tennessee, jkaiser2@vols.utk.edu

To the Graduate Council:

I am submitting herewith a dissertation written by Jordan Michael Kaiser entitled "Photochemical Control of Homogeneous Olefin Polymerization Catalysts." I have examined the final electronic copy of this dissertation for form and content and recommend that it be accepted in partial fulfillment of the requirements for the degree of Doctor of Philosophy, with a major in Chemistry.

Brian Long, Major Professor

We have read this dissertation and recommend its acceptance:

Michael Best, S. Michael Kilbey II, Siris Laursen

Accepted for the Council:

Dixie L. Thompson

Vice Provost and Dean of the Graduate School

(Original signatures are on file with official student records.)

Photochemical Control of Homogeneous Olefin Polymerization Catalysts

A Dissertation Presented for the
Doctor of Philosophy
Degree
The University of Tennessee, Knoxville

Jordan Michael Kaiser
May 2019

DEDICATION

No admirable accomplishment can be completed by a sole individual, it takes a team of quality individuals to scale great heights and accomplish one's dreams. This great achievement could not have been done without the help of so many amazing people and I thank you all!

This dissertation is especially dedicated to my Mom, Dad, and all my inspirational siblings. Without your timely visits, care packages, flight deals, free meals and continued moral support, I would not be where I am today. I can't thank you all enough.

ACKNOWLEDGEMENTS

First and foremost, I would like to thank my advisor Prof. Brian K. Long. I cannot thank you enough for believing in me and providing me with all the opportunities to achieve such success during my time in graduate school. Your ability to push me as a scientist and mold my way of thinking to address encountered problems is invaluable and will only benefit me in the next stage of my career. Aside from your professional mentoring, I am grateful for your personal mentoring, periodic life lessons, and laughs shared throughout my time at UTK.

Special thanks to my doctoral committee: Prof. Michael Best, Prof. S. Mike Kilbey, and Prof. Siris Laursen. Your time, guidance, comments, and critiques of my work have made me a better scientist for which I am truly grateful. To Prof. Jason Keleher, Prof. Joseph Kozminski, and Prof. Charles Crowder at Lewis University, I am proud to say that I wouldn't be where I am today without your mentorship and passion for science. This work would not be possible without the financial support from the U.S. Army Research Office and the University of Tennessee-Knoxville College of Arts and Sciences.

Finally, I would like to thank my parents for everything they have done for me during this adventure. My mom is the hardest working person I have ever met, and my dad holds family values in the highest regard. Without hard work and the best supporting family cast, I would not have been where I am today. I love you both and thank you for everything! To my siblings, Frank, Pauline, Dee, John, Josh, and Jeremy, ever since I can remember you were all role models to me in your own way and I thank you for setting such high standards that motivated me to raise the bar in everything I did. Finally, I would like to

thank all my high school coaches for teaching me mental toughness, family friends and Cincinnati family for your support and encouragement over the years, and Sam Rinehart for your priceless friendship that made this journey a lot easier.

ABSTRACT

Olefin polymerization catalysis is an ever-growing and ever-evolving field of strategic importance as scientists continually search for advanced polymeric materials. These catalysts regulate the incorporation of one or more monomers into a polymer chain, which can, in-turn, dictate the overall properties of the resultant material. If chemists can control when, how, and to what extent these monomers are enchained, researchers may selectively tailor materials for targeted applications. Traditionally, ligand scaffold design and metal-center identity have been utilized to control catalyst performance. However, this strategy is often limited by intricate and costly catalyst frameworks, as well as the inability to escape an inefficient "one catalyst, one polymer" mindset. To surpass these limitations, polymer chemists have begun to look for more versatile methods to enhance catalytic control.

Common methods to promote olefin polymerization control include incorporating small molecules (comonomers or chemical reagents) or manipulating reaction conditions (temperature and monomer pressure). Recent progress in the more general field of polymer synthesis has highlighted that photo-sensitive/responsive polymerizations are a burgeoning tactic, which is used to achieve both spatial and temporal control. In order to take the next step towards advanced catalytic control in the field of olefin polymerizations, the following fundamental questions must be addressed: (1) Can an external stimulus, such as light, be used to influence an olefin polymerization catalyst? (2) Can we expand the utility of this new tool to provide precise control over initiation, propagation, or termination events?

This dissertation addresses each of these questions in a series of investigations into how photochemistry may be used to influence olefin polymerizations. First, I address how the use of a photoreductant and light can be used to dictate the insertion mechanism of a redox-active catalyst. Following this work, I discuss how olefin polymerization precatalysts, differentiating in ligand structure and metal center, may be activated using UV light and photoacid generators. Lastly, I discuss how a photosensitizer in tandem with a photoacid generator permits visible light to activate olefin polymerization precatalysts. This work provides proof of concept that photochemical control of olefin polymerizations may be realized.

TABLE OF CONTENTS

LIST OF TABLES

LIST OF FIGURES

LIST OF ABBREVIATIONS AND SYMBOLS

α……..alpha
ad…… adamantyl
^{Ac}FcBAr^{F}…….acetylferrocenium tetrakis(3,5-bis(trifluoromethyl)phenyl)borate
AgBAr^{F}……...silver tetrakis(3,5-bis(trifluoromethyl)phenyl)borate
AgOTf…….silver triflate
ATRP……...atom transfer radical polymerization
β……...beta
B……..branching content per 1000 carbons
1B1……..methyl groups arising from sec-butyl branches
CFL…….compact fluorescent light bulb
CH_3CN……acetonitrile
$CoCp_2$……..cobaltocene
Cy……cyclohexyl
Đ…….polymer dispersity
DMSO……dimethylsulfide
DSC……differential scanning calorimetry
fac……..facial
Fc……ferrocene
Fc^+……...ferrocenium
[Fc][Bar^{F}]……ferrocenium tetrakis(3,5-bis(trifluoromethyl)phenyl)borate
GPC…….gel permeation chromatography
HCl……..hydrochloric acid
LED…….light emitting diode
MA……..methyl acrylate
MAO……...methylaluminoxane
Me……...methyl
MeOH…….methanol
MMAO……modified methylaluminoxane
M_n……number average molecular weight
M_w……weight average molecular weight
η……...intrinsic viscosity
NaBAr^{F}……sodium tetrakis(3,5-bis(trifluoromethyl)phenyl)borate
NHC…….*N*-heterocyclic carbene
NMR……nuclear magnetic resonance
o-MeO-C_6H_4……*ortho*-methoxy phenyl
PAG…….photoacid generator
PE……polyethylene
PET…….photoinduced electron transfer
PEX…….cross-linked polyethylene
PET-RAFT……..photo-induced electron transfer-reversible addition-fragmentation chain-transfer polymerization
Ph…….phenyl

PhLAG…….photo Lewis acid generator
PMAO-IP…….polymethylaluminoxane-improved performance
R_g……..radius of gyration
ROMP……..ring opening metathesis polymerization
T_m…….polymer melting transition temperature
UV……ultra-violet
VL…… visible light
X_{MA}……...methyl acrylate incorporation (mol %)

CHAPTER 1 – RECENT DEVELOMENTS IN REDOX-ACTIVE OLEFIN POLYMERIZATION CATALYSTS

A version of this chapter was originally published by Jordan M. Kaiser and Brian K. Long:

Kaiser, J. M., Long, B. K. *Coord. Chem. Rev.* **2018**, *372*, 141-152.

I was responsible for exhaustively surveying the literature and preparing the manuscript. Dr. Brian Long advised this work and aided in the preparation of the manuscript.

1.1 Introduction

Polyolefins are a class of polymers derived from simple, inexpensive, and readily abundant olefinic monomer sources, such as ethylene, propylene, and higher α-olefins. Today, polyolefins represent a significant percentage of all polymers produced annually and can be tailored to exhibit a wide variety of thermal and mechanical properties suitable for a plethora of applications. Polyolefins are most commonly synthesized using transition metal-based catalysts that enable polymerization via a coordination-insertion mechanism. Due to the complex relationship between ligand structure, the transition metal utilized, and overall reactivity, the development of advanced olefin polymerization catalysts remains a heavily investigated area of research in academia and industry alike. It is through these studies that scientists have gained a deep fundamental understanding of how catalysts may be manipulated to promote polymerization control and thereby facilitate the synthesis of polyolefins with precisely defined structure at the monomeric and polymeric levels.

Because of these efforts, olefin polymerization catalysis is an ever-growing and evolving field that continues to push the forefront of synthetic polymer chemistry.

Historically, olefin polymerization was first independently discovered by the teams of Hogan and Banks, and Ziegler and Natta in the early 1950's.[1-4] Their pioneering works demonstrated that heterogeneous catalysts composed of Cr, Ti, and V could produce high molecular weight polyolefins, such as high-density polyethylene and isotactic polypropylene, which would radically change many of the materials we encounter each and every day.[5] While these catalysts have proven to be exceptional for producing high molecular weight polymers with broad molecular weight dispersity, their heterogeneous nature presents a complex catalytic environment in which multiple distinct active sites are present, each with its own distinct rate constants for propagation, chain-transfer, and termination events. This catalytic complexity has encumbered detailed mechanistic and kinetic studies, and serves as a driving force to develop homogeneous, single-site catalyst analogues that may easily be studied, and thus controlled.

Homogeneous catalysts did not emerge as viable alternatives for olefin polymerization until the discovery of methylaluminoxane (MAO) by Kaminsky and coworkers.[6] MAO proved to be a crucial reagent for the efficient activation of homogeneous catalysts, and stimulated a paradigm-shift in how researchers studied, designed, and perceived catalysts for the coordination-insertion polymerization of olefins.[7-9] Early examples of homogeneous catalysts focused heavily on group 4 metallocenes, which were highly active and single-site in nature, often displaying uniform chain propagation rate constants and producing polyolefins with narrower molecular weight

dispersity than previously achievable using heterogeneous catalysts.[10] Following the success of metallocene-based catalysts, researchers soon expanded the scope of olefin polymerization catalysts to include ligands without cyclopentadienyl moieties.[11] These so-called post-metallocenes greatly expanded the breadth of applicable ligands and further promoted fine-tuning of ligand sterics and electronics surrounding the active transition metal center.

In 1995, the field of homogeneous single-site olefin polymerization catalysts was once again reinvigorated when Brookhart and coworkers demonstrated that late transition metal catalysts could also be employed to produce high molecular weight polyolefins.[12-13] These Ni and Pd α-diimine catalysts were shown to generate branched polyethylene microstructures using ethylene as a sole feedstock, which is a feat not possible with homogeneous group 4 catalysts.[14-15] Further investigations confirmed that these group 10 catalysts produce branched polymeric structures due to their strong propensity to migrate along the growing polymer chain via a process known as "chain-walking."[14] Chain-walking is accomplished through β-hydride elimination and subsequent reinsertion of the pendant olefin, which if repeated over and over, allows the active catalyst to shuttle along the polymeric backbone. If, during that process, a molecule of ethylene coordinates and inserts, a branch point is created. In addition to chain-walking, other attractive features of these group 10 catalysts include their ability to incorporate polar comonomers due to their decreased oxophilicity relative to their group 4 catalyst analogues and also their ability to polymerize various olefins in a controlled/living manner.[16-19]

Enticed by the many attractive features of Ni and Pd-based olefin polymerization catalysts, researchers soon directed their attention toward the development of innovative ways to modulate this unique catalytic behavior and improve overall polymerization control. One such example was described in 2005 by Guan and coworkers, who synthesized a series of group 10 α-diimine catalysts bearing various electron-withdrawing or electron-donating substituents.[20] Through this study, they discovered that catalysts bearing electron-donating groups produced more linear polyethylene microstructures, whereas those bearing electron-withdrawing moieties produce more highly branched materials. The authors concluded that the addition or removal of electron density at the active metal center alters the relative rates of monomer coordination-insertion to that of chain-walking. Although this report highlighted the pivotal role that ligand electronics play in regard to polymerization control, the need to iteratively synthesize multiple individual ligand/catalyst combinations with varying electron density ultimately limits this approach. Researchers soon turned to the possibility of utilizing redox-active ligands to bring about electronic modulation within a single catalyst. Redox-active ligands provide a unique opportunity to modulate the electronic properties of an active metal center via the addition or removal of electrons from a single ligand framework (Figure 1.1).

The first example of redox-switchable catalysis was reported by Wrighton and coworkers, who demonstrated this concept via a diphosphino-cobaltocene ligated rhodium(I) complex in which the reduced form was found to hydrogenate cyclohexene approximately 16 times faster than its oxidized analogue (Figure 1.2).

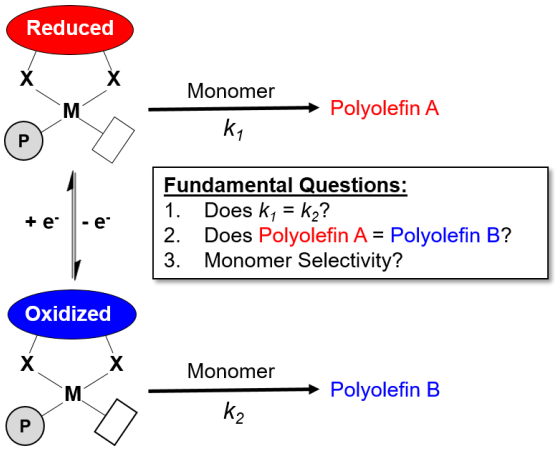

Figure 1.1 Demonstrates potential of redox-active catalysis for olefin polymerizations.

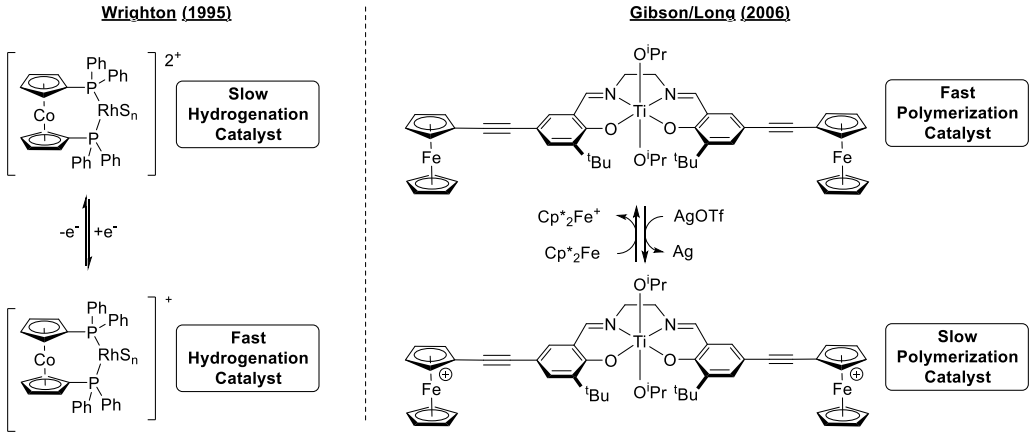

Figure 1.2 First examples of redox-active catalysts for small molecule transformations (left) and polymerizations (right).[21-22]

This dramatic rate enhancement was attributed to increased electron density at the rhodium center that facilitates oxidative addition of H_2.[21] This seminal work has since inspired the use of redox-active transition-metal catalysts for a plethora of small molecule transformations.[23-26] However, it wasn't until 2006 that this concept of redox-active catalysis would be applied to polymerization chemistry when Gibson, Long, and coworkers reported the first successful redox-switchable catalyst for the ring opening polymerization of lactide (Figure 1.2).[22] In this study, polymerization activity was turned "on" and "off" by adding or removing electrons from the ligands pendant ferrocenyl moieties, thereby altering its ability to coordinate and insert subsequent lactide monomers.

Inspired by the works highlighted above, analogous redox-active olefin polymerization catalysts were highly sought after and hypothesized to potentially provide a multitude of advantages stemming from the ability to precisely control catalytic activity and reactivity.[27] Though the first successful examples of redox-switchable, or redox-active, olefin polymerization catalysts have only recently emerged,[28-29] it should be noted that the idea of incorporating redox-switchable functionality into single-site olefin polymerization catalysts had been previously alluded to and/or attempted by the groups of Arnold, Gibson, and Stephan.[30-35]Unfortunately, in each of these cases no differentiation between reduced and oxidized catalytic species was observed. This lack of differentiation was often attributed to the use of methylaluminoxane (MAO), which is known to contain trialkylaluminum contaminants that were suspected of re-reducing the ferrocenium-containing (Fe^{III}) ligand frameworks back to their native state (Fe^{II}) during activation of the catalysts for olefin polymerization. These reports motivated researchers to investigate

a more diverse array of redox-active ligand frameworks, and eventually inspired the seminal reports of Chen and Long who provided fundamental evidence that ligand redox state could indeed be used to modulate olefin polymerization behavior.[28-29] It is these studies and the works that have followed that will be discussed in this review, as well as a brief perspective of the field as it moves forward.

1.2 Palladium-based Polymerization Catalysts

1.2.1 Phosphine-sulfonate Ligand Structure

Palladium-based catalysts bearing phosphine-sulfonate ligands were first introduced by Pugh and coworkers in 2002.[36-37] Since those reports, this class of catalysts has received significant attention in the olefin polymerization field due to their ability to polymerize ethylene without the need of an activating reagent, such as MAO. Furthermore, because they propagate via a neutral Pd active site, they are known to readily incorporate polar comonomers, a feat which is difficult for many other catalysts.[38-42] Because they do not require activation, it was realized that redox-active analogues might provide a tremendous opportunity to bypass the issues encountered when using MAO by Gibson and coworkers.[33-35] Additionally, the catalytic behavior of these phosphine-sulfonate Pd catalysts was shown to be sensitive to the electronic nature of their surrounding ligand,[43-44] thereby making them an ideal target for redox-active olefin polymerization catalysts.

In 2015, a series of Pd-based olefin polymerization catalysts bearing redox-active, phosphine-sulfonate ligands were reported by Chen and coworkers (**1**-**3**) (Figure 1.3).[28, 45]

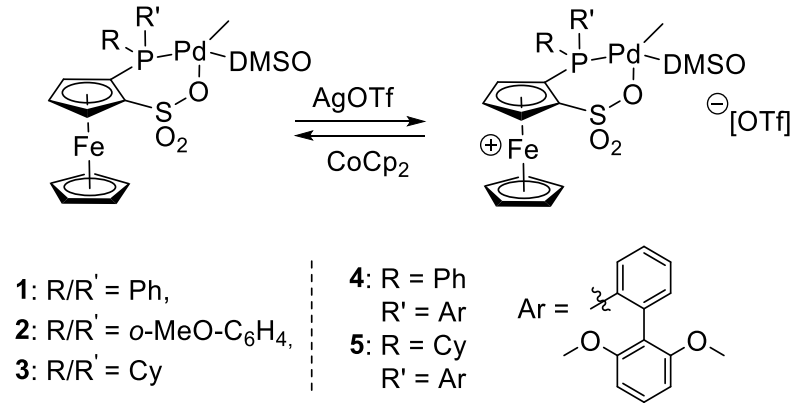

Figure 1.3 Pd-based catalysts **1-5** bearing redox-active phosphine-sulfonate ligands.[28, 45-46]

These catalysts were rendered redox-active via the incorporation of a ferrocenyl unit into the ligand backbone. It was found that native ferrocene-containing ligands could be readily oxidized to their ferrocenium analogues using silver trifluoromethanesulfonate (AgOTf), and could be subsequently re-reduced to their native oxidation state using cobaltocene ($CoCp_2$). These catalysts readily polymerize ethylene, norbornene, and were even found to copolymerize ethylene with polar comonomers, such as methyl acrylate, amino functionalized alkenes, and unsaturated esters making them ideal candidates to probe the effects that redox-activity has on olefin copolymerizations.[38, 41, 47-49]

Ethylene homopolymerizations using catalysts **1-3** and their oxidized analogues (**1_{ox}-3_{ox}**) clearly established differentiation in catalytic behavior between ligand redox states (Table 1.1). Catalysts **1-3** produced 1.21-2.50 g of polyethylene and achieved molecular weights ranging from 5860-9760 g/mol. In contrast, oxidized catalysts **1_{ox}-3_{ox}** exhibited decreased polymerization productivity, yielding only 0.29-0.53 g of polyethylene

with low molecular weights of 1420-3290 g/mol. An in-depth mechanistic study revealed that oxidized catalyst **1$_{ox}$** initially converted ethylene at a greater rate than its reduced counterpart (**1**), but then decomposes or deactivates during the course of the polymerization. It was found that oxidized catalysts **1$_{ox}$-3$_{ox}$** favored β-hydride elimination due to the electron-poor phosphine-sulfonate ligand which may be a source of this decomposition as complexes bearing Pd-H bonds are known to deactivate via formation of inactive Pd^0 species.[50] It was also noted that these oxidized catalysts favor chain-transfer over insertion events, causing the observed low yields and molecular weights.[43]

To further expand the catalog of phosphine-sulfonate ligated Pd catalysts, Chen and coworkers conducted a similar study in which the steric bulk surrounding the active metal center was increased by installing bulky bi-aryl substituents (**4-5**) (Figure 1.3).[46]

Table 1.1 Ethylene Polymerization Results using Phosphine-sulfonate Palladium Catalysts 1-3[a]

entry	catalyst	yield (g)	productivity[b]	M_n[c] (g/mol)	$Đ$[c]
1[a]	**1**	1.21	4.8	5860	2.40
2[a]	**1$_{ox}$**	0.29	1.2	2050	2.19
3[a]	**2**	2.01	8.0	7830	2.20
4[a]	**2$_{ox}$**	0.53	2.1	1420	2.04
5[a]	**3**	2.50	10.0	9760	2.34
6[a]	**3$_{ox}$**	0.44	1.7	3290	1.86

[a]Polymerization conditions: catalyst (5 μmol), toluene (48 mL), dichloromethane (2 mL), ethylene (9 atm), 80 °C, 30 min. [b]Productivity is in units of $\times 10^5$ g/(mol Pd·h). [c]Determined by gel permeation chromatography (GPC) using universal calibration. Data taken from literature.[28, 45]

This increased steric bulk was initially hypothesized to increase polyethylene molecular weights as previous reports advocate that increased steric bulk at the axial positions of the active metal center decreases chain-transfer events for both α-diimine derived catalysts [12, 51-58] as well as related phosphine-sulfonate based systems. [59-61] Unfortunately, this strategy was unsuccessful as catalysts **4** and **5** only yielded low molecular weight polyethylenes (M_n = 3361 and 4200 g/mol), which were lower than their less bulky catalyst analogues **1-3** (Table 1.2). Lastly, oxidized catalysts $\mathbf{4_{ox}}$ and $\mathbf{5_{ox}}$ exhibited a dramatic drop-off in productivity, producing no polymer and only small amounts of oligomers. The authors speculate that the decreased polymerization activity of oxidized catalysts $\mathbf{4_{ox}}$ and $\mathbf{5_{ox}}$ mimics the behavior observed by Chen and are believed to undergo similar deactivation processes, as was discussed above, but at an accelerated rate yielding oligomers instead of polymer.

Table 1.2 Ethylene Polymerization Results using Phosphine-sulfonate Palladium Catalysts 4-5[a]

entry	catalyst	yield (g)	productivity[b]	M_n[c] (g/mol)	$Đ$[c]
1	**4**	1.08	1.1	3361	1.42
2[e]	$\mathbf{4_{ox}}$	---	---	---	---
3	**5**	0.85	0.9	4200	1.92
4[e]	$\mathbf{5_{ox}}$	---	---	---	---

[a]Polymerization conditions: catalyst (10 μmol), toluene (48 mL), dichloromethane (2 mL), ethylene (8 atm), 80 °C, 1 h. [b]Productivity is in units of $\times 10^5$ g/(mol Pd·h). [c]Determined by gel permeation chromatography (GPC) in trichlorobenzene at 150 °C. [e]No solid product was observed. A small amount of butene and hexene were observed by GC-MS. Data taken from literature.[46]

As mentioned previously, the ability of Pd phosphine-sulfonate precatalysts to readily copolymerize ethylene and polar comonomers is one of their most attractive features. To investigate the effects that ligand based redox-state has on the copolymerization of ethylene and methyl acrylate, Chen and coworkers utilized catalysts **1-3** and their oxidized analogues $\mathbf{1_{ox}}$-$\mathbf{3_{ox}}$ (Table 1.3). Specifically, when comparing the copolymerization results of catalysts **2** and $\mathbf{2_{ox}}$, $\mathbf{2_{ox}}$ exhibited a 4-fold slower polymerization productivity (0.7×10^4 g/mol·h) as compared to its reduced analogue **2** (2.8×10^4 g/mol·h), and much lower molecular weight polymers were achieved (Table 1.3, entries 3-4). These results were in perfect agreement with the ethylene polymerization results described in Table 1.1 in which all oxidized catalysts displayed lower productivities and molecular weights as compared to their reduced counterparts due to catalyst instability. Furthermore, the ability of catalyst $\mathbf{2_{ox}}$ to incorporate methyl acrylate (MA), a polar comonomer, was found to decrease by over 50% (X_{MA} = 25.0→10.5). When analyzing MA incorporation results, the authors hypothesize that the oxidized ferrocenium containing ligand decreases the electron density at the active metal site, thereby increasing its electrophilic nature and the propensity of oxygen chelation, leading to lower MA incorporations.

In addition to incorporating polar monomers, phosphine-sulfonate palladium precatalysts are known to be highly active for the polymerization of cyclic olefin monomers, such as norbornene.[62-70] In contrast to the ethylene polymerization trends observed above for catalysts **1-5**, the oxidized analogues ($\mathbf{1_{ox}}$-$\mathbf{5_{ox}}$) were found to be the most active species for the oligomerization/polymerization of norbornene, while their reduced catalyst analogues **1-5** were virtually inactive. Surprisingly, less bulky catalysts

1_{ox}-3_{ox} were only active for norbornene oligomerization, whereas the bulkier catalysts **4_{ox}** and **5_{ox}** were found to polymerize norbornene. Most importantly however, each catalyst pair (**1/1_{ox}-5/5_{ox}**) was able to be cycled between their "on" and "off" states successfully proving that these catalysts are not only redox-active, but are redox-switchable catalytic systems. Examples of these redox-switchable norbornene oligomerizations/polymerizations can be seen in Figure 1.4 in which catalyst **3** (left) and catalyst **5** (right) were specifically chosen to demonstrate this behavior. Both of these plots represent the enhanced catalytic control that can be provided through the incorporation of redox-active ligands into olefin polymerization precatalysts.

Table 1.3 Copolymerization of Ethylene and Methyl Acrylate using Catalysts 1-3 and 1_{ox}-3_{ox}[a]

entry	catalyst	productivity[b]	X_{MA}[c]	M_n[d]	$Đ$[d]
1	**1**	0.8	12.0	1570	2.40
2	**1_{ox}**	0.2	8.2	---[e]	2.19
3	**2**	2.8	25.0	1600	2.20
4	**2_{ox}**	0.7	10.5	400	2.04
5	**3**	1.0	18.8	2130	2.34
6	**3_{ox}**	0.2	12.0	330	1.86

[a]Polymerization conditions: catalyst (20 μmol), [MA] = 2.5 M, total volume of toluene and MA (48 mL), dichloromethane (2 mL), ethylene (9 atm), 100 °C, 1 h. [b]Productivity is in units of $\times 10^4$ g/(mol Pd·h). X_{MA} = MA incorporation (mol %); determined by ^{1}H NMR spectroscopy. [d]Determined by gel permeation chromatography (GPC) using universal calibration. [e]Molecular weight too small to be accurately determined by GPC. Data obtained from literature.[28]

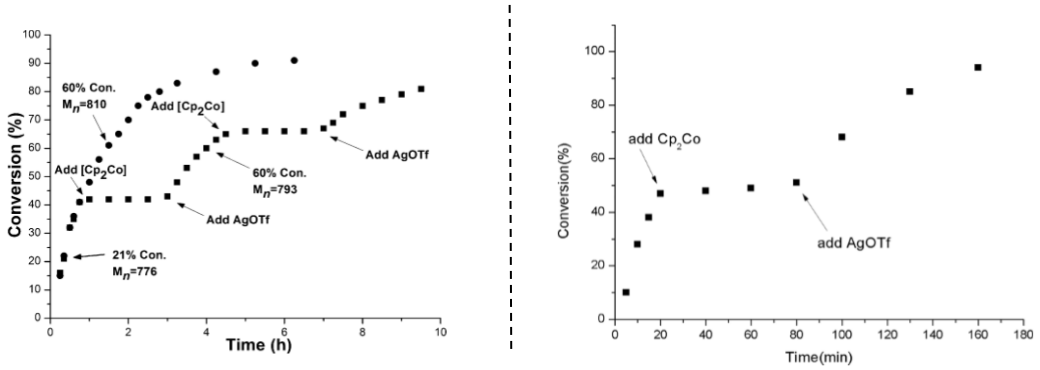

Figure 1.4 (Left) Oligomerization of norbornene (squares) using catalysts redox-switchable catalyst **3/3$_{ox}$,** oxidant = AgOTf, reductant = $CoCp_2$. A control oligomerization shows norbornene conversion using **3$_{ox}$** (circles).[28] (Right) Oligomerization of norbornene (squares) using catalysts redox-switchable precatalyst **5/5$_{ox}$,** oxidant = AgOTf, reductant = $CoCp_2$.[46] Both figures reproduced with permission from Refs.[28, 46] Copyright 2015, John Wiley and Sons. Copyright 2017, John Wiley and Sons.

1.2.2 α-Diimine Ligand Structure

As previously mentioned, α-diimines have become one of the most ubiquitous ligand scaffolds in late transition metal catalyzed olefin polymerizations. Efforts to explore and expand the potential utility of α-diimine ligands have relied heavily on ligand modifications that finely tune their sterics and/or electronics.[12, 20] Capitalizing on the versatility of these ligands, Chen and coworkers designed a Pd α-diimine olefin polymerization catalyst (**6**) that does not require MAO for activation (Figure 1.5).[71] Once again, ferrocenyl units were selected as the redox-active moieties, which were installed as substituents off the ligands *N*-aryl rings.

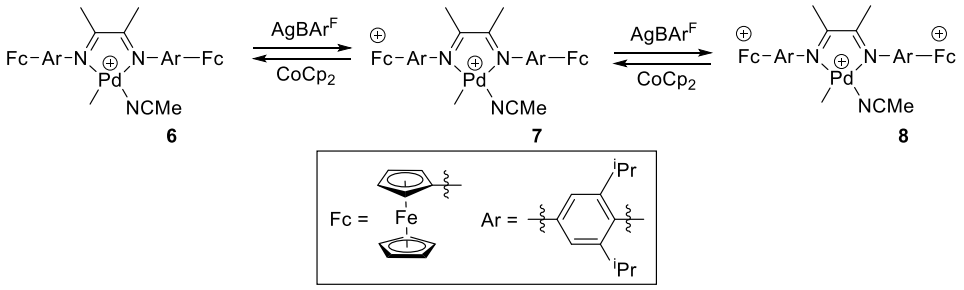

Figure 1.5 Pd-based catalysts **6-7** bearing redox-active, ferrocenyl substituted α-diimine ligands.[71]

They found that silver tetrakis(3,5-bis(trifluoromethyl)phenyl)borate ($AgBAr^F$) was a suitable oxidant and that cobaltocene was an effective reductant. Because this ligand contains two redox-active sites, it was hypothesized that two distinct oxidized states may be accessed via stepwise oxidation of the ferrocenyl moieties. This would test not only the effects of electron withdrawing substituents for olefin polymerizations, but would also provide additional insight into how catalysts containing multiple redox moieties effect overall catalytic performance.

The catalytic behavior of catalysts **6-8** were evaluated for ethylene polymerizations (Table 1.4, entry 1-3). Analysis of the polymerization results revealed that catalytic activity decreased from 1.36 $x10^5$ down to 0.22 $x10^5$ g/(mol Pd·h) as the ferrocenyl moieties were oxidized in a stepwise fashion. The authors speculate that the change in activity is a result of catalyst deactivation when Pd black formation was observed during polymerization for catalysts **7** and **8**. This catalyst degradation was also hypothesized to be responsible for the low molecular weight polyethylenes obtained with doubly oxidized catalyst **8** (M_n = 0.61 x 10^4 g/mol).

Table 1.4 Polymerization of Ethylene and 1-hexene with Catalysts 6-8[a]

entry	catalyst	monomer	activity[c]	M_n[d] ($\times 10^{-4}$)	$Đ$[d]	1B1%[e]
1[a]	**6**	ethylene	1.36	15.78	2.13	15.2 (±0.3)
2[a]	**7**	ethylene	0.74	17.04	2.31	18.2 (±0.8)
3[a]	**8**	ethylene	0.22	0.61	1.48	19.3 (±1.0)
4[b]	**6**	1-hexene	95	2.04	1.34	---
5[b]	**7**	1-hexene	33	2.23	1.42	---
6[b]	**8**	1-hexene	0	---	---	---

[a]Ethylene polymerization conditions: catalyst (10 μmol), volume of toluene (20 mL), ethylene (8 atm), 40 °C, 3 h. [b]1-Hexene polymerization conditions: catalyst (10 μmol), total volume of toluene and 1-hexene (20 mL), 1-hexene (2 mL), 20 °C, 3 h. [c]Catalyst activity is in units of $\times 10^5$ g/(mol Pd·h). [d]Determined by gel permeation chromatography (GPC) using polystyrene standards. [e]1B1% = % methyl branches in *sec*-butyl ended branches. Determined by ^{13}C NMR spectroscopy and reported values are averages over multiple trials. Data obtained from literature.[71]

Detailed branching analysis was performed using ^{13}C NMR spectroscopy, and the percentage of methyl groups arising from *sec*-butyl branches (1B1%) was used to highlight the effects of the ligand oxidation state. This percentage was found to increase as a function of added oxidant in which native catalyst **6** yielded 15.2%, catalyst **7** had 18.2% (1 equivalent of oxidant added), and catalyst **8** displayed 19.3% (2 equivalents of oxidant added) methyl branches arising from *sec*-butyl branches. These results are in perfect agreement with reports by Guan and coworkers who previously found *α*-diimines bearing electron withdrawing functionalities generate more branch-on-branch structures during ethylene polymerization.[20] To further support these observations, gel permeation chromatography (GPC) was used to generate a log-log plot of radius of gyration (R_g) versus molecular weight (M_n) for the polymers produced using catalysts **6-8** (Figure 1.6).

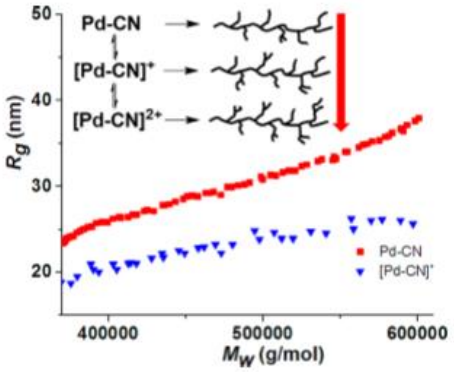

Figure 1.6 Log-log plot of R_g vs. M_w for polymers produced using catalysts **6** and **7.** Reproduced with permission from Ref.[71]. Copyright 2017, The American Chemical Society.

As expected, polymers produced by catalyst **6** (■) exhibit higher R_g values across all molecular weights as compared to those produced via singly oxidized catalyst **7** (▲), which have significantly lower R_g values clearly indicating that it has a more branched polymer microstructure.[14, 72] Polymers produced using catalyst **8** did not achieve high enough molecular weights for R_g to be accurately measured.

Lastly, 1-hexene polymerizations further accentuated the differentiation between catalyst oxidation states in which catalyst **6** displayed an activity of 95 $\times 10^5$ g/(mol Pd·h), whereas doubly oxidized catalyst **8** was completely inactive (Table 4, entry 4-6). In this case, it was proposed that the strongly electrophilic Pd center of doubly oxidized catalyst **8** stabilizes olefin coordination, but disfavors the subsequent insertion step relative to chain-transfer processes.[73-75] Similar catalytic behavior was observed when copolymerizing ethylene and polar comonomers, such as methyl acrylate (MA) and norbornene. As an example, catalyst **6** copolymerized ethylene and MA with modest

activity (9.7×10^3 g/(mol Pd·h)) and incorporated 5.5 mol% MA. Oxidized species **7** and **8** lead to lower catalyst activities (0.12 and 0.06×10^3 g/(mol Pd·h)) and with MA incorporation decreasing to 4.9 and 3.9%.

1.2.3 Heteroscorpionate Ligand Structure

Each of the palladium catalysts discussed above (**1-8**) utilize bidentate ligand frameworks in combination with a labile coordinating species (DMSO or CH_3CN), which is then displaced via monomer coordination during polymerization. Because the vinyl-addition polymerization of norbornene and norbornene derivatives is usually accomplished using catalysts that employ either bidentate or monodentate ligands,[63-65, 76-78] catalysts **1-8** were able to successfully polymerize these bulky monomers. An alternative to using these minimalistic ligand sets is to use tridentate ligands that contain a hemilabile component that may be dislodged by a more nucleophilic monomer species. This concept has been successfully utilized by Mecking and coworkers for allyl palladium-based catalysts for olefin oligomerization.[79] Furthermore, the weakly coordinating nature of these ligands may be leveraged to regulate the coordination of monomers based upon the nucleophilic competition between the hemilabile coordinating component and the olefinic monomer. This may additionally eliminate the need for an activator, such as MAO, which is advantageous for redox-active systems due to the reducing power of alkylaluminum contaminants, as described above.

Literature also teaches us that hemilabile ligands may be regulated via the incorporation of redox-active functionality, and thereby control the activity of transition-metal catalysts for many small molecule organic transformations.[23] Diaconescu and

coworkers expanded this concept to the vinyl addition polymerization of norbornene with the development of catalyst **9,** which includes a redox-switchable hemilabile component within its ligand structure (Figure 1.7).[80] The redox-active ferrocenyl moiety of catalyst **9** was readily oxidized to $\mathbf{9_{ox}}$ using acetyl ferrocenium tetrakis(3,5-bis(trifluoromethyl)-phenyl)borate ($^{Ac}FcBAr^{F}$) while cobaltocene was found to be an effective reductant for catalyst $\mathbf{9_{ox}}$ back to **9**. Oxidation of the ferrocene containing hemilabile ligand is believed to withdraw electron density from the adjacent phosphine chelating group and enhance its lability.

Catalysts **9** and $\mathbf{9_{ox}}$ were both tested for polymerization activity using a variety of substituted norbornene monomers, as Pd catalysts are known to be highly active towards these sterically encumbered olefins. Catalyst **9** was found completely inactive towards these monomers, presumably due to its electron rich ligand coordinating in a tripodal fashion which occupies any potential monomer coordination sites around the Pd center. In contrast, oxidized catalyst $\mathbf{9_{ox}}$ readily polymerized each norbornyl monomer tested.

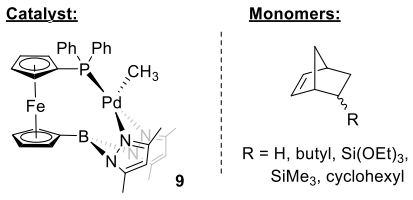

Figure 1.7 Pd-based catalyst **9** bearing a redox-active heteroscorpionate ligand and the monomers used for subsequent polymerization studies.[80]

This was attributed to the oxidized ligand's decreased electron density and therefore more weakly coordinating hemilabile component that could be displaced by monomer and enter into the coordination-insertion process. Most importantly, it was discovered that this catalyst can oscillate *in situ* between its dormant (**9**) and active (**9$_{ox}$**) states upon the addition of chemical oxidants or reductants. To display this redox-switchable behavior, 5-(triethoxysilyl)-bicyclo[2.2.1]hept-2-ene was selected as a representative monomer. As can be seen in Figure 1.8, catalyst **9$_{ox}$** actively consumes monomer until cobaltocene is added to reduce **9$_{ox}$** back to **9** and effectively turn "off" the polymerization (■). Re-oxidation using ^{Ac}FcBAr^{F} was then able to turn the polymerization back "on" ultimately reaching similar monomer conversions as the control reaction in which no redox-switching was performed (●).

1.2.4 *N*-Heterocyclic Carbene (NHC) Ligand Structure

N-heterocyclic carbenes (NHCs) are prevalent in numerous scientific fields, but have perhaps been most impactful in the field of transition metal-based catalysis due to their ability to act as coordinating ligands in a similar fashion as the phosphines mentioned above.[81] In regard to transition metal catalyzed polymerizations, NHCs have found particular utility as strongly electron-donating ligands for ruthenium catalyzed ring-opening metathesis polymerizations (ROMP).[82]

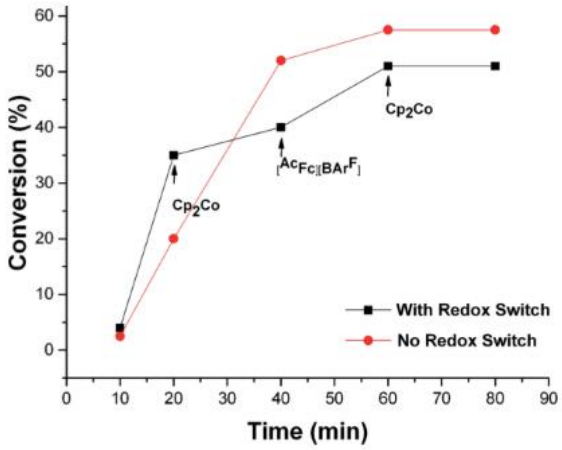

Figure 1.8 Polymerization of 5-(triethoxysilyl)bicyclo[2.2.1]hept-2-ene using redox-active catalyst **9.** Reductant ($CoCp_2$) and oxidant ($^{Ac}FcBAr^F$) were added *in situ* to switch (■) between the active ($\mathbf{9_{ox}}$) and dormant species (**9**). A control polymerization without redox switching is also shown (●). Reproduced with permission from Ref.[80] Copyright 2016, John Wiley and Sons.

Furthermore, researchers have also developed redox-active versions of these NHCs and applied them to both small molecule transformations [83] as well as ROMP.[84-85] Inspired by these works, Chen and coworkers have recently developed a class of palladium-based olefin polymerization catalysts containing redox-active NHCs (**11-12**) (Figure 1.9).[86] These catalysts are activated for polymerization via halide abstraction with sodium tetrakis(3,5-bis(trifluoromethyl)phenyl)borate) ($NaBAr^F$), generating a neutral active center. They also found that cobaltocene readily reduced the redox-active naphthoquinimidazolylidene ligand while ferrocenium tetrakis(3,5-bis(trifluoromethyl)phenyl)borate) ([Fc][BAr^F]) was able to re-oxidize the catalyst to its

native state. As a note, this is the first example discussed in this review that examines a redox-active ligand that is not based upon the oxidation of a ferrocenyl moiety.

In these polymerization tests, native catalysts **11** and **12** successfully polymerized norbornene, whereas their reduced analogues **11$_{red}$** and **12$_{red}$** were virtually inactive for all polymerizations. They hypothesized that the increased electron density of the reduced NHC ligand decreased the electrophilicity of the active-metal center, which in turn increased the energy barrier for monomer coordination and insertion. Comparing the polymerization results of the active species, catalyst **11** polymerized norbornene to 96% yield in 2 minutes, while the more sterically bulky catalyst **12** required 5 minutes to reach the same yield. The authors hypothesize that this difference in activity is simply due to ligand sterics. To expand the scope of applicable monomers, catalysts **11** and **12** were also used to polymerize 5-norbornene-2-yl acetate and 1-chloro-1-octyne.

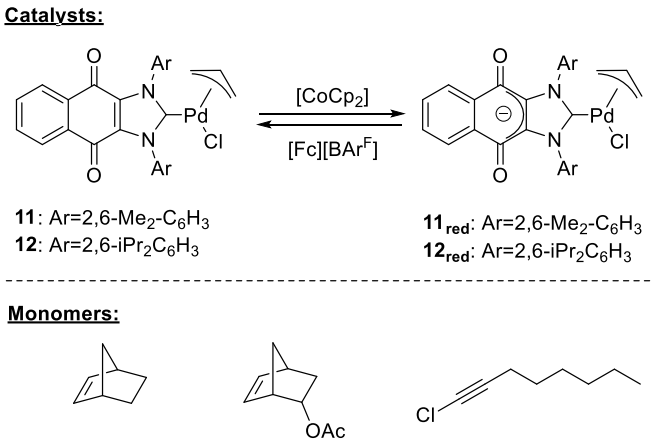

Figure 1.9 Pd-based catalysts **11-12** bearing redox-active NHC ligands, and the monomers selected for polymerization.[86]

For both monomers, **11**$_{red}$ and **12**$_{red}$ were both dormant while their oxidized analogues **11** and **12** were polymerization active. To showcase the reversible nature of the redox-active catalysts, redox-switching experiments were performed in which catalyst **11** was used to polymerize 5-norbornene-2-yl acetate (Figure 1.10 left) and catalyst **12** was used to polymerize 1-chloro-1-octyne (Figure 1.10 right). As can be seen in Figure 1.10, addition of cobaltocene to either polymerization essentially halted any monomer insertion, which could then be reinstated upon addition of FcBAr^F which re-oxidized **11**$_{red}$→**11** and **12**$_{red}$→**12**, respectively.

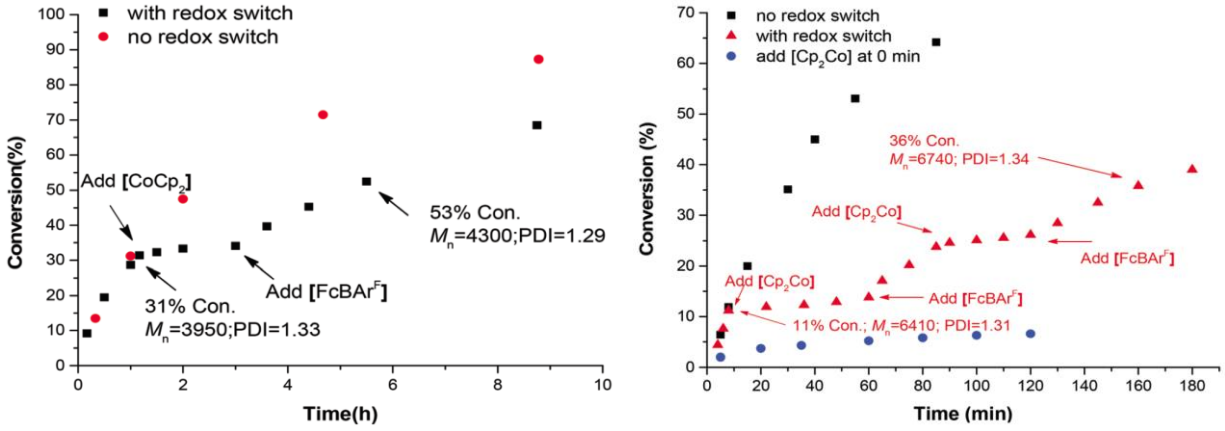

Figure 1.10 (Left) Redox-switchable polymerization of 5-norbornene-2-yl acetate with **11/11**$_{red}$**.** (Right) Redox-switchable polymerization of the 1-chloro-1-octyne with **12/12**$_{red}$**.** Reproduced from Ref.[86] with permission from the Chinese Chemical Society (CCS), Peking University (PKU), and the Royal Society of Chemistry.

1.3 Nickel Polymerization Catalysts

1.3.1 Phosphine-sulfonate Ligand Structure

As noted above, phosphine-sulfonate ligands are heavily studied for olefin polymerizations. In 2017, Chen and coworkers expanded the redox-active phosphine-sulfonate catalyst catalog by introducing nickel species **13** (Figure 1.11).[46] This species was inspired by a previous report by Scott and coworkers in which they found that increased steric bulk at the axial position of nickel phosphine-sulfonate catalysts led to increases in achievable polyethylene molecular weights.[61] With hopes of applying this same concept to Ni-based redox-active phosphine-sulfonate catalysts, they increased the steric bulk via the incorporation of bulky bi-aryl substituents in similarity to their previous work with Pd-based catalysts **4** and **5** described above. Silver triflate (AgOTf) and cobaltocene ($CoCp_2$) were found to be suitable oxidants and reductants, respectively, to access the catalyst's different redox states (**13/13$_{ox}$**).

Catalyst **13** polymerized ethylene with an activity of 2.14×10^5 g/(mol Ni·h), whereas oxidized catalyst **13$_{ox}$** exhibited an approximately 5-fold lower activity (0.43×10^4 g/(mol Ni·h)). Though this clearly established differentiation between catalyst redox states, only low molecular weight polyethylene was obtained using catalyst **13** (6190 g/mol) and **13$_{ox}$** (4400 g/mol). Though these results contradicted their original hypothesis, single crystal X-ray diffraction revealed that the bulky bi-aryl substituent used was positioned over the ferrocenyl unit in the solid state. Because of this, this ligand fails to fully block the axial position of the Ni center, and is likely responsible for the low polymer molecular weight observed.

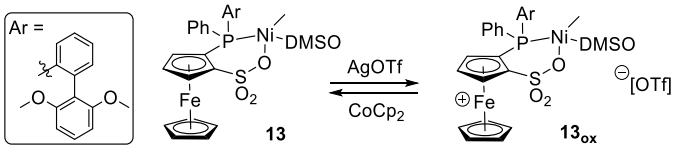

Figure 1.11 Redox-active nickel phosphine-sulfonate catalyst **13** for olefin polymerizations.[46]

Lastly, though clear differentiation between **13** and $\mathbf{13_{ox}}$ was established, the authors note that they were unable to establish an *in situ* redox-switchable system.

1.3.2 α-Diimine Ligand Structure

Similar to the palladium α-diimine catalysts discussed above, the analogous nickel catalysts have drawn significant attention following Brookhart's seminal report in 1995.[12] To capitalize on these catalysts remarkable ability to produce various branched polyethylene structures using ethylene as a sole monomer feedstock, it was well understood that the extent of chain-walking could be controlled by one, or any combination of three methods: a) controlling reaction temperature,[87] b) controlling ethylene feed pressure,[14] or c) utilizing catalysts bearing ligands with specifically tuned electron-donating or electron-withdrawing properties.[20] Although these routes are effective for controlling the extent of polyethylene branching each of them rely exclusively on tuning limited reaction attributes while modulating ligand electronics or on the iterative synthesis of individual ligand frameworks and catalysts.

To provide an alternate method, Long and coworkers hypothesized that redox-active Ni α-diimine precatalysts may facilitate control over polyethylene branching in similarity

to the electronic modifications mentioned above, albeit by using only a single redox-active catalyst species that may be modulated via the addition of an oxidant or reductant.[29] In 2016, the first redox-active nickel α-diimine catalyst was reported and is shown in Figure 1.12.[29] As a note, olefin polymerization catalyst **14** was previously reported by Brookhart, but its redox-activity had not been explored.[12] Cyclic voltammetry showed that precatalyst **14** displays a quasi-reversible one-electron redox couple at $E_p^{1/2}$ = −0.8 V (vs Fc/Fc^+), which suggested that cobaltocene would serve as an ideal reductant. It is important to note that this redox-center is in stark contrast to most other reports in that the redox-active moiety is the organic acenaphthenequinone derived α-diimine ligand rather than the more commonly encountered ferrocenyl moieties.

Ethylene homopolymerizations using catalyst **14** and $\mathbf{14_{red}}$ each showed remarkably similar behavior, yielding 1.75-1.78 g of polyethylene and achieving very high molecular weight polymers (M_w) of 200-217 kg/mol (Table 1.5, entries 1 and 3).

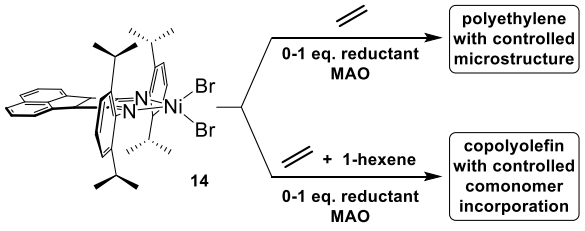

Figure 1.12 Redox-active olefin polymerization precatalyst **14** is used to control polyethylene microstructure and higher α-olefin incorporation rate.[29, 88]

Despite these similarities, analysis of these polymers branching content via ^{1}H NMR spectroscopy revealed that polyethylene produced using the native catalyst **14** reproducibly produced ~30% more branches/1000 carbons than polyethylenes produced using reduced catalyst **14$_{red}$**. This notable difference is highlighted in Figure 1.13. Furthermore, it was discovered that by adding partial equivalents of $CoCp_2$ reductant, a near-linear relationship between polyethylene branching and added $CoCp_2$ equivalents could be achieved (114 → 88 branches/1000 C's) (Figure 1.13). This signified that polyethylene branching content could be specifically tailored without sacrificing activity or compromising the molecular weight. The authors hypothesized that the observed decrease in polyethylene branching is due to a more electron-rich nature of the reduced acenaphthenequinone derived α-diimine ligand. This, in turn, decreases the propensity of that catalyst to undergo "chain-walking" relative to ethylene coordination and insertion, thereby yielding polymers with more linear structures.

Table 1.5 Ethylene Polymerizations using Precatalyst 14 With and Without Added Cobaltocene Reductant[a]

entry	$CoCp_2$ (equiv.)	yield (g)	activity[b]	M_w (kg mol^{-1})[c]	$Đ$[c]
1	0.0	1.75	3.50	217	1.54
2	0.5	1.95	3.90	271	1.77
3	1.0	1.78	3.56	200	2.04

[a]Polymerization conditions: catalyst (10 μmol), toluene (148 mL), 2 mL of dichloromethane, ethylene (15 psi), 20 °C, 30 min, and 100 equiv. of PMAO-IP. [b]Catalyst activity is in units of 10^5 g/(mol Pd·h). [c]Determined using triple detection GPC at 140 °C in 1,2,4-trichlorobenzene. Data obtained from literature.[29]

These results are in perfect agreement with the previous report of Guan and coworkers, [20] who found similar trends in a series of discretely synthesized α-diimine catalysts.

Polymers produced using the redox-active olefin polymerization pair **14/14$_{red}$**, were further analyzed using quantitative ^{13}C NMR spectroscopy, which also revealed that as the amount of added reductant approaches 1 equiv. relative to precatalyst, the presence of any branch-on-branch structure is virtually eliminated. More specifically, precatalyst **14** yielded polyethylene with 6.0 *sec*-butyl branches/1000 carbons, whereas precatalyst **14$_{red}$** only produced 0.8 *sec*-butyl branches/1000 carbons. This change is hypothesized to be a direct result of precatalyst **14$_{red}$**'s increased ligand-based electron density.

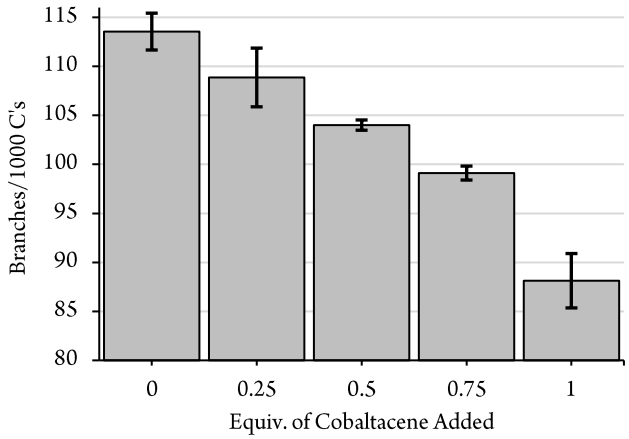

Figure 1.13 Plot of polyethylene branching content produced using precatalyst **14** as a function of equiv. of added chemical reductant ($CoCp_2$). Reprinted with permission from Ref. with permission from W.C. Anderson, J.L. Rhinehart, A.G. Tennyson, B.K. Long, *J. Am. Chem. Soc.*, 138 (2016) 774-777. Copyright 2016, American Chemical Society.

The authors also note that attempts to directly characterize the active, reduced precatalyst **14**$_{red}$ were unsuccessful, and that further elucidation of the reduced precatalyst's structure are required to fully understand the source of this behavior.[29, 89]

To expand the utility of redox-active catalyst **14**, homopolymerizations of propylene and 1-hexene were investigated, as well as copolymerizations of ethylene and 1-hexene.[88] As can be seen in Figure 1.14, homopolymerizations of 1-hexene using native catalyst **14** (●) reached complete monomer consumption within ~2 h. In contrast, catalyst **14**$_{red}$ (■) required almost 6 h to reach the same conversion. Similar results were obtained for propylene polymerizations. This polymerization activity dependence on catalyst redox state was unexpected as prior results clearly demonstrated that catalyst activities remained virtually identical for ethylene homopolymerizations, regardless of redox-state (Table 1.5, entries 1 and 3).

To capitalize on this unique behavior, Long and coworkers investigated the copolymerization of ethylene and 1-hexene. They hypothesized that 1-hexene incorporation rates may be controlled as a function of catalyst **14**'s ligand redox-state, albeit while the turnover frequency of ethylene is maintained constant regardless of redox-state, leading to copolymers with finely tuned comonomer incorporation levels. As seen in Figure 1.15, this was indeed observed as the number of butyl branches/1000 carbons decreased from 33.2 to 18.1 as the amount of added reductant was increased to 1 equiv.

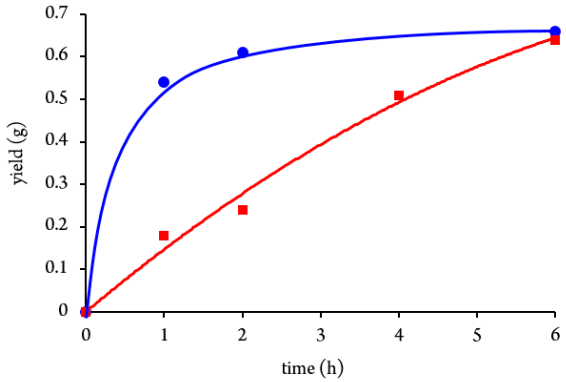

Figure 1.14 Homopolymerization of 1-hexene using precatalysts **14** (●) and **14**$_{\mathbf{red}}$ (■). Reprinted with permission from Ref. W.C. Anderson, B.K. Long, *ACS Macro Lett*, 5 (2016) 1029-1033. Copyright 2016, American Chemical Society.

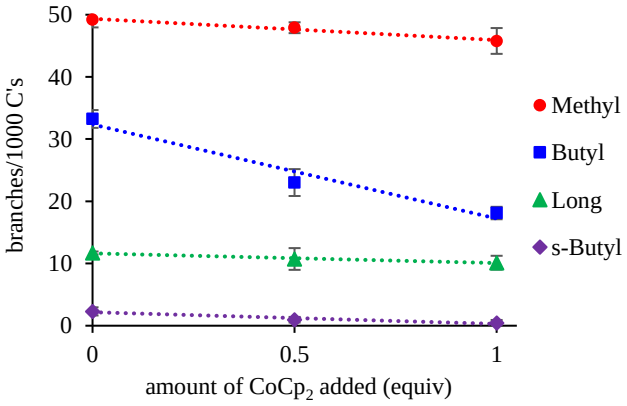

Figure 1.15 Plot of methyl (●), butyl (■), C-6 and longer (▲), and *sec*-butyl (♦) branches/1000 C's for copolymers of ethylene and 1-hexene produced by **14** as a function of added cobaltocene equivalents. Reprinted with permission from Ref. W.C. Anderson, B.K. Long, *ACS Macro Lett*, 5 (2016) 1029-1033. Copyright 2016, American Chemical Society.

This was attributed to a decrease in the incorporation of 1-hexene as the amount of added cobaltocene increased, and was further confirmed via reaction mixture monitoring that showed that 13.0%, 7.9%, and 4.5% of the included 1-hexene was consumed per gram of polymer produced when 0.0, 0.5, and 1.0 equiv of $CoCp_2$ was added, respectively. Although the absolute reasoning for this observation is not fully understood by the authors, they speculate that the reduced catalyst **14$_{red}$** exists as a ligand centered, radical anion that lowers the electrophilic nature of the nickel metal center, which lowers the rate of 1-hexene coordination and insertion more dramatically than it affects ethylene coordination and insertion.

Having thoroughly investigated the catalytic tendencies of catalyst **14** and its reduced analogue **14$_{red}$**, Long and coworkers also reported a series of α-diimine catalysts bearing ferrocenyl substitutents (**15-17**) (Figure 1.16).[90] It was hypothesized that these ferrocene-containg ligands would be more electron rich than their unsubstituted counterparts, yielding more linear polyethylene with high melting transitions, and that the incorporation of additional redox-active sites might open opportunities to acces a single catalytic species with multiple accesible redox-states. Cyclic voltametry studies showed that the ferrocenyl units could be readily oxidized using silver [tetrakis(bis-3,5-trifluoromethylphenyl) borate] ($AgBAr^F$) while the α-diimine backbone could be reduced using $CoCp_2$.

Upon activation with MAO, catalysts **15-17** each proved to readily polymerize ethylene.

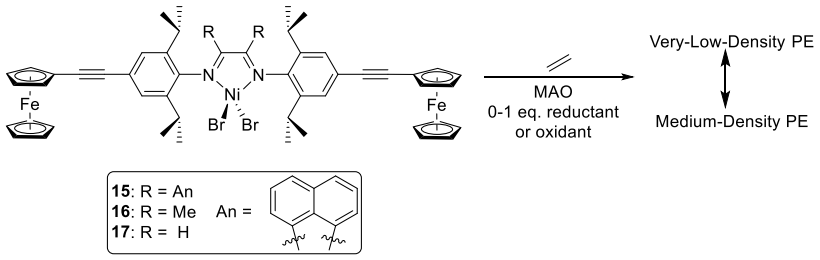

Figure 1.16 Redox-active olefin polymerization precatalysts **15-17** bearing ferrocenyl substituted α-diimine ligands.

However, only catalyst **15** exhibited reversible redox activity for the the α-diimine ligand backbone as well as the ferrocenyl units, which was determined using cyclic voltametry. Perhaps not too surprisingly, native catalyst **15** and oxidized catalyst $\mathbf{15_{ox}}$ in which both ferrocenyl moieties were oxidized using 2 equiv. of $CoCp_2$ exhibited no differentiation between ligand-based redox states. As can be seen in Table 1.6, both catalysts polymerized ethylene with similar activities (yields = 1.05 and 1.09 g) and produced polymers of similar molecular weight (222-235 kg/mol) and branch content (39-40 branches/1000 C's) (Table 1.6, entries 1-2). This lack of differentiation between the native and oxidized catalysts was initially hypothesized, and later proven, to be due to the use of MAO, which contains excess trimethylaluminum. Trialkylaluminum species are known to reduce ferrocenium-containing species (Fe^{III}) to their Fe^{II} oxidation state, which in this case means that activation of catalyst $\mathbf{15_{ox}}$ using MAO simultaneously reduced its redox-active ferrocenium units to recreate catalyst **15** *in situ*. Similar issues were encountered by Gibson and coworkers as was previously discussed in these reviews.[33-35]

Table 1.6 Ethylene Polymerization Results using Precatalyst 15 and Redox Agents[a]

entry	catalyst	yield (g)	M_w (kg/mol)[b]	B[c]	density (g/mL)[d]	T_m (°C)[e]
1	**15$_{ox}$**[f]	1.09	235	39	0.90	107
2	**15**	1.05	222	40	0.90	107
3	**15$_{red}$**[f]	0.66	264	9	0.93	119

[a]Polymerization conditions: catalyst (5 μmol), 98 mL of toluene, 2 mL of dichloromethane, ethylene (15 psi), 20 °C, 15 min, and 500 equiv. of MMAO. [b]Determined using triple detection GPC at 140 °C in 1,2,4-trichlorobenzene. [c]Branches per 1000 total C's, determined by ^{1}H NMR spectroscopy, reported values are averages over multiple trials. [d]Determined using Archimedes Principal. [e]Determined using differential scanning calorimetry (DSC), second heating cycle. [f]2 equiv. of AgBAr^F was added to trials labeled "ox", whereas 1 equiv. of cobaltocene was added to trails labeled "red". Data obtained from literature.[90]

In contrast, reduced catalyst **15$_{red}$** displayed a drastic change in branching content (9 branches/1000 C's) as compared to native catalyst **15** (40 branches/1000 C's) (Table 1.6, Entry 2-3). As mentioned above, this is hypothesized to be a result of the more electron-rich nature of the reduced acenaphthenequinone derived α-diimine ligand, which increases the rate of ethylene coordination and insertion relative to the rate of chain-walking. Measurements of polymer density made utilizing Archimedes' Principal showed that the polymer produced using native catalyst **15** is categorized as very-low-density polyethylene (density = 0.90 g/mL), whereas the polyethylene produced using the cobaltocene-reduced catlayst **15$_{red}$** is categorized as medium-density polyethylene (density = 0.93 g/mL). This observation marked the first example in which more than one grade (or density) of polyethylene was obtained using a redox-active olefin polymerization catalyst.

1.4 Conclusion and Outlook

The first successful examples of redox-active olefin polymerization catalysts have recently been realized with seminal reports of Chen and Long. Following these reports, a variety of palladium and nickel-based catalysts have been developed that take full advantage of well-known ligand frameworks such as phosphine-sulfonates, α-diimines, heteroscorpionates, and *N*-heterocyclic carbenes. These catalysts have been tested for a variety of monomeric substrates, such as ethylene, higher α-olefins, substituted and unsubstituted norbornenes, alkynes, and a plethora of polar comonomers, and have been shown to exhibit catalytic differentiation based on redox state for one or more of these monomers. In general, Pd-based redox-active olefin polymerization catalysts have found particular utility in modulating polar comonomer incorporation levels in redox-switchable norbornene and alkyne polymerizations, leading to "on-off-on" type behavior. In contrast, Ni-based redox-active olefin polymerization catalysts are able to control polyolefin microstructure as a function of ligand redox-state, control higher α-olefin comonomer incorporation levels in copolyethylenes, and achieve high molecular weight polyolefins in each case.

Although the field of redox-active olefin polymerization catalysts has grown tremendously over the past few years, there are still a number of obstacles that must be overcome for redox chemistry to become a reliable tool for enhanced olefin polymerization control. First, redox-active catalysts are often limited based on their need to be activated by reagents such as MAO. As highlighted herein, multiple reports have shown that trialkylaluminum contaminants in MAO may re-reduce previously oxidized moieties. This

ultimately limits redox-active ligand design criteria and their potential for *in situ* redox-switching capabilities. A second limitation is that currently known redox-active olefin polymerization catalysts have been unable to demonstrate monomer selectivity switching. If redox-switching is able to bring about inversion of monomer selectivity, it can be envisioned that advanced polymer architectures, such as block copolymers, may be accessed. As a note, the ability to invert monomer selectivity based upon ligand/catalyst redox state has recently been demonstrated for the redox-switchable ring-opening polymerization of lactide and cyclic ethers via chemical additives and electrochemical pulses.[91-101] Lastly, many of the redox-switchable catalysts systems presented in this chapter suffer from limited catalyst stability/lifetime that will also impact the ability of these catalysts to one day access advanced polymer architectures. This issue is further compounded in that many industrial used polymerizations, such as fluidized bed rectors for ethylene polymerization, operate at elevated temperatures that are known to accelerate catalyst decomposition and/or deactivation.[87, 102-113] Though a handful of thermally robust Ni and Pd-based catalysts have been developed,[56, 114-126] it is unclear if redox-switchable functionality may be incorporated into those catalyst systems. In closing, redox-active olefin polymerization catalysts have expanded the toolbox of the modern synthetic polymer chemist. Although the list of current limitations in the field may seem extensive, I hope that you will view it as both an opportunity and a challenge.

CHAPTER 2 – PHOTOCHEMICAL CONTROL OF A REDOX-ACTIVE OLEFIN POLYMERIZATION CATALYST

A version of this chapter was originally published by Jordan M. Kaiser, W. Curtis Anderson, Jr., and Brian K. Long:

Kaiser, J. M., Anderson, W. C. Jr., Long, B. K. *Polymer Chemistry*. **2018**, *9*, 1567-1570

I was responsible for the synthesis and characterization of the nickel precatalyst used, conducted all polymerizations, characterized the resultant polymers, and lead the preparation of the manuscript. Dr. W. Curtis Anderson aided in preparation of the manuscript and provided experimental insight. Dr. Brian Long advised this work and aided in the preparation of the manuscript.

2.1 Introduction

The ability to exact spatial and temporal control during a polymerization using external stimuli presents a unique opportunity by which tailored polymeric materials may be accessed.[127] Although various external stimuli may be employed for this purpose, such as applied voltage, chemical reagents, and mechanical force, the ability to manipulate reactions using light has become increasingly popular. As an example, photoredox agents have been shown to effectively control small-molecule organic transformations via the oxidation or reduction of catalytic species.[25, 128-135] In the field of polymer chemistry, photo-active molecules have been used to influence the initiation, propagation, and termination events in many polymerization methodologies, such as atom transfer radical

polymerization (ATRP),[136-145] ring opening metathesis polymerization (ROMP),[146] photo-induced electron transfer-reversible addition-fragmentation chain-transfer polymerizations (PET-RAFT),[147-152] thiol-ene polymerization,[153] and most recently, cationic polymerizations.[154-156]

Although each of these methods represent an amazing demonstration of catalytic control, they are limited in that they provide no means to dictate the resultant polymer's microstructure. In contrast, it has been shown that simple changes in reaction temperature and/or ethylene feed pressure can result in varied polyethylene microstructures (branching content) while using only a single group 10 transition metal-based olefin polymerization precatalyst.[14, 157-159] Inspired by this work and fundamental studies by Guan et al.,[20] researchers have recently expanded the ability to influence polyethylene microstructure to include control via redox-active ligands. The electronic nature of these ligands may be altered in situ to modulate olefin polymerization behavior.[28-29, 71, 88, 90-91] As a specific example, Anderson *et al.* recently demonstrated that the *α*-diimine ligand backbone of Ni complex **14** could be reduced using an added chemical reductant, thereby resulting in the generation of polyethylene with reduced branching content and virtual elimination of all branch-on-branch microstructure.[29]

Inspired by these reports, we hypothesized that polyethylene microstructure could likewise be modulated via visible light if a compatible photoredox agent was employed. If successful, the presence or absence of light would dictate the electronic nature of the active polymerization catalyst, ultimately controlling the resultant polymer's microstructure with the "flick-of-a-switch".

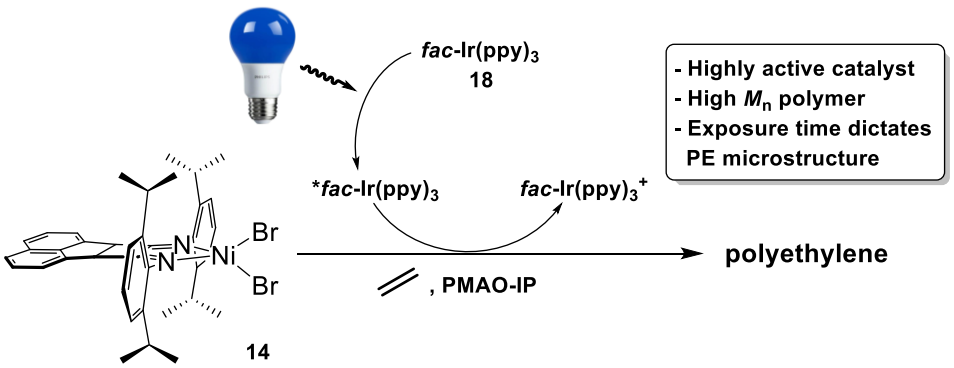

Figure 2.1 Photochemical regulation of polyethylene microstructure using precatalyst **14** and *fac*-Ir(ppy)$_3$ (**18**).

To the best of my knowledge, no examples of a photoredox olefin polymerization have been reported to date. Toward this goal, we present the photo-modulation of polyethylene branching content using a redox-active α-diimine precatalyst (**14**) and the photoreductant, tris[2-phenylpyridinato-C2,*N*] iridium(III) (18) (Figure 2.1).

2.2 Results and Discussion

Redox-active precatalyst **14** has a reported half-wave potential of $E_{1/2}$ = -0.80 V (vs Fe^{II}/Fe^{III}) as measured via cyclic voltammetry.[29] This moderate potential permitted the use of the well-known one electron reductant cobaltocene ($CoCp_2$), which has a reduction potential of $E_{1/2}$ = -1.33 V. However, for this study a stoichiometric photoreductant with similar reduction potential is required. We chose to use tris[2-phenylpyridinato-C^2,N] iridium(III) (*fac*-Ir(ppy)$_3$) (**18**) that has a photo-excited reduction potential of $E_{1/2}^{IV/*III}$ = -1.73 V.[160] To irradiate this photoreductant, multiple light sources were investigated in order to determine the optimal source to yield consistent results.

Considering that molecule **18** has a maximum absorbance in the blue region (450 nm),[142] We selected three light sources (14 W CFL, 3 W blue LED, and 36 W UV lamp) that show emission at this particular wavelength. Each light source irradiated separate ethylene polymerizations containing catalyst **14** and photoreductant **18**. The microstructure of the resultant polymers were analyzed via SEC on a HT-GPC. The Mark-Houwink plot presented in Figure 2.2 indicates that there are structural differences between each polymer produced. At any given molecular weight, an increase in intrinsic viscosity correlates to a decrease in polyethylene branching content. As expected, the polymerization that was shielded from light consistently displayed lower intrinsic viscosity as a function of molecular weight to indicate a branched polyethylene microstructure. When using a polychromatic light source, 14 W CFL (green trace), there is a noticeable increase in intrinsic viscosity at a given molecular weight to represent a more linear polyethylene polymer. The most significant difference in branching content was observed when using a monochromatic light source, 3 W blue LED (blue trace), and a high-powered polychromatic light source, 36 W UV lamp (red trace). While the polymer microstructure of these resultant polymers are similar, Table 2.1 displays the influence of light source on catalyst activity. All the light sources, except the 36 W UV lamp, show no effect on catalyst activity as each polymerization produced 2.24-2.54 g of polyethylene. On the other hand, the polymerization exposed to the UV lamp yielded 0.62 g of polymer. We attribute this decrease in polymer yield to the high-wattage light source leading to catalyst decomposition/deactivation. To ensure the most consistent results for the following polymerizations, the 3 W blue LED light was chosen as the optimal light source.

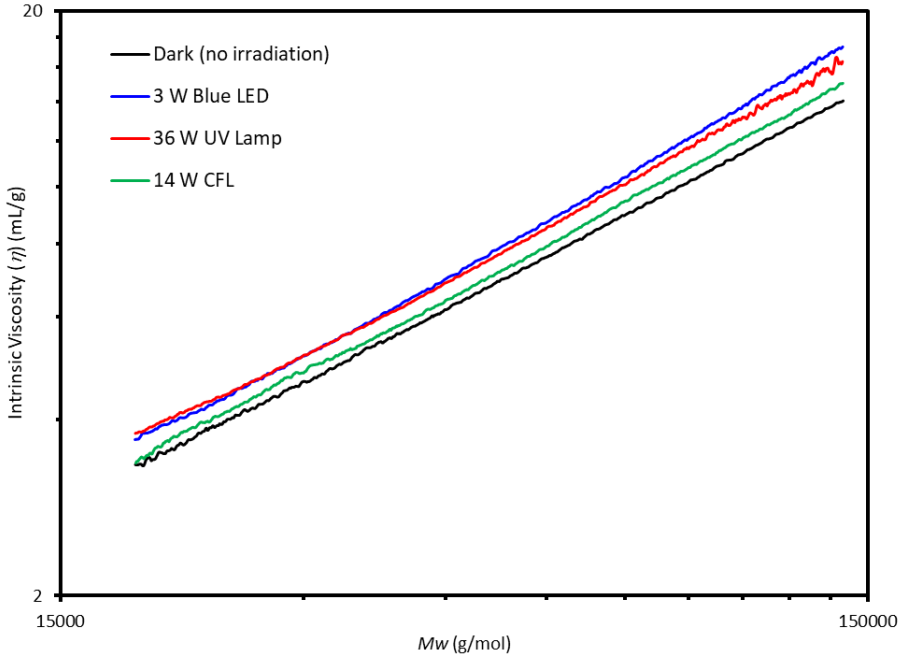

Figure 2.2 Log-log plot of intrinsic viscosity (η) vs M_w for polyethylene produced using precatalyst **14** and photoreductant **18** under irradiation by different light sources. (No light source (black), 3 W blue LED (blue), 36 W UV lamp (red), and 14 W CFL (green))

To ensure that photoreductant **18** and the applied light source do not instigate any unwanted polymerization behavior, control experiments were conducted to confirm their compatibility in standard PMAO-IP-activated ethylene polymerizations. First, we determined that irradiation of photoreductant **18** in the absence of precatalyst **14** yielded no ethylene polymerization activity (Table 2.1, entry 1). Next, We confirmed that irradiation of precatalyst **14** in the absence of photoreductant **18** has no effect on the polymer produced (Table 2.1, entry 2).

Table 2.1 Comparing Polyethylene Yield with Irradiation Light Source[a]

entry	light source	polymer yield (g)
1	Dark (no irradiation)	2.24
2	3 W blue LED	2.37
3	36 W UV	0.61
4	14 W CFL	2.54

[a]Polymerization Conditions: Precatalyst **14** = 10.0 µmol, **18** = 10.0 µmol, 150 mL of toluene, 20 °C, 15 PSI ethylene, 30 min polymerization, 30 min irradiation, and 100 equiv. of PMAO-IP.

These control experiments indicate that the results discussed in the following sections are not due to undesirable reactions involving the photoreductant and/or light source individually, but a synergy of the two that together are able to reduce the nickel α-diimine precatalyst **14**.

All subsequent ethylene polymerizations were conducted by employing equimolar amounts of **14** and **18** in toluene, 100 equivalents of PMAO-IP for catalyst activation, and a predetermined exposure time using a 3 W blue LED light (Table 2.2, entry 3-9). This data shows that the activity of precatalyst **14** is virtually unaffected by the presence of **18** and exposure to light, as similar amounts of polyethylene were obtained in each case (yield = 2.20-2.50 g). Furthermore, all of the resultant polymers have similar molecular weights (M_w = 174-221 kg/mol), as analyzed via gel permeation chromatography (GPC). However, as irradiation time is increased, a concomitant increase in polymer dispersity is observed ($Đ$ = 1.54-1.97). As a note, this trend was also observed in a previous report in which $CoCp_2$ was employed as an added chemical reductant, suggesting similar catalyst reduction behavior.[29, 88]

Table 2.2 Polymerization of Ethylene using Ni Precatalyst 14 and Photoreductant 18 as a Function of Exposure Time[a]

entry	exposure time[b] (min)	yield (g)	M_w[c] (kg/mol)	$Đ$[c]	B[d]
1[e]	30	0	-	-	-
2[f]	30	2.46	174	1.78	111 (± 2.2)
3	0	2.24	180	1.54	113 (± 1.9)
4	1	2.48	186	1.64	106 (± 1.8)
5	3	2.50	214	1.78	102 (± 1.9)
6	5	2.38	219	1.79	101 (± 2.1)
7	10	2.26	221	1.85	99 (± 2.3)
8	20	2.20	214	1.84	96 (± 1.9)
9	30	2.37	212	1.97	93 (± 1.6)

[a]Polymerization Conditions: Precatalyst **14** = 10.0 µmol, **18** = 10.0 µmol, 150 mL of toluene, 20 °C, 15 psi ethylene, 30 min, and 100 equiv. of PMAO-IP. [b]Irradiated using a 3 W blue LED light. [c]Determined using triple detection GPC at 140 °C in 1,2,4-trichlorobenzene. [d]Branches per 1000 total C's as determined by ^{1}H NMR reported values are averages over multiple trials. [e]No precatalyst **14** added. [f]No photoreductant **18** added.

Analysis of the resultant polyethylene samples by ^{1}H NMR spectroscopy shows that there is a notable decrease in polyethylene branching content (B = 113 - 93 branches/1000 C) as a function of visible light exposure time (Table 2.2, entries 3-9). This data is represented graphically in Figure 2.3 in which polyethylene branching content is plotted relative to exposure time for ethylene polymerizations containing precatalyst **14** and photoreductant **18** (■), and control polymerizations containing precatalyst **14** without any photoreductant present (●). In Figure 2.3, an exponential decay in polyethylene branching density is observed for polymerizations containing photoreductant **18** depending on the duration of visible light exposure. This clearly suggests that as exposure time increases, a greater concentration of the reduced, catalytically-active species is present, which ultimately leads to a more linear polyethylene microstructure.

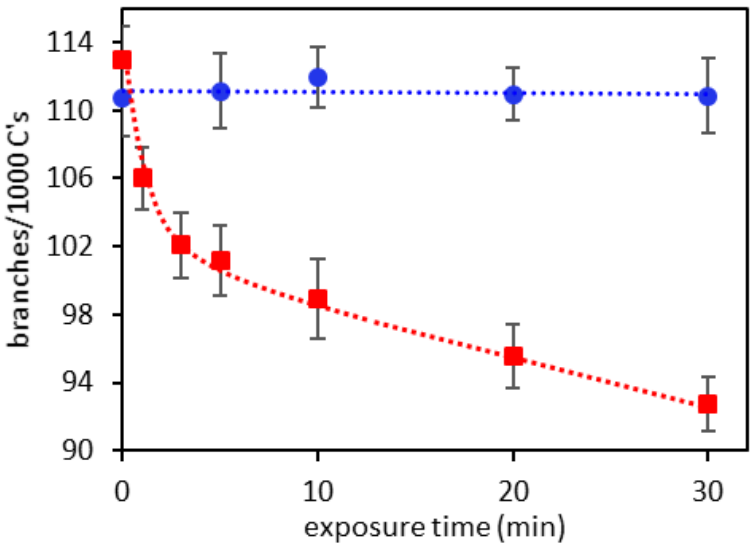

Figure 2.3 Plot of polyethylene branches/1000 C's versus exposure time for a polymerization containing *fac*-Ir(ppy)$_3$ (■) and a control polymerization containing no *fac*-Ir(ppy)$_3$ (●).

To further analyze the microstructure of the resultant polyethylene samples, their dilute solution behavior was evaluated using GPC. In similarity to the results obtained via ^{1}H NMR analysis, Mark-Houwink log-log plots of intrinsic viscosity (η) versus weight average molecular weight (M_w) further confirm the differentiation in branching content between ethylene polymerizations exposed to visible light irradiation (Figure 2.4, red trace), and those that were not exposed (Figure 2.4, blue trace). As a note, a highly linear polyethylene sample is also plotted in Figure 2.4 (green trace) as a reference.[29] From this data, noticeably lower intrinsic viscosities are observed across all molecular weights for polymerizations that were not exposed to visible light irradiation.

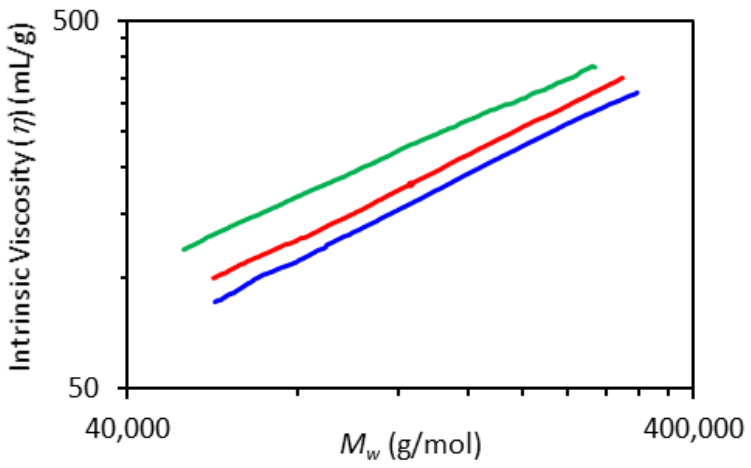

Figure 2.4 Log-log plot of intrinsic viscosity (η) vs M_w for polyethylene produced using precatalyst **14** and photoreductant **18** under irradiation (—, red) or without irradiation (—, blue). For comparison, a highly linear PE sample is also plotted (—, green).

This result is in strong agreement with a previous report in which a chemical reductant was used,[29] and further supports a change in polyethylene microstructure as a function of visible light exposure in the presence of photoreductant **18**.

To quantify the difference in polymer branching content as a function of visible light exposure time, quantitative ^{13}C NMR analysis was used following the procedures of Galland and co-workers (Table 2.3).[161-162] As exposure time is increased, the percentage of methyl branches increases from 53.4% to 61.7%, whereas the percentage of ethyl, propyl, butyl, and long branches were each found to decrease by a small percentage. More interestingly, long exposure times led to a dramatic reduction in *sec*-butyl branches (6.1% - 1.4%), which is significant as *sec*-butyl branches have distinct shifts in their ^{13}C NMR spectra and are the smallest form of branch-on-branch structure distinguishable via NMR

analysis. The observed decrease in overall branching content and near elimination of all branch-on-branch microstructure are in perfect agreement with the previous report,[29] and further suggests that photoreductant **18** can effectively reduce the α-diimine backbone of precatalyst **14** upon exposure to visible light. We hypothesize that the decreased propensity of the reduced catalytic species to undergo chain-walking is due to the more electron-rich nature of the reduced catalytic species. This hypothesis is supported by the work of Guan and coworkers who demonstrated that catalysts bearing strongly electron-donating α-diimine ligands display increased rates of ethylene coordination-insertion relative to their rate of chain-walking.[20]

Table 2.3 Polyethylene Branching Identity Analysis as Determined via Quantitative ^{13}C NMR[a]

	LED exposure time[b] (min)		
	0	10	30
methyl	53.4 (±2.0)	58.0 (±0.7)	61.7 (±1.9)
ethyl	8.3 (±0.3)	7.5 (±0.6)	7.0 (±0.4)
propyl	4.8 (±0.4)	4.5 (±0.4)	4.3 (±0.9)
butyl	7.3 (±0.5)	6.8 (±0.2)	5.6 (±0.4)
amyl	5.2 (±0.3)	5.0 (±0.5)	6.0 (±0.6)
long[c]	15.0 (±1.3)	14.5 (±0.4)	14.0 (±2.4)
sec-butyl	6.1 (±1.3)	3.8 (±0.4)	1.4 (±0.2)

[a]Values represent the percent (%) of total branching content. [b]3 W Blue LED light. [c]Branches six carbons and longer.

2.3 Conclusions

To the best of my knowledge, this report marks the first successful example in which polyolefin microstructure is modulated using light as an external stimulus. More specifically, by combining the redox-activity of precatalyst **14** and photoreductant **18** as a stoichiometric one electron donor, We were able to effectively modulate polyethylene branching density and microstructure as a function of exposure to visible light. Furthermore, ^{1}H NMR, ^{13}C NMR, and GPC analyses were used to quantitate and confirm the change of the branching density of polymers. This capability serves as a fundamental proof-of-principle, emphasizes the versatility of redox-active catalysts, and showcases the ability to tailor high-molecular weight polyolefins via externally regulated stimuli.

2.4 Experimental

2.4.1 General Methods and Materials

All reactions were performed under an inert nitrogen atmosphere using an MBraun UniLab glovebox or using standard Schlenk techniques, unless otherwise noted. All solvents were dried using an Innovative Technologies PureSolv Solvent Purification System and degassed via three freeze-pump-thaw cycles. Precatalyst **14** was prepared according to literature.[12] Photoreductant **18** was purchased from Sigma Aldrich and used as received. PMAO-IP was purchased from Akzo Nobel and used as received. All other reagents were purchased from commercial vendors and used without further purification. Gel permeation chromatography (GPC) was performed at 160 °C in 1,2,4-trichlorobenzene at a flow rate of 1.0 mL/min on a Malvern Viscotek HT-GPC equipped with triple detection. Quantitative

^{13}C NMR spectra were obtained using a Varian 500 MHz NMR and analyzed following literature procedures.[161-163] Polymer ^{1}H NMR spectra were obtained using a Varian 500 MHz NMR. All NMR spectra are referenced relative to their residual solvent signal. Branching content was determined by ^{1}H NMR spectroscopy using the formula $(CH_3/3)/[(CH + CH_2 + CH_3)/2] \times 1000$.[164]

2.4.2 General Ethylene Polymerization Conditions

Under an inert atmosphere and shielded from ambient light, a Fisher-Porter bottle was charged with precatalyst **14** (10 μmol), photoreductant **18** (10 μmol), toluene (150 mL), and a magnetic stir bar. The Fisher-Porter bottle was sealed, placed in a thermostated room temperature water bath (the reactor was submerged to 1/3rd the solvent level), and covered with aluminum foil to shield from ambient light (see Figure S1). The vessel was pressurized with ethylene gas while stirring and allowed to equilibrate for 10 minutes. PMAO-IP (100 equivalents) was injected to initiate polymerization and the reaction was stirred continuously for the desired time. All polymerizations were quenched via the addition of MeOH (10 mL) and the polymer was precipitated using excess acidic MeOH (5% HCl in MeOH). The polymer was stirred in the acidic methanol for 24 hours then filtered, washed with excess methanol, and dried to constant weight in a vacuum oven.

2.4.3 General Ethylene Polymerization Conditions (Reduced Catalyst)

Polymerizations requiring the reduced catalyst form were performed using the same procedure described above, except after MAO was injected, the reaction was irradiated using a Sunlite 3 W blue LED bulb for the desired amount of time. The Fisher-Porter bottles

used are Lab Crest® 6 oz pressure reactors (glass side-wall thickness is ~4 mm) purchased from Andrews Glass Co. The bulb was positioned 2 cm from the Fisher-Porter bottle (Figure 2.5a) and an aluminum foil shield was placed around the apparatus to ensure maximum irradiation while also shielding from ambient light (Figure 2.4b). As described above, the reactor was submerged in the water bath to 1/3rd the solvent level to provide temperature control, yet not greatly diminish the intensity of light reaching the reaction solution.

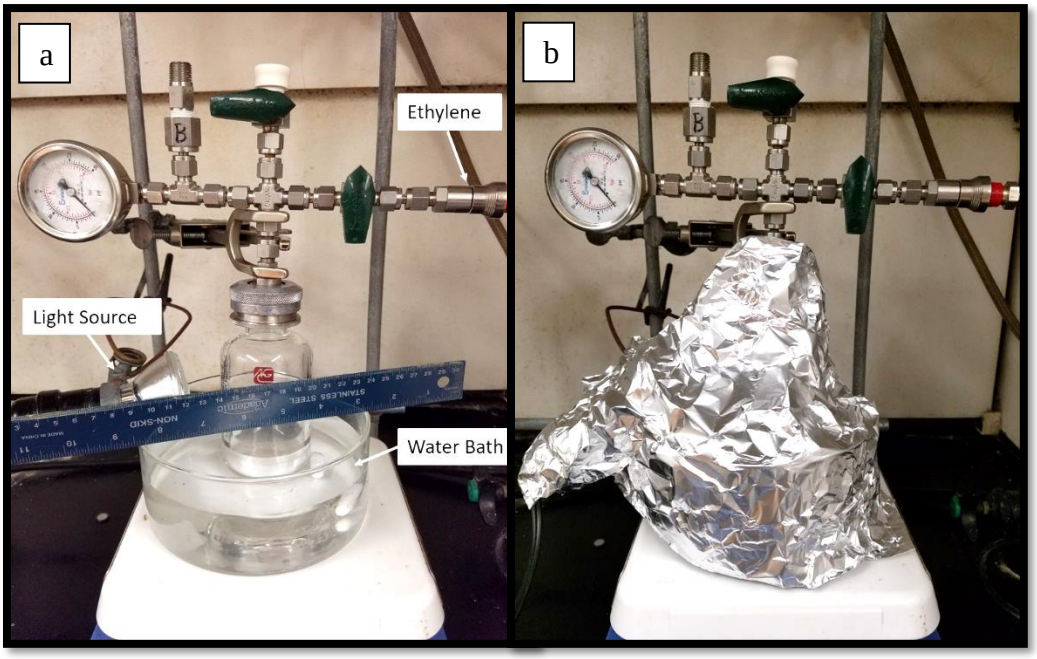

Figure 2.5 a) Polymerization set-up. b) Polymerization set up with aluminum foil shield.

CHAPTER 3 – LIGHT STIMULATED OLEFIN POLYMERIZATION AND APPLICATIONS THEREOF

A version of this chapter is disclosed in a provisional patent by Jordan M. Kaiser and Brian K. Long:

Kaiser, J. M., Long, B. K., "Olefin Polymerizations and Printing Methods Thereof" Application number: 62720589, Filed: August 21, 2018. Patent Pending.

I was responsible for the synthesis and characterization of the nickel catalyst used, conducted all polymerizations, characterized the resultant polymers, and prepared the manuscript. Dr. Brian Long advised this work and aided in the preparation of the manuscript.

3.1 Introduction

3.1.1 Overview of Homogeneous Olefin Polymerization Catalyst Activation

The majority of homogeneous olefin polymerization precatalysts, regardless of ligand design, are inherently polymerization inactive. To become active, they need an open coordination site and an orthogonal alkyl, aryl, or H group to insert monomers via coordination-insertion (Figure 3.1). This activation is typically accomplished via the addition of an added chemical reagent referred to as a "cocatalyst" or "activator" in the literature.[14, 21, 29, 58, 165-167] Research on activators is ever-growing, but these essential reagents are generally organized into the following categories: aluminoxanes, perfluoro borate salts, perfluoro borate Brønsted acids, and perfluoroaryl borane Lewis acids.

Aluminoxane reagents, the most popular of which is methylaluminoxane (MAO), have a general oligomeric structure of $[-Al(R)-O-]_n$ and are very effective olefin polymerization precatalyst activators due to their high reactivity. While the structure of these aluminoxane complexes is still under dispute, they can behave as both an alkylating reagent and Lewis acid to generate the active catalytic species via routes A, B, or C (Figure 3.1). In the case where a dihalide precatalyst is used (Figure 3.1, route A), MAO will alkylate the metal center and then abstract the remaining halide, ultimately generating the required open coordination site. This halide abstraction can also be used to activate monohalide precatalysts via route B. Finally, aluminoxanes can simply act as Lewis acids to abstract an alkyl ligand (Figure 3.1, route C) when a dialkyl substituted precatalyst is employed.

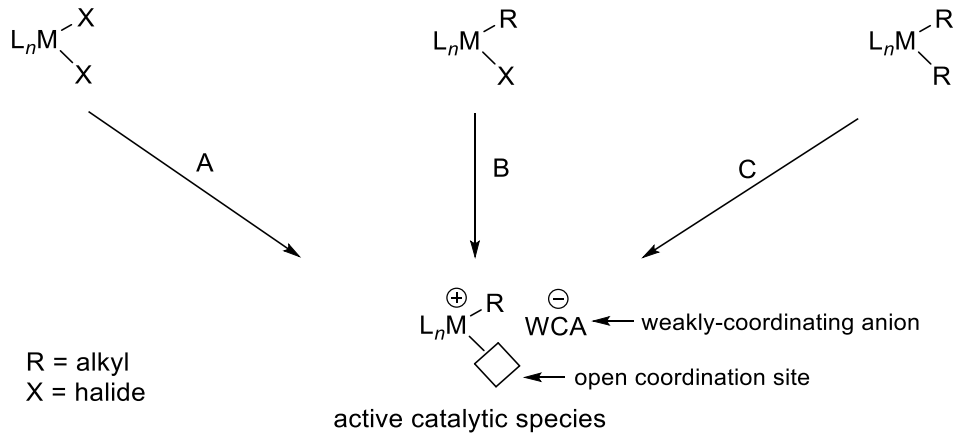

Figure 3.1 Routes to access the active olefin polymerization catalytic species.

Because most catalytically-active olefin polymerization catalysts propagate via a cationic metal species, it is important to select proper activating reagents that contain weakly- or non-coordinating anions to complete the ion pair and ensure optimal catalytic activity and longevity. If a strong coordinating counter-anion is present, then a tight ion-pair association prevents olefin monomers from coordinating to an active metal center at the open coordination site, ultimately retarding monomer insertion. In specific cases where MAO is used as the activator, a weakly-coordinating alkyl aluminoxane anion is produced, which stabilizes the cationic metal species without hindering olefin coordination and insertion. The remaining activators that will be discussed include perfluoroaryl substituents (e.g. pentafluorophenyl) that have been reported to minimize nucleophilic character by delocalizing the incumbent negative charge; therefore, creating a weak ionic attraction to the cationic metal center permitting the coordination-insertion of monomer. This weak cation-anion interaction leads to high catalytic activities that are superior to traditional counterions, such as $[BF_4]^-$ and $[PF_6]^-$.

Perfluoroborate salts (BAr^F), such as $NaBAr^F$ and $AgBAr^F$, are commonly used to activate monohalide precatalysts (Figure 3.1, route B) by halide abstraction and elimination of a salt. Other ionic perfluoroborate species with a hydrocarbon-centered cation (e.g. trityl BAr^F) are strong Lewis acids capable of effectively abstracting alkyl ligands from dialkyl precatalysts (Figure 3.1, route C). In addition, borate complexes can also behave as Brønsted acids by promoting proton transfers. Ammonium (e.g. HNR_3^+) and oxonium acid (e.g $H(OR_2)_2^+$) derivatives paired with a borate anion can also abstract an alkyl ligand generating methane via protonolysis. While charged borate complexes can facilitate

precatalyst activation through several mechanisms, neutral perfluoroarylborane complexes (e.g. $B(C_6F_5)$) are competent cocatalysts for activating dialkyl substituted precatalysts (Figure 3.1, route C), as well. The trisubstituted borane is a strong Lewis acid that abstracts the alkyl substituent to generate an open-coordination site. This resulting monoalkyl borate product behaves as a suitable weakly-coordinating anion to stabilize the cationic metal-center due to the delocalized nucleophilic character provided by the perfluoroaryl substituents.

While each of these activation methods have found utility in the field of olefin polymerization catalysis, they do not permit spatially and/or temporally controlled activation via external stimuli. The ability to use this type of control over the polyolefin polymerization precatalyst activation process could prove to be advantageous for numerous applications due to the availability of olefin monomer feedstocks. Toward this goal, this chapter will focus on the development of light-activated olefin polymerization precatalysts and their potential use to enable the light-based 3-D printing of polyolefins.

3.1.2 Opportunities for Photoinduced Olefin Polymerizations in 3-D Printing

The ability to generate usable materials and devices via three-dimensional (3-D) printing has become an incredibly relevant field of research in both industry and academia alike.[168-170] Perhaps the most readily accessible and popular 3-D printing method for polymers is fused deposition modeling (FDM). FDM involves the extrusion of a polymer filament in a line-by-line manner to form a targeted structure. While FDM is routinely used in industrial, academic, and even hobbyist settings, it has a restricted range of extrudable polymeric materials and limited fine-detail resolution. In contrast, 3-D printing via

stereolithography (SLA) and dynamic light processing (DLP) methods have attracted significant interest due to their enhanced printing precision and versatility. Both SLA and DLP use light projection that induces polymerization or cross-linking of a liquid resin to form their desired features.[171-172]

Although SLA and DLP printing both demonstrate an impressive ability to produce detailed and complex 3-D printed structures, they are limited to a restricted monomer/resin catalog, which contains only those species capable of undergoing photoinitiated polymerization or cross-linking.[173] Unfortunately, these requirements disqualify olefinic monomers such as ethylene, propylene, and higher α-olefins from being eligible 3-D printed materials. These monomers are among the cheapest and most versatile feedstocks known today and are the essential building blocks of polyolefins: the world's most widely produced polymers. To enable the 3-D printing of polyolefins via SLA or DLP-like methods, corresponding chemistries must be developed that will facilitate the photoinduced polymerization of ethylene and higher α-olefins.

In an effort to fill this gap in current capabilities, we herein describe the initial development of photoinduced olefin polymerizations. This is accomplished via the combination of an olefin polymerization precatalyst, a photoacid generator (PAG), and exposure to UV light. Because this is a photoinduced process, it is able to provide both spatial and temporal resolution of the polymerization process. As a note, PAG's have been previously used to photoinitiate other polymerizations, such as ring opening metathesis polymerization (ROMP),[174-175] cationic polymerization,[176-177] and the curing of some resins;[178] however, to the best of my knowledge, this represents the first example in which

light is used to initiate the coordination-insertion polymerization of ethylene and higher α-olefins. Finally, we will provide evidence that this methodology may be used to "print" polyolefins and generate layered conformal polyolefin films and/or patterned polyolefin films via light activated, gas phase polymerizations, which draw analogy to the SLA printing process.

3.2 Results and Discussion

3.2.1 UV Light Stimulated Olefin Polymerizations

Inspired by the ability to activate alkyl substituted olefin polymerization catalysts using Brønsted acids, we hypothesize that replacing traditionally used proton sources with a PAG might enable light-stimulated precatalyst activation.[179] To test this hypothesis, we chose to investigate the polymerization of 1-hexene using common metallocene olefin polymerization precatalysts, dimethylbis(indenyl) zirconium (**19**), dimethylbis(tert-butylcyclopentadienyl) halfnium (**20**), and a non-metallocene ONNO-type catalyst (**21**) in combination with the iodonium PAG, 4-isopropyl-4'-methyldiphenyliodonium tetrakis(pentafluorophenyl) borate (**I-PAG**) as an initial test platform (Figure 3.2). We chose this PAG due to its commercial availability and weakly coordinating borate anion, which is known to prevent tight ion-pair association between the active, cationic olefin polymerization catalyst and the corresponding counter anion following activation.[180] The light source employed was a handheld 4 W compact UV lamp (254 nm).

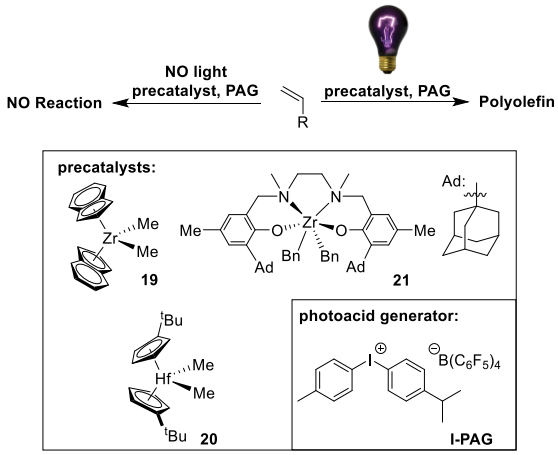

Figure 3.2 Polymerization of olefinic monomers using precatalysts **19-21** activated by an iodonium PAG (**I-PAG**) in the presence of UV light.

3.2.2 UV Activated Polymerization of 1-hexene

To establish optimal polymerization conditions for all precatalysts, 1-hexene was polymerized using precatalyst **19** with varying amounts of **I-PAG** activator and UV light exposure. My first study altered the equivalence of **I-PAG** (0.5-1.5) to precatalyst **3** while holding exposure time at a prolonged 30 minutes (Table 3.1, entries 1-3). Modulating the equivalence of **I-PAG** lead to 38-60% monomer conversion, consistent molecular weights (M_w = 17.0-25.3 kg/mol), and broad dispersity ($Đ$ = 1.57-2.23). Comparing the conversion decrease from entry 2 to entry 3, We hypothesize that adding excess **I-PAG** can generate excess protons and promote higher rates of chain-transfer and catalyst deactivation. The results of this study support the use of a catalyst-activator ratio of 1:1 for optimal conversion.

Table 3.1 Polymerization of 1-hexene using precatalyst 19 varying I-PAG equivalence and UV exposure time[a]

entry	activator	equivalence of activator	exposure time (min)[b]	% conv.	M_w[c] (kg/mol)	$Đ$[c]
1	**I-PAG**	0.5	30	38 ± 1.3	17.2	1.76
2	**I-PAG**	1.0	30	60 ± 1.6	25.0	2.23
3	**I-PAG**	1.5	30	50 ± 1.9	25.3	1.57
4	**I-PAG**	1.0	1	6 ± 1.7	18.6	1.53
5	**I-PAG**	1.0	5	48 ± 3.8	25.4	1.63
6	**I-PAG**	1.0	15	64 ± 2.3	19.7	2.60
7	**I-PAG**	1.0	30	60 ± 1.6	25.3	1.57
8	**AB**	1.0	0	61 ± 1.7	25.3	1.82
9[d]	**I-PAG**	1.0	15	0	---	---
10	**I-PAG**	1.0	0	0	---	---

[a]Polymerization conditions: Polymerization time = 3 h, precatalyst **19** = 10.0 μmol, 3 mL of 1-hexene, and 1 mL of DCM at 20 °C. [b]Irradiated using a handheld 4 W compact UV lamp operating at 254 nm. [c]Determined using triple detection GPC at 150 °C in 1,2,4-trichlorobenzene. [d]No precatalyst was added.

Following the equivalence study, we chose to change UV exposure time (1-30 minutes) to understand how this variable impacts my polymerizations (Table 3.1, entries 4-7). Increasing the light exposure time leads to a range of monomer conversion between 6-64%, consistent polymer molecular weights (M_w = 18.6-25.4 kg/mol), and broad polymer dispersity ($Đ$ = 1.53-2.60). At short exposure time, a small concentration of precatalyst is activated, leading to low monomer conversion. As exposure time increases, monomer conversion increases until maximum precatalyst activation is reached at 15 minutes of UV light exposure. Future polymerizations using **I-PAG** will include 15 minutes of UV light exposure for maximum precatalyst activation.

Optimizing the conditions for my light-activated olefin polymerizations, we conducted several control experiments to compare and support this unique activation method. First, we activate precatalyst **19** by using the traditional Brønsted acid activator, *N*,*N*-dimethylanilinium tetra(pentafluoro-phenyl)borate (**AB**), in replace of **I-PAG** (Table 3.1, entry 8). **AB** activates olefin polymerization precatalysts via protonolysis of bound alkyl substituents, and for the polymerization of 1-hexene was found to reach 61% monomer conversion. The polymer produced using **AB** as the activator is comparable in molecular weight (M_w = 25.3 kg/mol) and dispersity ($Đ$ = 1.82) to polymerizations using **I-PAG** (Table 3.1, entry 8). On the other hand, productivity of precatalyst **19** in combination with **I-PAG**/UV yielded slightly better conversions at 64% when precatalyst:activator equivalence and UV exposure is optimized. The next two control polymerizations were conducted to ensure that UV irradiation of my system and incorporation of **I-PAG** had no additional effect on my results (Table 3.1, entries 9-10).

First, **I-PAG** was irradiated under identical polymerization conditions, except that no olefin precatalyst was present. As expected, no poly(1-hexene) was produced (Table 3.1, entry 9). Second, to demonstrate that **I-PAG** cannot activate the precatalyst without UV light exposure, we selected precatalyst **19** as an example and combined it with **I-PAG** under identical polymerization conditions, and shielded the polymerization from any light exposure. Again, no polymer was formed (Table 3.1, entry 10). These control reactions, in conjunction with the successful polymerization results (Table 3.1, entries 1-8), allow us to safely conclude that a) precatalyst, **I-PAG**, and UV irradiation are each required for polymerization activity, and b) that **I-PAG** is indeed a competent olefin polymerization catalyst photoactivator that yields comparable results to precatalysts activated using traditional chemical reagents.

To further probe the activation process and test my hypothesis that protons resulting from UV irradiation of **I-PAG** results in precatalyst activation via protonolysis of the metal-alkyl substituents, we used proton NMR spectroscopy to monitor the protonolysis of Zr-bound methyl groups present in precatalyst **19** (Figure 3.3), which is known to occur during activation with Brønsted acidic activators such as **AB**.[181] We were able to track the Zr-CH_3 signal integration as it decreased linearly as a function of UV exposure time. We attribute this decrease to more and more protons being released into solution as **I-PAG** is irradiated and the Zr-CH_3 bonds are cleaved via protonolysis, thereby releasing methane and generating the olefin polymerization active cationic Zr center.

After optimizing and confirming the mechanism of our PAG activation method using precatalyst **19**, we expanded the precatalyst catalog applicable for this activation method

to test an alternative metallocene bearing a different active metal center (**20**) (Table 3.2, entries 1 & 3). Holding activator concentration at optimal conditions determined in Table 3.1, precatalyst **20** reached 17% monomer conversion, molecular weight of 4.1 kg/mol, and a dispersity of 2.77 upon activation with **AB** (Table 3.2, entry 1). When using **I-PAG** as the activator, precatalysts **20** polymerized 1-hexene to 43% monomer conversion, molecular weight of 1.6 kg/mol, and a dispersity 2.73 to their **AB** activated polymerizations (Table 3.2, entry 3). It is important to note that when comparing the activation performance of **AB** and **I-PAG** with precatalyst **19** and **20**, the polymerizations using **I-PAG** reached higher monomer conversions. I hypothesize that this behavior is due to the improved acidic nature of the protic acid produced from the photodecomposition of the iodonium salt than the protonated amine, leading to more active catalytic species, ultimately improving polymer yield.

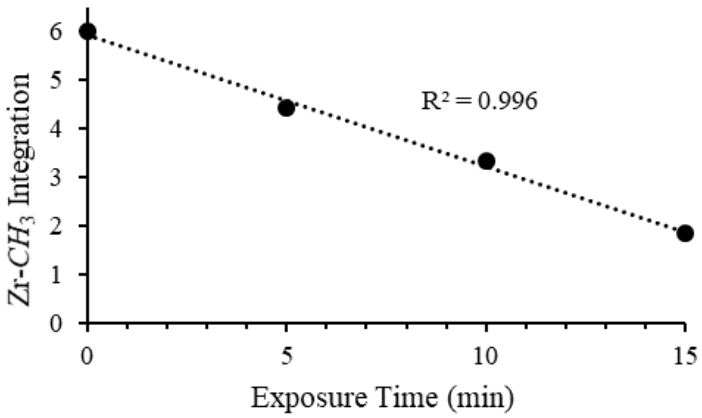

Figure 3.3 Monitoring the Zr-CH_3 peak integration of precatalyst 19 as a function of UV exposure time using ^{1}H NMR spectroscopy.

Table 3.2 Polymerization of 1-hexene using precatalysts 20 & 21 activated by AB or I-PAG[a]

entry	precatalyst	activator	exposure time (min)[b]	% conv.	M_w[c] (kg/mol)	$Đ$[c]
1	**20**	**AB**	0	17 ± 0.1	4.1	2.77
2	**21**	**AB**	0	41 ± 0.9	47.9	2.12
3	**20**	**I-PAG**	15	43 ± 3.1	1.6	2.73
4	**21**	**I-PAG**	5	28 ± 2.0	46.1	2.09

[a]Polymerization conditions: Polymerization time = 3 h, precatalyst = 10.0 μmol, activator = 10.0 μmol, 3 mL of 1-hexene, and 1 mL of DCM at 20 °C. [b]Irradiated using a handheld 4 W compact UV lamp operating at 254 nm. [c]Determined using triple detection GPC at 150 °C in 1,2,4-trichlorobenzene.

To develop the precatalyst library applicable to this photoinduced activation method, we selected a non-metallocene ONNO-type precatalyst (**21**) that is commonly activated via protonolysis for olefin polymerizations as reported by Kol and Busico.[182-185] Following optimal polymerization conditions previously established, precatalyst **21** lead to 41% monomer conversion, poly(1-hexene) molecular weight of 47.9 kg/mol, and dispersity of 2.12 when activated using **AB** (Table 3.2, entry 2). When using **I-PAG** as the activator I had to adjust the UV exposure time because initially irradiating precatalyst **21** for 15 minutes lead to low monomer conversion (10%). Following this result, we conducted several additional polymerizations altering UV exposure time to determine an optimal irradiation time of 5 minutes (Figure 3.4). We hypothesize that exposure times longer than 5 minutes lead to photoinduced catalyst deactivation/decomposition due to metallocene catalysts ability to absorb UV light, while exposure times shorter than 5 minutes limit the production of protons required to effectively activate precatalyst **21**. When using the

optimal exposure time of 5 minutes, precatalyst **21** reached 28% monomer conversion, poly(1-hexene) molecular weight of 46.1 kg/mol, and dispersity of 2.09 when activated using **I-PAG** (Table 3.2, entry 4). Future polymerizations of other olefins using precatalyst **21** will include a 5-minute exposure time for optimal results.

3.2.3 UV Activated Polymerization of Ethylene

Having successfully demonstrated the ability to activate a variety of olefin polymerization precatalysts for the polymerization of 1-hexene, we then chose to evaluate this methodology using the more industrially-relevant gaseous feedstock, ethylene. Therein, ethylene polymerizations were conducted using precatalysts **19-21** using the optimized conditions established above, as well as corresponding control experiments (Table 3.3).

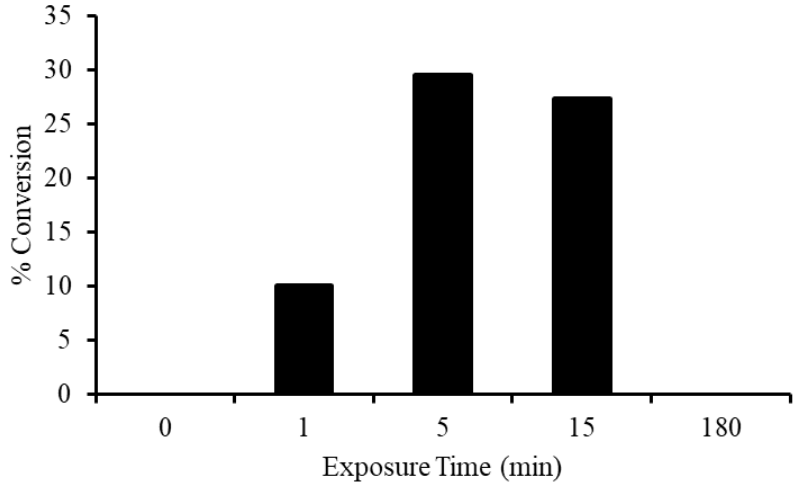

Figure 3.4 Polymerization of 1-hexene using precatalyst **21** and **I-PAG** varying UV exposure time.

Table 3.3 Polymerization of ethylene using precatalysts 19-21 activated by I-PAG and UV exposure[a]

entry	precatalyst	activator	exposure time (min)[b]	yield (mg)	M_w[c] (kg/mol)	$Đ$[c]
1	**19**	**AB**	0	120 ± 12.1	228.3	4.83
2	**20**	**AB**	0	87 ± 14.3	89.1	2.77
3	**21**	**AB**	0	46 ±8.5	44.3	3.03
4	**19**	**I-PAG**	0	0	---	---
5	**20**	**I-PAG**	0	0	---	---
6	**21**	**I-PAG**	0	0	---	---
7	**19**	**I-PAG**	15	335 ± 11.4	183.5	3.54
8	**20**	**I-PAG**	15	189 ± 10.2	74.7	2.23
9	**21**	**I-PAG**	5	17.9 ± 7.7	25.6	2.48

[a]Polymerization conditions: precatalyst = 10.0 μmol, activator = 10.0 μmol, ethylene = 15 psi, 1 mL of DCM, 19 mL of toluene, 20 °C, and polymerization time = 30 min. [b]Irradiated using a handheld 4 W compact UV lamp operating at 254 nm. [c]Determined using triple detection GPC at 150 °C in 1,2,4-trichlorobenzene. [d]Precatalyst and monomer were not exposed to UV light.

First, a baseline of polymerization activity for precatalysts **19-21** was established using the chemical activator **AB** (Table 3.3, entries 1-3), which produced between 46-120 mg of polyethylene depending upon the precatalyst used. The resultant polymer produced contained a broad range of molecular weights (M_w = 44.3-228.3 kg/mol) and broad dispersity ($Đ$ = 2.77-4.83). Additional control experiments were also performed in which **I-PAG** was introduced to the polymerization reactor, but without any UV irradiation to ensure that no unwanted "dark" polymerizations occur (Table 3.3, entries 4-6). As expected, no polyethylene was produced, once again confirming that both UV irradiation and **I-PAG** are required to generate the active catalyst form. Light activated ethylene polymerizations were conducted by irradiating reactions containing precatalysts **19-21** and **I-PAG** for 5 or 15 min (Table 3.3, entries 7-9). As expected, polyethylene was produced in comparable yields (17.9-335 mg) to those produced using the traditional chemical activator **AB**. The polyethylene produced displayed comparable properties such as, molecular weight (M_w = 25.6-183.5 kg/mol) and polymer dispersity ($Đ$ = 2.23-3.54) when compared to the polymers produced using activator **AB**.

3.2.4 Gas-phase, 3-D Printing of Polyolefins Using UV Light-activated Olefin Polymerizations

As stated before, we hypothesized that the ability to 3-D print polyolefins in the gas-phase, in a similar fashion to SLA and DLP printing, could be accomplished via light-activated olefin polymerization. Having demonstrated that UV light can be used as an external stimulus to provide temporal control over the activation of olefin polymerization precatalysts, we then turned our efforts to: 1) ascertain if polyolefin films could be grown

from a gas-phase monomer feed, and 2) could polyolefin film growth be spatially regulated via controlled UV light exposure (exposed vs. unexposed areas).

To determine if polyolefin films could be grown by a gas-phase, light-activated olefin polymerization process, ethylene was used as our monomer of choice. Therein, a solution of desired precatalyst (**19-21**) and **I-PAG** were prepared in DCM and shielded from ambient light. The precatalyst/**I-PAG** solution was then deposited onto a support substrate via either drop-casting or spray coating. The casting solvent quickly evaporated leaving a precatalyst-activator residue on the substrate surface, which was loaded into a quartz pressure reactor. The polymerization reactor was pressurized with ethylene gas (30 psi) and exposed to UV irradiation using the same handheld 4 W compact UV lamp (254 nm) as used for the previous solution state polymerizations above. When conducting gas-phase polymerizations, the precatalyst and activator concentration was increased 3-5 times compared to solution-phase polymerizations in order to produce enough polymer to use for GPC characterization. Table 3.4 contains the properties of the polyethylene films produced by precatalysts **19-21**. Precatalyst **19** and **20** produce high molecular weight polyethylene films (M_w = 0.7 - 3.8 x 10^6 g/mol) with broad dispersity ($Đ$ = 2.01-5.42) and routine film thickness of 15-30 μm. It is not uncommon for gas-phase polymerizations to reach high molecular weights compared to solution-phase due to the absence of a polymerization solvent that causes polymer to become insloluble, increasing the viscosity of the solution, ultimately limiting obtainable molecular weights.[186-187] On the other hand, precatalyst **21** was unable to produce a polyethylene film, and we hypothesize that this is due to the UV light instigating photoinduced deactivation/decomposition.

Table 3.4 Polymer film properties following gas-phase polymerizations with precatalysts 19-21 and I-PAG/UV light[a]

entry	precatalyst	M_w[b] (g/mol)	$Đ$[b]
1	**19**	3.8 x 10^6	2.01
2	**20**	0.7 x 10^6	5.42
3[c]	**21**	n/a	n/a

[a]Polymerization conditions: precatalyst = 50.0 μmol, **I-PAG** = 50.0 μmol, ethylene = 30 psi, 20 °C, irradiated using a handheld 4 W compact UV lamp operating at 254 nm for 15 min., and polymerization time = 30 min. [b]Determined using triple detection GPC at 150 °C in 1,2,4-trichlorobenzene. [c]Precatalyst prepped substrate was irradiated for 5 min.

Following the confirmation of polyethylene thin films on flat substrates, we successfully demonstrated the ability to grow conformal films over topology, such as is pictured in Figure 3.5 in which conformal polyethylene films were grown from the surface of a U.S. quarter. These films were lifted from the support substrate by submersing in non-solvent (methanol) to yield free-standing films that retained the topology and detail of the substrate.

After demonstrating the ability of polyolefin thin films to mimic surface topology, we needed to determine if polyolefin film formation could be spatially controlled using light-activated olefin polymerization. In addition to temporal control, spatial control is also a fundamental requirement in SLA and DLP printing processes. Spatial control allows polymer to only be printed in areas exposed to light, whereas no polymer is produced in unexposed regions.

Figure 3.5 Producing conformal polyethylene films using precatalyst **20** and light-activated olefin polymerization. The pictures shown are of a U.S. quarter a) after deposition and evaporation of the precatalyst **20**/**I-PAG** solution, b) after UV exposure, and c) after the film is lifted from the support via submerging in methanol.

For these experiments, the precatalyst **20**/**I-PAG** solution was deposited onto a glass slide and dried. A photomask, which allows a defined portion of the substrate to be irradiated while all other areas remain unexposed, was placed on top of the coated slide and then flooded with UV light. As can be seen in Figure 3.6, both negative-tone masks (top images) are transferred to the substrate only in the regions not covered by the photomask. The exposed regions turn from colorless to orange as the irradiated **I-PAG** activates precatalyst **20** and begins olefin polymerization (bottom images). Submerging these films in a nonsolvent (methanol) decomposes the remaining catalyst and the colorless, patterned polyethylene films can then be lifted from the substrate. In addition to establishing fundamental proof that light-activated olefin polymerization catalysts may provide both temporal and spatial control for future 3-D printing applications, we also explored if this methodology could be used to generate multi-layer structures.

Since precatalyst **19** has demonstrated superior polymerization activity, we used it for a study focused on maximizing the thickness of films.

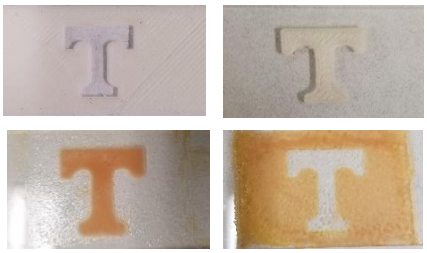

Figure 3.6 Images of the photomasks used (top images) and the resultant spatially controlled, patterned polyolefin films (bottom images). Note: the orange color results when precatalyst **20** is activated using **I-PAG** and UV exposure.

To determine if multi-layer structures could be produced, a polyethylene film was grown from a glass substrate as described above. After production of the first layer, a subsequent precatalyst **19**/**I-PAG** layer was deposited and a second polymer layer is grown upon exposure to UV light and ethylene gas. These films were measured using a micrometer, and in a specific example, the layer thicknesses were found to be 20 and 18 μm for the first and second layers, respectively (38 μm total thickness of both layers) (Figure 3.7). With the results presented, we have demonstrated that a PAG with light can be used to implement temporal and spatial control over the activation of olefin polymerization precatalysts to create thin polyolefin films. This type of control warrants an in-depth investigation in 3-D printing the world's cheapest plastic.

3.2.5 Visible Light Stimulated Olefin Polymerizations

While synthesizing polyethylene thin films using an iodonium salt and UV light to activate olefin polymerization precatalysts, we encountered several issues.

1 layer 2 layers

Figure 3.7 Image of a polyolefin monolayer (left) and bilayer (right) film grown on a glass substrate using precatalyst **19/I-PAG** and UV light.

First, the exposure time required to reach maximum precatalyst activation was 15 minutes, which is a lengthy period of time. In order for this photoinduced activation method to become a practical tool to achieve 3-D printed polyolefin materials, exposure times need to be vastly improved. Second, the UV light source, used to generate the activating species, interfered with the ONNO-type catalyst activity and longevity. A plethora of metallocene and non-metallocene precatalysts absorb UV light, so observations that this region can be detrimental to catalyst lifetime reduces the applicable precatalyst library. Lastly, the fragile quartz pressure vessels required low-pressure gas-phase polymerizations, ultimately leading to thin, delicate patterned and conformal olefin films that were difficult to handle and isolate. An attractive quality in 3-D printing is the ability to produce large-scale robust materials, which would be difficult using low-pressured polymerizations. The utility of a short wavelength light source with an onium salt to release protic acid has provided similar problems for other polymerization mechanisms (e.g. cationic polymerizations).[188-190] Introduction of a photosensitizer has become a prominent method used to shift the short wavelength absorbance of iodonium salts to a longer wavelength range for a more efficient photoinduced process.[191-192]

Heterocyclic compounds, polycyclic hydrocarbons, and organic dyes are common photosensitizers used to induce photolysis of onium salts.[188, 191, 193-195] These complexes absorb light, creating an excited species, that undergoes a photoinduced electron transfer (PET) to reduce the onium salt, generating an unstable cationic radical complex that can further react and produce protic acid.[196] When selecting the photosensitizer-PAG pair, it is important that the energetics are thermodynamically feasible.[191-192, 197-198] As an electron is excited to the LUMO of the photosensitizer, it must be able to relax to the LUMO of the PAG in order to generate the reactive cationic radical species. Kohl and coworkers recently studied several polynuclear aromatic hydrocarbons and their photosensitization compatibility with **I-PAG**.[196]

From this study, we selected to use 5,12-bis(phenylethynyl)tetracene (**BPET**) as the photosensitizer for my photoinduced system because its high molar extinction coefficient in the visible region, lack of heteroatoms, and favorable thermodynamics of the PET in comparison to other photosensitizers studied. Incorporation of this photosensitizer with **I-PAG** will allow me to use a visible light source to photoinduce precatalyst activation for olefin polymerizations (Figure 3.8). The light source selected for the following polymerizations is a 3 W green LED.

3.2.6 Visible Light Activated Polymerization of 1-hexene

Incorporating **BPET** with precatalyst and PAG will require proper optimization to better understand its role in the polymerization. Based on the optimization studies previously completed in section 3.2.1, the ratio of **I-PAG**:precatalyst will be held constant at 1:1.

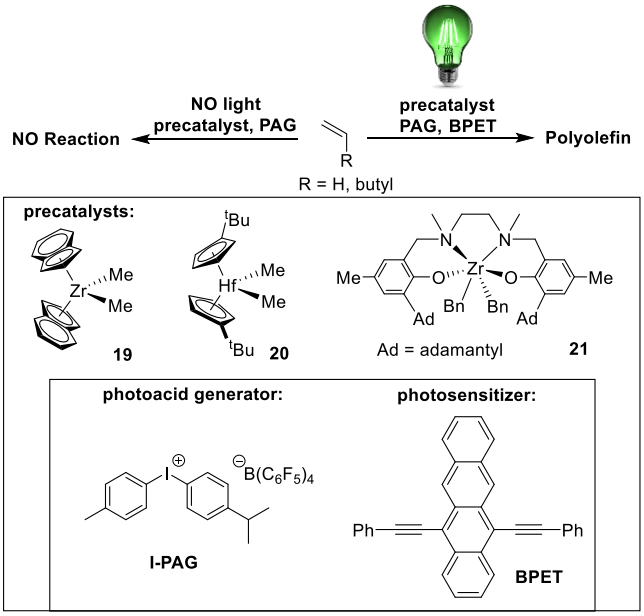

Figure 3.8 Polymerization of olefinic monomers by precatalysts **19-21** using a photosensitizer (**BPET**) with a PAG (**I-PAG**) and green light to induce photochemical activation.

The first experiment conducted with **BPET** includes varying its equivalence (0.01-1.0 equiv.) to precatalyst and PAG, while holding exposure time at a prolonged 30 minutes for the polymerization of 1-hexene (Table 3.5, entries 1-4).Altering the equivalence of **BPET** to precatalyst and PAG lead to 70-93% monomer conversion, consistent molecular weights (M_w = 19.4-26.2 kg/mol), and broad dispersity ($Đ$ = 1.54-2.65). Introducing a photosensitizer into the polymerization has improved the monomer conversion by >30%. In addition, polymer production was optimal using substoichiometric amounts of **BPET**. Even a photosensitizer equivalence of 0.1 lead to the conversion of 10% more monomer then compared to polymerizations using **I-PAG** and UV light.

Table 3.5 Polymerization of 1-hexene using precatalyst 19 varying photosensitizer equivalence and LED exposure time[a]

entry	photosensitizer	equivalence of photosensitizer	exposure time (min)[b]	% conversion	M_w[c] (kg/mol)	$Đ$[c]
1	**BPET**	0.01	30	trace	---	---
2	**BPET**	0.1	30	70 ± 3.8	26.2	2.65
3	**BPET**	0.5	30	93 ± 1.1	19.4	1.85
4	**BPET**	1.0	30	90 ± 0.9	24.7	1.54
5	**BPET**	0.5	1	69 ± 2.8	26.4	2.63
6	**BPET**	0.5	5	90 ± 1.9	26.5	1.51
7	**BPET**	0.5	15	91 ± 0.8	25.4	1.31
8	**BPET**	0.5	30	93 ± 1.1	19.4	1.85
9[d]	none	n/a	0	61 ± 1.7	25.3	1.82
10[e]	**BPET**	0.5	5	0	---	---
11[f]	**BPET**	0.5	5	0	---	---
12[g]	none	n/a	5	0	---	---
13	**BPET**	0.5	0	0	---	---

[a]Polymerization conditions: Polymerization time = 3 h, precatalyst **19** = 10.0 μmol, activator **I-PAG** = 10.0 μmol, 3 mL of 1-hexene, and 1 mL of DCM at 20 °C. [b]Irradiated using a handheld 3 W green LED operating at 565 nm. [c]Determined using triple detection GPC at 150 °C in 1,2,4-trichlorobenzene. [d]Activator *N*,*N*-dimethylanilinium tetra(pentafluorophenyl)borate = 10.0 μmol. [e]No precatalyst was added. [f]No **I-PAG** was added. [g]No **BPET** was added.

Previous reports support this observation and discuss the improved photolysis of onium salts when photosensitizers are present.[199] The addition of **BPET** permits the absorbance of longer wavelengths compared to onium salts which absorb broad band UV light. This absorbance at longer wavelengths captures a higher fraction of the emitted light, ultimately leading to a higher concentration of initiating species present to activate more precatalyst and polymerize more monomer.[188] Due to the results from the equivalence study, we have determined the optimal ratio of photosensitizer:PAG:precatalyst for future polymerizations will be 0.5:1.0:1.0.

As previously discussed, using **I-PAG** and UV light to activate olefin precatalysts required an extensive exposure time of 15 minutes. Since the photosensitization of onium salts is an efficient electron transfer process, we expect that the irradiation time required to reach maximum active catalyst concentration will occur in a reduced time period. To test this hypothesis, we conducted several polymerizations varying exposure time (1-30 minutes) while holding all other variables constant (Table 3.5, entries 5-8). Increasing the light exposure time leads to efficient monomer conversion between 69-93%, consistent poly(1-hexene) molecular weight (M_w = 19.4-26.5 kg/mol), and broad dispersity ($Đ$ = 1.31-2.63). Figure 3.9 compares the drastic change in catalyst activity with the addition of a photosensitizer versus the original PAG system. Higher monomer conversions were achieved using an exposure time of 1 minute of green LED light versus 15 minutes of UV light in the previous study. This observation supports my hypothesis that photosensitized onium salts lead to a more efficient production of protic acid. Since maximum monomer conversion was reached after only 5 minutes of LED irradiation, future polymerizations

using **BPET** will use 5 minutes of green light exposure.

To further confirm that the photosensitizer is responsible for these active polymerizations, we conducted several control experiments to compare and support this unique activation method. As previously disclosed, precatalyst **19** activated using the traditional Brønsted acid activator, *N*,*N*-dimethylanilinium tetra(pentafluoro-phenyl)borate (**AB**), in replace of a photoacid generator was found to reach 61% monomer conversion (Table 3.5, entry 8). The polymer produced was comparable in molecular weight (M_w = 25.3) and dispersity ($Đ$ = 1.82) to polymerizations using **BPET**+**I-PAG**. It is important to note that incorporating equivalence of **BPET** as low as 0.1, or limiting the exposure time to 1 minute, produced more poly(1-hexene) than traditional activation methods using **AB**. The next two control polymerizations were conducted to ensure that production of a Brønsted acid in the absence of precatalyst (Table 3.5, entry 9), and **BPET**'s excited state in the absence of **I-PAG** (Table 3.5, entry 10), could not lead to the polymerization of 1-hexene. The following control polymerizations confirm that **I-PAG** cannot produce acid in the presence of green light, and that **BPET** and **I-PAG** cannot undergo PET without green light (Table 3.5, entries 10-11). These control reactions, in conjunction with the successful polymerization results, allow us to safely conclude that a) precatalyst, **I-PAG**, **BPET**, and a green light source are each required for polymerization activity, and b) that the photosensitization of **I-PAG** is indeed a superior photoactivation method for precatalyst **19** versus **I-PAG**/UV light or **AB**.

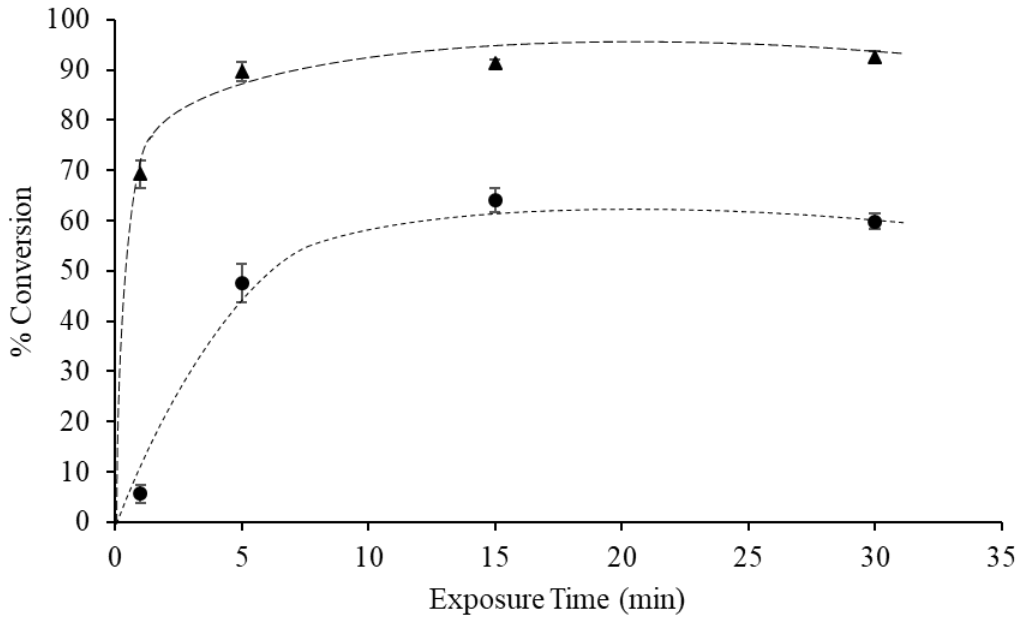

Figure 3.9 Plot of monomer conversion as a function of exposure time using precatalyst **19** and **I-PAG**/UV (●) or **BPET**+**I-PAG**/LED (▲) photoinduced activation methods for 1-hexene polymerizations.

After manipulating the conditions of this elegant photoactivation method as they pertain to a zirconium metallocene olefin polymerization catalyst, we began to confirm the utility of this activation process to other precatalyst designs. Precatalyst **20** remains in the metallocene family, but with an alternative metal-center, hafnium. Polymerizing 1-hexene with precatalyst **20** after photoinduced activation lead to 54% monomer conversion, low molecular weight (M_w = 5.0 kg/mol), and broad dispersity ($Đ$ = 2.80) (Table 3.6, entry 3). This activation method yields comparable polymer characteristics to traditional activation methods, while improving the monomer conversion by 37% (Table 3.6, entry 1). Expanding outside of the metallocene group, ONNO-type metallocene's are common

precatalysts well studied and activated by Brønsted acids. Testing the success of this effective activation method to precatalyst **21** resulted in 51% monomer conversion, moderate molecular weight (M_w = 47.9 kg/mol), and broad dispersity ($Đ$ = 2.18) (Table 3.6, entry 4). This polymerization result was an important data point in supporting previous shortcomings encountered with the **I-PAG** /UV system.

Activating precatalyst **21** with UV light and **I-PAG** lead to photoinduced catalyst deactivation/decomposition from the short wavelength light source. We hypothesized that utilization of a photosensitizer will eliminate this problem and lead to improved catalyst activity due to the longer wavelength required to induce protic acid production. Incorporating **BPET** and shifting the irradiation wavelength to the visible region lead to a 182% increase in monomer conversion (28%→51%).

Table 3.6 Polymerization of 1-hexene using precatalysts 20 & 21 activated by AB or BPET+I-PAG[a]

entry	precatalyst	photosensitizer	exposure time (min)[b]	% conv.	M_w[c] (kg/mol)	$Đ$[c]
1[d]	**20**	none	0	17 ± 0.1	4.1	2.77
2[d]	**21**	none	0	41 ± 0.9	47.9	2.12
3	**20**	**BPET**	5	54 ± 4.8	5.0	2.80
4	**21**	**BPET**	5	51 ± 3.9	47.9	2.18

[a]Polymerization conditions: Polymerization time = 3 h, precatalyst = 10.0 μmol, activator **I-PAG** = 10.0 μmol, 3 mL of 1-hexene, and 1 mL of DCM at 20 °C. [b]Irradiated using a handheld 4 W compact UV lamp operating at 254 nm. [c]Determined using triple detection GPC at 150 °C in 1,2,4-trichlorobenzene. [d]Activator *N*,*N*-dimethylanilinium tetra(pentafluorophenyl)borate = 10.0 μmol.

In addition, this photochemical activation method improved the monomer conversion by 10% compared to activator **AB**, while producing polymer with similar characteristics (M_w = 47.9 kg/mol, $Đ$ = 2.18) (Table 3.6, entry 4). This result supports the hypothesis that using a different irradiation wavelength minimizes photochemical deactivation/decomposition. Also, when comparing the efficiency of the photoactivation methods, **BPET**+**I-PAG** vs. **I-PAG** vs. **AB**, the photosensitized activation process yielded the highest monomer conversion for all three precatalysts.

3.2.7 Visible Light Activated Polymerization of Ethylene

After demonstrating the use of this photoinduced activation method for several olefin polymerization precatalysts bearing different ligand scaffolds and metal centers, I expanded the monomer library by testing a more industrially-relevant olefin feedstock, ethylene. Ethylene polymerizations were conducted using precatalysts **19-21** and optimal conditions established with 1-hexene. Photosensitized light-activated ethylene polymerizations were conducted by irradiating reactions containing precatalysts **19-21**, **BPET**, and **I-PAG** for 5 minutes (Table 3.7, entries 4-6). As expected, polyethylene was produced (46-512 mg) in comparable yields to those produced using traditional activator **AB**. The polyethylene produced displayed comparable properties such as, molecular weight (M_w = 44.0-544.7 kg/mol) and polymer dispersity ($Đ$ = 1.83-3.53) when compared to the polymers produced using **AB**.

Further analyzing the polymerization results, precatalyst **19** produced 426% and 153% more polyethylene than **AB** and **I-PAG**/UV activation methods. Precatalyst **20** produced less polyethylene than its zirconium counterpart, but the PET process improved

the production of polyethylene compared to **AB** and **I-PAG** activators. In the distinct case of precatalyst **21**, the photoinduced activation with **I-PAG** produced 37% less polymer than **AB** activated polymerizations. Incorporating the photosensitizer with precatalyst **21** and **I-PAG** restores the polymer produced back to yields obtained with **AB**. While we were still surprised the polyethylene yields are low, previous reports by Busico and coworkers disclosed that ONNO-type zirconium catalysts have shortened lifetimes and are subject to high chain-transfer rates for ethylene polymerizations, which could help explain these polymerization results.[185] Overall, the improved catalytic performance instigated by the addition of a photosensitizer for precatalysts **19-21** in solution-phase olefin and α-olefin polymerizations will become valuable when testing the gas-phase polymerization capabilities with this photoinduced activation method.

Table 3.7 Polymerization of ethylene using precatalysts 19-21 activated by I-PAG, BPET, and visible light exposure[a]

entry	precatalyst	activator	exposure time (min)[b]	yield (mg)	M_w[c] (kg/mol)	$Đ$[c]
1	**19**	**AB**	0	120 ± 12.1	228.3	4.83
2	**20**	**AB**	0	87 ± 14.3	89.1	2.77
3	**21**	**AB**	0	46 ± 8.5	44.3	3.03
4	**19**	**BPET**	5	512 ± 30.0	544.7	3.50
5	**20**	**BPET**	5	194 ± 8.7	96.5	1.83
6	**21**	**BPET**	5	46 ± 9.3	44.0	2.72

[a]Polymerization conditions: precatalyst = 10.0 μmol, **I-PAG** = 10.0 μmol, ethylene = 15 psi, 1 mL of DCM, 19 mL of toluene, 20 °C, and polymerization time = 30 min. [b]Irradiated using a 3 W green LED lightbulb operating at 565 nm. [c]Determined using triple detection GPC at 150 °C in 1,2,4-trichlorobenzene.

3.2.8 Gas-phase, 3-D Printing of Polyolefins Using Visible Light Activated Olefin Polymerizations

Having demonstrated that UV light can indeed be used as an external stimulus to provide temporal control over the activation olefin polymerization precatalysts, we then turned our efforts to studying the ability to harness spatial control for gas-phase olefin polymerizations using visible light induced activation method. Similar to the procedure described above in section 3.2.4, a solution of desired precatalyst (**19-21**), **I-PAG**, and **BPET** were prepared in DCM and shielded from ambient light. The precatalyst/**I-PAG/BPET** solution was then deposited onto a support substrate via either drop-casting or spray coating. The casting solvent quickly evaporated leaving a precatalyst-activator residue on the substrate surface, which was loaded into a borosilicate pressure reactor. An added advantage to shifting the absorbance wavelength into the visible region is eliminating the innate pressure restrictions that come with using quartz materials. These borosilicate vessels safely permit pressures up to 100 psi without influencing transmittance of our green light source. Unlocking this ability to access high monomer pressures will be invaluable when optimizing these gas-phase polymerizations to produce durable 3-D polyolefin materials.

In order to understand how monomer pressure will influence film formation, we conducted an experiment monitoring film thickness as a function of ethylene pressure (Figure 3.10). At constant precatalyst **19** (30 μmol), **I-PAG** (30 μmol), and **BPET** (15 μmol) loading, film thickness increases with increasing pressure. These films were prepared using the drop-cast method, which allows for maximum reagent loading.

At 30 psi of ethylene, a film of 11 µm was obtained. As we increased monomer pressure to 60 and 90 psi, we were able to obtain films as thick as 70 µm, which will be easier to handle and isolate compared to the 15-30 films produced using **I-PAG** and UV light. Future gas-phase polymerizations will be conducted at 90 psi for maximum film thickness.

Following this study, each precatalyst was loaded onto a glass slide with the required activating reagents, to produce a polyethylene film to be analyzed via GPC (Table 3.8). Precatlysts **19**-**21** generated high molecular weight polymer (M_w = 158.9-1.6 x 10^4 kg/mol) with broad dispersity ($Đ$ = 1.58-5.59) (Table 3.8, entries 1-3). For the gas-phase ethylene polymerization using precatalyst **21**, we were able to synthesize a high molecular weight thin film due to the longer wavelength light source.

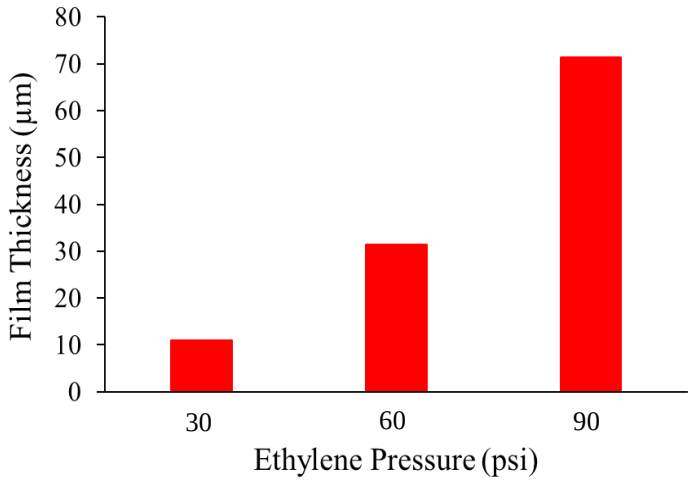

Figure 3.10 Polyethylene film thickness measurements as a function of olefin feedstock pressure.

Table 3.8 Polymer film properties following gas-phase polymerizations with precatalysts 19-21, BPET, and I-PAG/UV light[a]

entry	precatalyst	M_w[b] (kg/mol)	$Đ$[b]
1[c]	**19**	931.1	1.58
2	**20**	1.638×10^4	5.28
3	**21**	158.9	5.59

[a]Polymerization conditions: precatalyst = 50.0 μmol, **I-PAG** = 50.0 μmol, **BPET** = 25.0 μmol, ethylene = 90 psi, 20 °C, irradiated using a 3W green LED lightbulb operating at 565 nm for 5 min, and polymerization time = 30 min. [b]Determined using triple detection GPC at 150 °C in 1,2,4-trichlorobenzene. [c]Precatalyst = 30.0 μmol, **I-PAG** = 30.0 μmol, and **BPET** = 15 μmol.

After using GPC to analyze the polymer produced, we conducted experiments testing the spatial control of this photosensitized photoinduced activation method. Using the same negative-tone masks as before, precatalyst **19**, **BPET**, and **I-PAG** were dissolved in an organic solvent and drop-casted on a glass slide (Figure 3.11). Following proper placement of the mask, the slide was placed in a Fisher Porter pressure tested vessel and green LED light was used to initiate polymerization at exposed areas. Due to the addition of **BPET**, the precatalyst-activator residue is a dark purple, but after exposure the active catalyst deposit turns black. This color change is consistent with observations reported by Kohl and coworkers using this photosensitizer with an iodonium salt and is suspected to be due to the extension of conjugation between BPET biproducts.[188, 196]

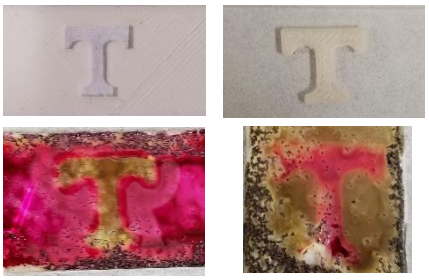

Figure 3.11 Photographs of the photomasks used (top images) and the resultant spatially controlled, patterned polyolefin films (bottom images). Note: the black color results when precatalyst **19** is activated using **BPET**, **I-PAG** and green light exposure, while the purple color represents inactivated precatalyst.

Following the polymerization, the films were submerged in methanol to decompose the remaining catalyst, and then soaked in chloroform to remove photosensitizer biproducts, resulting in a colorless, patterned polyethylene film.

3.3 Conclusions

In summary, we have demonstrated that light activated olefin polymerization may be accomplished via the combination of alkyl substituted olefin polymerization precatalysts, a photoacid generator (**I-PAG**), and exposure to light. This methodology provides temporal control over the precatalyst activation process and was used for the solution state polymerization of the olefinic monomers, 1-hexene and ethylene. Detailed ^{1}H NMR analysis was used to confirm that UV exposure triggers the incorporated photoacid generator to release protic acid, which activates olefin polymerization precatalysts **19-21** via protonolysis, yielding the required cationic, active metal site. In

addition, we have confirmed that the addition of a photosensitizer (**BPET**), in conjunction with **I-PAG,** can be used to instigate Brønsted acid production via green LED light exposure.The polymerization results with this visible light activation method generally lead to improved monomer conversion or polymer yield regardless of precatalyst or monomer source.

Drawing inspiration from current SLA and DLP 3-D printing techniques, these UV and visible light-activated olefin polymerization methods were then used to produce conformal, as well as spatially patterned polyolefin films from a gas-phase printing process. This finding confirms the ability to spatially regulate polyolefin growth and brings this methodology closer to a potential next-generation 3-D printing process. It is our desire that these fundamental results will stimulate the ability to use light-based 3-D printing techniques to print the world's most widely used and produced polymers, polyolefins, and that this light-activated olefin polymerization process brings us one step closer to that reality.

3.4 Experimental

3.4.1 General Methods and Materials

All reactions were performed under an inert nitrogen atmosphere using an MBraun UniLab glovebox or using standard Schlenk techniques, unless otherwise noted. All solvents were dried using an Innovative Technologies PureSolv Solvent Purification System and degassed via three freeze-pump-thaw cycles. Precatalyst **19** and **20** were purchased from Strem Chemicals Inc. and used as received. Photoreductant **I-PAG** was

purchased from TCI and used as received. Precatalyst **21** and **BPET** was prepared according to literature procedures.[185, 196] All other reagents were purchased from commercial vendors and used without further purification. Gel permeation chromatography (GPC) was performed at 150 °C in 1,2,4-trichlorobenzene at a flow rate of 1.0 mL/min on a Malvern Viscotek HT-GPC equipped with triple detection.

3.4.2 General 1-hexene Polymerization Conditions

Under an inert atmosphere and shielded from ambient light, a quartz flask was charged with precatalyst **19**, **20**, or **21** (10 μmol), photoacid generator **I-PAG** (10 μmol), 1-hexene (3 mL), dichloromethane (1 mL), and a magnetic stir bar. To initiate the polymerization, the reaction flask was irradiated using a handheld 4 W compact UV lamp operating at 254 nm for a pre-determined time. Following irradiation, the reaction was stirred continuously until the total desired reaction time was reached. All polymerizations were quenched, and polymer precipitated, by the addition of MeOH (10 mL). The polymer was collected and dried to constant weight in vacuo.

3.4.3 General Ethylene Polymerization Conditions

Under an inert atmosphere and shielded from ambient light, a solution of precatalyst **19**, **20**, or **21** (10 μmol), photoacid generator **I-PAG** (10 μmol), toluene (19 mL), dichloromethane (1 mL) and a magnetic stir bar were added to a quartz pressure tube reactor and sealed. The vessel was removed from the glove box, pressurized with ethylene gas (15 psi) while stirring, and equilibrated for 10 min prior to photoinitiation. The vessel was irradiated using a handheld 4 W compact UV lamp operating at 254 nm. After 15 min

of exposure time, the polymerizations were quenched after an additional 15 minutes via the addition of MeOH (10 mL) and the polymer was precipitated using excess acidic MeOH (5% HCl in MeOH). The polymer was stirred in the acidic methanol for 24 hours then filtered, washed with excess methanol, and dried to constant weight in vacuo.

3.4.4 General Photosensitized 1-hexene Polymerization Conditions

Under an inert atmosphere and shielded from ambient light, a quartz flask was charged with precatalyst **19**, **20**, or **21** (10 μmol), photoacid generator **I-PAG** (10 μmol), photosensitizer **BPET** (5 μmol), 1-hexene (3 mL), dichloromethane (1 mL), and a magnetic stir bar. To initiate the polymerization, the reaction flask was irradiated using a 3 W green LED lightbulb operating at 565 nm for a pre-determined time. Following irradiation, the reaction was stirred continuously until the total desired reaction time was reached. All polymerizations were quenched, and polymer precipitated, by the addition of MeOH (10 mL). The polymer was collected and dried to constant weight in vacuo.

3.4.5 General Photosensitized Ethylene Polymerization Conditions

Under an inert atmosphere and shielded from ambient light, a solution of precatalyst **19**, **20**, or **21** (10 μmol), photoacid generator **I-PAG** (10 μmol), photosensitizer **BPET** (5 μmol), toluene (19 mL), dichloromethane (1 mL) and a magnetic stir bar were added to a quartz pressure tube reactor and sealed. The vessel was removed from the glove box, pressurized with ethylene gas (15 psi) while stirring, and equilibrated for 10 min prior to photoinitiation. The vessel was irradiated using a 3 W green LED lightbulb operating at 565 nm. After 5 min of total exposure time, the polymerizations were quenched after 25

minutes of additional polymerization time via the addition of MeOH (10 mL) and the polymer was precipitated using excess acidic MeOH (5% HCl in MeOH). The polymer was stirred in the acidic methanol for 24 hours then filtered, washed with excess methanol, and dried to constant weight in vacuo.

3.4.6 General Method of Polyolefin Film Growth in the Gas-phase (Both Conformal and Patterned)

Conformal Films

Under an inert atmosphere and shielded from ambient light, a solution of precatalyst **20** (20 μmol), photoacid generator **I-PAG** (20 μmol), and dichloromethane (1 mL) was prepared. This solution was drop-cast onto a quarter. After solvent evaporation, the coated substrate was loaded into a quartz pressure tube reactor and sealed. The vessel was removed from the glove box, pressurized with either ethylene gas (30 psi), and equilibrated for 10 min prior to photoinitiation. The substrate was then irradiated using a handheld 4 W compact UV lamp operating at 254 nm for 15 minutes to initiate polymerization. After an additional 15 minutes (Total polymerization time = 30 minutes), the reaction was exposed to air and the reaction quenched using excess MeOH. The resultant films were collected and dried to constant weight in vacuo.

Patterned Films

Under an inert atmosphere and shielded from ambient light, a solution of precatalyst **19** or **20** (50 μmol), photoacid generator **I-PAG** (50 μmol), and dichloromethane (5 mL) was prepared. This solution was drop-cast or spray-coated onto a glass substrate. After solvent evaporation, the coated substrate was loaded into a quartz pressure tube reactor and

sealed. A photomask was also placed on top of the coated substrate after loading into the reactor. The vessel was removed from the glove box, pressurized with ethylene gas (30 psi), and equilibrated for 10 min prior to photoinitiation. The substrate was then irradiated using a handheld 4 W compact UV lamp operating at 254 nm for 15 minutes to initiate polymerization. After a total polymerization time of 30 minutes, the reaction was exposed to air and the reaction quenched using excess MeOH. The resultant films were collected and dried to constant weight in vacuo.

3.4.7 General Method of Photosensitized Polyolefin Film Growth in the Gas-phase

Under an inert atmosphere and shielded from ambient light, a solution of precatalyst **19** or **20** (50 μmol), photoacid generator **I-PAG** (50 μmol), photosensitizer **BPET** (25 μmol), and dichloromethane (5 mL) was prepared. This solution was drop-cast or spray-coated onto a glass substrate. After solvent evaporation, the coated substrate was loaded into a quartz pressure tube reactor and sealed. A photomask was also placed on top of the coated substrate after loading into the reactor. The vessel was removed from the glove box, pressurized with ethylene gas (90 psi), and equilibrated for 10 min prior to photoinitiation. The substrate was then irradiated using a 3 W green LED lightbulb operating at 565 nm for 5 minutes to initiate polymerization. After a total polymerization time of 30 minutes, the reaction was exposed to air and the reaction quenched using excess MeOH. The resultant films were collected and dried to constant weight in vacuo.

CHAPTER 4 – CONCLUSIONS AND OUTLOOK

The synthesis of polyolefins typically includes a transition-metal based catalyst that undergoes three complex steps: activation, propagation, and termination. In this work, we studied how external stimuli, such as redox reagents and light, can manipulate the activation and propagation events during the production of polyolefins, the world's cheapest and most versatile commodity plastics. The first portion of this dissertation (Chapters 1 & 2) described how visible light can be used to influence the coordination-insertion mechanism of a redox-active *α*-diimine nickel olefin polymerization catalyst (**14**). Previous reports from our research group, as well as others, have established that ligand electronics can be manipulated *in situ* using chemical oxidants and reductants. To further expand this capability, we used photoreductant **18** to reduce the α-diimine precatalyst **14** *in situ* upon irradiation using a blue LED light source. The native redox-active catalyst **14** underwent more chain-walking events, rather than coordination-insertion, in order to produce branched polyethylene with 113 branches per 1000 carbons. When photoreductant **18** is added to the reaction mixture and irradiated with visible light, the reduced catalytically active species generated polymer with a less branched polyethylene microstructure, having 93 branches per 1000 carbons. We hypothesize that this decrease in branching content was a result of the electron-rich catalyst favoring a coordination-insertion mechanism in competition with chain-walking. ^{13}C NMR analysis supported this hypothesis and showed that branch-on-branch formation, a characteristic of polymers produced with a catalyst that readily undergoes chain-walking, was nearly eliminated with the reduced catalytic species. Finally, we demonstrated that exposure time could be manipulated to generate polymers with varying branching content, albeit from a single

precatalyst. This concept avoids the long-standing "one catalyst, one polymer" mindset and provides the first example in which light is used as an external stimulus to control polyethylene microstructure.

The second portion of this dissertation (Chapter 3) described how we have developed the ability to use UV and visible light to instigate precatalyst activation and demonstrated its potential to access 3-D printed polyolefins. Polyolefins have been 3-D printed using Fused Deposition Modeling techniques, but they are not compatible with light driven printing processes. Considering the surge of interest and research into light-based 3-D printing processes for biomedical and manufacturing purposes, polyolefins remain an untapped polymer resource that could provide cost-effective and versatile 3-D printed materials. Currently, light-based 3-D printing techniques such as stereolithography (SLA) and dynamic light printing (DLP), are precise processes demonstrating spatial and temporal control to generate well-defined complex structures, but they are restricted by the catalog of printable monomers. we have demonstrated proof-of-principle evidence that we may expand this restricted monomer pool by using light-activated olefin polymerization precatalysts. Specifically, by using both metallocene and non-metallocene group 4 catalysts (**19**-**21**), an iodonium salt (**I-PAG**), and the presence of UV light, we demonstrated temporal control over the activation of precatalysts for solution-phase polymerizations of 1-hexene and ethylene. Precatalyst **19** and precatalyst **20** produced more polymer when activated with UV light and **I-PAG** compared to using the traditional Brønsted acidic activator, **AB**. Non-metallocene precatalyst **21** required shorter irradiation times (5 minutes) in order to maximize monomer conversion, and even then, the

photoactivation of this precatalyst was not as effective as using the activator, **AB**. We hypothesize that this is due to photoinduced catalyst deactivation/decomposition upon extended light exposure. Following demonstration of temporal control, gas-phase polymerizations were used to validate spatial control. Using a quartz pressure reactor, we were able to grow layered polyethylene films and use negative tone masks to selectively grow polymer in irradiated areas. While this was a successful first attempt at 3-D printing polyolefins, the activation process was not efficient requiring 15 minutes of UV light and the light source proved detrimental for precatalyst **21**.

In order to enhance the photoactivation of these olefin polymerization precatalysts, as well as red-shift the wavelength required to produce protic acid, we selected the photosensitizer, **BPET**, to facilitate a photoinduced electron transfer (PET) to instigate acid production that is activated with visible light. The addition of this photosensitizer in combination with **I-PAG** and precatalyst lead to improved polymerization yields for both 1-hexene and ethylene polymerizations for all three precatalysts. Since the activating wavelength shifted to the visible region, the activity of precatalyst **21** escalated leading to competitive polymer production. In addition, the implementation of a visible light source permitted the use of pressure-tested borosilicate glass vessels to synthesize polyethylene thin films via gas-phase olefin polymerizations. The ability to use pressure-tested vessels allowed us to conduct polymerizations at high monomer pressures, which allowed thicker films to be produced. Similar to the UV printed films, these polymerizations displayed temporal and spatial control, only producing polymer upon irradiation and where irradiated. These results demonstrate the first instance where olefin polymerization

catalysts are activated via light stimulus, in turn providing temporal and spatial control over the synthesis of polyolefins. This advanced methodology has the potential to be a valuable addition to the breadth of 3-D printed materials, and may also result in the generation of a new gas-phase 3-D printing technique.

The future of this light-activated gas-phase olefin polymerization project will first focus on conducting additional experiments to support the increase in polymer produced from using the different activation techniques (**AB**, **I-PAG**/UV light, **BPET**/**I-PAG**/visible light). We hypothesize that the protic acid produced by the PAG is more effective at activating many olefin polymerization precatalysts than traditional anilinium perfluoroborate species. Additionally, there is a literature presence that believes photosensitized PAG systems lead to more efficient activating species,[191-192] which is consistent with what we observed. To confirm an increase in activating species for photosensitized PAG systems, there are several applicable NMR techniques that can be used to quantify the number of active catalyst sites present following activation events.[200] An easy experiment that can be conducted to determine the relative concentration of active metallocene species includes quenching a polymerization with bromine, which halogenates the propagating chain ends and active catalyst species.[201] This distinct end-group will cause a chemical shift for respective peaks within the NMR spectrum and with the help of an internal standard, integrations can be used to calculate the concentration of active catalyst present. We hypothesize that **AB** will generate the lowest concentration of activated metallocenes, while **BPET**/**I-PAG**/visible light activated polymerizations will have the

highest. Overall, this study would provide important insight into the effectiveness of these photoinduced activation methods.

Another aspect of this photoinduced activation method requiring further investigation is the mechanism of PET between **BPET** and **I-PAG**, ultimately identifying the species that leads to the targeted Brønsted acid. Literature provides contradicting mechanisms that hypothesize either a cationic photosensitizer species or cationic PAG species is responsible for proton generation.[192, 196, 202] In the photosensitized PAG activation method described in Chapter 3, we were able to use catalytic amounts of **BPET** with respect to **I-PAG** and precatalyst. This leads us to speculate that the cationic **I-PAG** species is responsible for producing a majority of the essential protic acid. In addition, it poses an interesting question as to how the cationic **BPET** species regenerates its native state to undergo PET with subsequent PAGs.

Aside from obtaining in-depth understanding regarding the mechanism of the precatalyst activation process, practical applications of light-activated olefin polymerization precatalysts includes 3-D printing polyolefins. This work demonstrated temporal and spatial control over the activation of 1-hexene and ethylene polymerizations, but supplemental work will include polymerizing and printing other olefins (e.g. propylene). Precatalyst **21** has been previously reported to synthesize isotactic polypropylene, while the metallocene precatalysts (**19-20**) can produce a variety of tactic polypropylene. The mechanical properties of these polyolefins are attractive to the 3-D printing field, making the ability to access these materials using abundant gaseous monomer feedstocks will only add to its impact.[185]

REFERENCES

1. Chadwick, J. C., Ziegler-Natta Catalysts. In *Encyclopedia of Polymer Science and Technology*, 2003.

2. Sailors, H. R.; Hogan, J. P., *J. Macromol. Sci. Part A Chem.* **1981**, *A 15* (7), 1377.

3. American Chemical Society National Historic Chemical Landmarks. . http://www.acs.org/content/acs/en/education/whatischemistry/landmarks/polypropylene.html (accessed March 27).

4. Hogan, J. P.; Banks, R. L., History of Polypropylene. In *History of Polyolefins*, Seymour, R., Ed. Netherlands: Kluwer Academic: 1986.

5. Hlatky, G. G., *Chem. Rev.* **2000**, *100* (4), 1347.

6. Sinn, H.; Kaminsky, W.; Vollmer, H. J.; Woldt, R., *Angew. Chem. Int. Edit.* **1980**, *19* (5), 390.

7. Kuhlman, R. L., Metallocenes. In *Encyclopedia of Polymer Science and Technology*, 2016; pp 1.

8. Heurtefeu, B.; Vaultier, F.; Leino, R.; Boisson, C.; Cramail, H., Single-Site Catalysts. In *Encyclopedia of Polymer Science and Technology*, 2012.

9. Coates, G. W., *Chem. Rev.* **2000**, *100* (4), 1223.

10. Alt, H. G.; Koppl, A., *Chem. Rev.* **2000**, *100* (4), 1205.

11. Gibson, V. C.; Spitzmesser, S. K., *Chem. Rev.* **2003**, *103* (1), 283.

12. Johnson, L. K.; Killian, C. M.; Brookhart, M., *J. Am. Chem. Soc.* **1995**, *117* (23), 6414.

13. Ittel, S. D.; Johnson, L. K.; Brookhart, M., *Chem. Rev.* **2000**, *100* (4), 1169.

14. Guan, Z.; Cotts, P. M.; McCord, E. F.; McLain, S. J., *Science* **1999**, *283* (5410), 2059.

15. Guan, Z., *Chem. Eur. J.* **2002**, *8* (14), 3086.

16. Killian, C. M.; Tempel, D. J.; Johnson, L. K.; Brookhart, M., *J. Am. Chem. Soc.* **1996**, *118* (46), 11664.

17. Coates, G. W.; Hustad, P. D.; Reinartz, S., *Angew. Chem. Int. Edit.* **2002**, *41* (13), 2236.

18. Chen, E. Y., *Chem. Rev.* **2009**, *109* (11), 5157.

19. Boffa, L. S.; Novak, B. M., *Chem. Rev.* **2000**, *100* (4), 1479.

20. Popeney, C.; Guan, Z. B., *Organometallics* **2005**, *24* (6), 1145.

21. Lorkovic, I. M.; Duff, R. R.; Wrighton, M. S., *J. Am. Chem. Soc.* **1995**, *117* (12), 3617.

22. Gregson, C. K.; Gibson, V. C.; Long, N. J.; Marshall, E. L.; Oxford, P. J.; White, A. J., *J. Am. Chem. Soc.* **2006**, *128* (23), 7410.

23. Allgeier, A. M.; Mirkin, C. A., *Angew. Chem. Int. Edit.* **1998**, *37* (7), 894.

24. Romero, N. A.; Nicewicz, D. A., *Chem. Rev.* **2016**, *116* (17), 10075.

25. Prier, C. K.; Rankic, D. A.; MacMillan, D. W., *Chem. Rev.* **2013**, *113* (7), 5322.

26. Luca, O. R.; Crabtree, R. H., *Chem. Soc. Rev.* **2013**, *42* (4), 1440.

27. Teator, A. J.; Lastovickova, D. N.; Bielawski, C. W., *Chem. Rev.* **2016**, *116* (4), 1969.

28. Chen, M.; Yang, B.; Chen, C., *Angew. Chem. Int. Edit.* **2015**, *54* (51), 15520.

29. Anderson, W. C., Jr.; Rhinehart, J. L.; Tennyson, A. G.; Long, B. K., *J. Am. Chem. Soc.* **2016**, *138* (3), 774.

30. Shafir, A.; Power, M. P.; Whitener, G. D.; Arnold, J., *Organometallics* **2000**, *19* (19), 3978.

31. Shafir, A.; Arnold, J., *Inorg. Chim. Acta* **2003**, *345*, 216.

32. Multani, K.; Stanlake, L. J.; Stephan, D. W., *Dalton Trans.* **2010**, *39* (38), 8957.

33. Gibson, V. C.; Long, N. J.; Oxford, P. J.; White, A. J. P.; Williams, D. J., *Organometallics* **2006**, *25* (8), 1932.

34. Gibson, V. C.; Gregson, C. K. A.; Halliwell, C. M.; Long, N. J.; Oxford, P. J.; White, A. J. P.; Williams, D. J., *J. Organomet. Chem.* **2005**, *690* (26), 6271.

35. Gibson, V. C.; Halliwell, C. M.; Long, N. J.; Oxford, P. J.; Smith, A. M.; White, A. J. P.; Williams, D. J., *Dalton Trans.* **2003**, (5), 918.

36. Drent, E.; van Dijk, R.; van Ginkel, R.; van Oort, B.; Pugh, R. I., *Chem. Commun.* **2002**, (9), 964.

37. Drent, E.; van Dijk, R.; van Ginkel, R.; van Oort, B.; Pugh, R. I., *Chem. Commun.* **2002**, (7), 744.

38. Carrow, B. P.; Nozaki, K., *Macromolecules* **2014**, *47* (8), 2541.

39. Nakamura, A.; Ito, S.; Nozaki, K., *Chem. Rev.* **2009**, *109* (11), 5215.

40. Nozaki, K., Polymerization of Polar Monomers. In *Organometallic Reactions and Polymerization*, Osakada, K., Ed. Springer Berlin Heidelberg: Berlin, Heidelberg, 2014; pp 217.

41. Nakamura, A.; Anselment, T. M.; Claverie, J.; Goodall, B.; Jordan, R. F.; Mecking, S.; Rieger, B.; Sen, A.; van Leeuwen, P. W.; Nozaki, K., *Acc. Chem. Res.* **2013**, *46* (7), 1438.

42. Ito, S.; Nozaki, K., *Chem. Rec.* **2010**, *10* (5), 315.

43. Cai, Z. G.; Shen, Z. L.; Zhou, X. Y.; Jordan, R. F., *ACS Catal.* **2012**, *2* (6), 1187.

44. Wucher, P.; Goldbach, V.; Mecking, S., *Organometallics* **2013**, *32* (16), 4516.

45. Chen, M.; Yang, B. P.; Chen, C. L., *Synlett* **2016**, *27* (9), 1297.

46. Yang, B. P.; Pang, W. M.; Chen, M., *Eur. J. Inorg. Chem.* **2017**, (18), 2510.

47. Jian, Z. B.; Wucher, P.; Mecking, S., *Organometallics* **2014**, *33* (11), 2879.

48. Conley, M. P.; Jordan, R. F., *Angew. Chem. Int. Edit.* **2011**, *50* (16), 3744.

49. Leicht, H.; Gottker-Schnetmann, I.; Mecking, S., *Angew. Chem. Int. Edit.* **2013**, *52* (14), 3963.

50. Runzi, T.; Tritschler, U.; Roesle, P.; Gottker-Schnetmann, I.; Moller, H. M.; Caporaso, L.; Poater, A.; Cavallo, L.; Mecking, S., *Organometallics* **2012**, *31* (23), 8388.

51. Ota, Y.; Ito, S.; Kuroda, J.; Okumura, Y.; Nozaki, K., *J. Am. Chem. Soc.* **2014**, *136* (34), 11898.

52. Guo, L.; Chen, C., *Sci. China Chem.* **2015**, *58* (11), 1663.

53. Guo, L. H.; Dai, S. Y.; Sui, X. L.; Chen, C. L., *ACS Catal.* **2016**, *6* (1), 428.

54. Chen, Z.; Liu, W.; Daugulis, O.; Brookhart, M., *J. Am. Chem. Soc.* **2016**, *138* (49), 16120.

55. Long, B. K.; Eagan, J. M.; Mulzer, M.; Coates, G. W., *Angew. Chem. Int. Edit.* **2016**, *55* (25), 7106.

56. Rhinehart, J. L.; Brown, L. A.; Long, B. K., *J. Am. Chem. Soc.* **2013**, *135* (44), 16316.

57. Deng, L. Q.; Woo, T. K.; Cavallo, L.; Margl, P. M.; Ziegler, T., *J. Am. Chem. Soc.* **1997**, *119* (26), 6177.

58. Camacho, D. H.; Guan, Z., *Chem. Commun.* **2010**, *46* (42), 7879.

59. Chen, M.; Chen, C., *ACS Catal.* **2017**, *7* (2), 1308.

60. Guironnet, D.; Roesle, P.; Runzi, T.; Gottker-Schnetmann, I.; Mecking, S., *J. Am. Chem. Soc.* **2009**, *131* (2), 422.

61. Perrotin, P.; McCahill, J. S.; Wu, G.; Scott, S. L., *Chem. Commun.* **2011**, *47* (24), 6948.

62. He, X.; Liu, Y.; Chen, L.; Chen, Y.; Chen, D., *J. Polym. Sci., Part A: Polym. Chem.* **2012**, *50* (22), 4695.

63. Hu, T.; Li, Y. G.; Li, Y. S.; Hu, N. H., *J. Mol. Catal. A: Chem.* **2006**, *253* (1-2), 155.

64. Tian, J.; Zhu, H.; Liu, J.; Chen, D.; He, X., *Appl. Organomet. Chem.* **2014**, *28* (9), 702.

65. Hennis, A. D.; Polley, J. D.; Long, G. S.; Sen, A.; Yandulov, D.; Lipian, J.; Benedikt, G. M.; Rhodes, L. F.; Huffman, J., *Organometallics* **2001**, *20* (13), 2802.

66. Walter, M. D.; Moorhouse, R. A.; Urbin, S. A.; White, P. S.; Brookhart, M., *J. Am. Chem. Soc.* **2009**, *131* (25), 9055.

67. Casares, J. A.; Espinet, P.; Salas, G., *Organometallics* **2008**, *27* (15), 3761.

68. Yamashita, M.; Takamiya, I.; Jin, K.; Nozaki, K., *Organometallics* **2006**, *25* (19), 4588.

69. Blank, F.; Scherer, H.; Janiak, C., *J. Mol. Catal. A: Chem.* **2010**, *330* (1-2), 1.

70. Blank, F.; Scherer, H.; Ruiz, J.; Rodriguez, V.; Janiak, C., *Dalton Trans.* **2010**, *39* (15), 3609.

71. Zhao, M. H.; Chen, C. L., *ACS Catal.* **2017**, *7* (11), 7490.

72. Cotts, P. M.; Guan, Z. B.; McCord, E.; McLain, S., *Macromolecules* **2000**, *33* (19), 6945.

73. Popeney, C. S.; Guan, Z., *Macromolecules* **2010**, *43* (9), 4091.

74. Popeney, C. S.; Levins, C. M.; Guan, Z. B., *Organometallics* **2011**, *30* (8), 2432.

75. Sui, X.; Hong, C.; Pang, W.; Chen, C., *Mater. Chem. Front.* **2017**, *1* (5), 967.

76. Huo, P.; Liu, W.; He, X.; Wei, Z.; Chen, Y., *Polym. Chem.* **2014**, *5* (4), 1210.

77. Kim, D.-G.; Bell, A.; Register, R. A., *ACS Macro Lett.* **2015**, *4* (3), 327.

78. Xiang, P.; Ye, Z., *J. Organomet. Chem.* **2015**, *798*, 429.

79. Mecking, S.; Keim, W., *Organometallics* **1996**, *15* (11), 2650.

80. Abubekerov, M.; Shepard, S. M.; Diaconescu, P. L., *Eur. J. Inorg. Chem.* **2016**, (15-16), 2634.

81. Peris, E.; Crabtree, R. H., *Coord. Chem. Rev.* **2004**, *248* (21-24), 2239.

82. Sussner, M.; Plenio, H., *Angew. Chem. Int. Edit.* **2005**, *44* (42), 6885.

83. Tennyson, A. G.; Lynch, V. M.; Bielawski, C. W., *J. Am. Chem. Soc.* **2010**, *132* (27), 9420.

84. Savka, R.; Foro, S.; Gallei, M.; Rehahn, M.; Plenio, H., *Chem. Eur. J.* **2013**, *19* (32), 10655.

85. Varnado, C. D., Jr.; Rosen, E. L.; Collins, M. S.; Lynch, V. M.; Bielawski, C. W., *Dalton Trans.* **2013**, *42* (36), 13251.

86. Zou, W. P.; Pang, W. M.; Chen, C. L., *Inorg. Chem. Front.* **2017**, *4* (5), 795.

87. Gates, D. P.; Svejda, S. A.; Oñate, E.; Killian, C. M.; Johnson, L. K.; White, P. S.; Brookhart, M., *Macromolecules* **2000**, *33* (7), 2320.

88. Anderson, W. C.; Long, B. K., *ACS Macro Lett.* **2016**, *5* (9), 1029.

89. Gao, W.; Xin, L.; Hao, Z.; Li, G.; Su, J. H.; Zhou, L.; Mu, Y., *Chem. Commun.* **2015**, *51* (32), 7004.

90. Anderson, W. C.; Park, S. H.; Brown, L. A.; Kaiser, J. M.; Long, B. K., *Inorg. Chem. Front.* **2017**, *4* (7), 1108.

91. Wang, X.; Thevenon, A.; Brosmer, J. L.; Yu, I.; Khan, S. I.; Mehrkhodavandi, P.; Diaconescu, P. L., *J. Am. Chem. Soc.* **2014**, *136* (32), 11264.

92. Broderick, E. M.; Guo, N.; Wu, T.; Vogel, C. S.; Xu, C.; Sutter, J.; Miller, J. T.; Meyer, K.; Cantat, T.; Diaconescu, P. L., *Chem. Commun.* **2011**, *47* (35), 9897.

93. Quan, S. M.; Wei, J. N. A.; Diaconescu, P. L., *Organometallics* **2017**, *36* (22), 4451.

94. Lowe, M. Y.; Shu, S. S.; Quan, S. M.; Diaconescu, P. L., *Inorg. Chem. Front.* **2017**, *4* (11), 1798.

95. Quan, S. M.; Wang, X. K.; Zhang, R. J.; Diaconescu, P. L., *Macromolecules* **2016**, *49* (18), 6768.

96. Broderick, E. M.; Guo, N.; Vogel, C. S.; Xu, C.; Sutter, J.; Miller, J. T.; Meyer, K.; Mehrkhodavandi, P.; Diaconescu, P. L., *J. Am. Chem. Soc.* **2011**, *133* (24), 9278.

97. Delle Chiaie, K. R.; Biernesser, A. B.; Ortuno, M. A.; Dereli, B.; Iovan, D. A.; Wilding, M. J. T.; Li, B.; Cramer, C. J.; Byers, J. A., *Dalton Trans.* **2017**, *46* (38), 12971.

98. Delle Chiaie, K. R.; Yablon, L. M.; Biernesser, A. B.; Michalowski, G. R.; Sudyn, A. W.; Byers, J. A., *Polym. Chem.* **2016**, *7* (28), 4675.

99. Biernesser, A. B.; Delle Chiaie, K. R.; Curley, J. B.; Byers, J. A., *Angew. Chem. Int. Edit.* **2016**, *55* (17), 5251.

100. Biernesser, A. B.; Li, B.; Byers, J. A., *J. Am. Chem. Soc.* **2013**, *135* (44), 16553.

101. Qi, M.; Dong, Q.; Wang, D.; Byers, J. A., *J. Am. Chem. Soc.* **2018**, *140* (17), 5686.

102. Tempel, D. J.; Johnson, L. K.; Huff, R. L.; White, P. S.; Brookhart, M., *J. Am. Chem. Soc.* **2000**, *122* (28), 6686.

103. Liu, F.-S.; Hu, H.-B.; Xu, Y.; Guo, L.-H.; Zai, S.-B.; Song, K.-M.; Gao, H.-Y.; Zhang, L.; Zhu, F.-M.; Wu, Q., *Macromolecules* **2009**, *42* (20), 7789.

104. Xie, T. Y.; Mcauley, K. B.; Hsu, J. C. C.; Bacon, D. W., *Ind. Eng. Chem. Res.* **1994**, *33* (3), 449.

105. Berkefeld, A.; Mecking, S., *J. Am. Chem. Soc.* **2009**, *131* (4), 1565.

106. Berkefeld, A.; Mecking, S., *J. Am. Chem. Soc.* **2009**, *131* (4), 1565.

107. Meinhard, D.; Wegner, M.; Kipiani, G.; Hearley, A.; Reuter, P.; Fischer, S.; Marti, O.; Rieger, B., *J. Am. Chem. Soc.* **2007**, *129* (29), 9182.

108. Ionkin, A. S.; Marshall, W. J., *Organometallics* **2004**, *23* (13), 3276.

109. Hu, H.; Zhang, L.; Gao, H.; Zhu, F.; Wu, Q., *Chem. Eur. J.* **2014**, *20* (11), 3225.

110. Liu, J.; Chen, D.; Wu, H.; Xiao, Z.; Gao, H.; Zhu, F.; Wu, Q., *Macromolecules* **2014**, *47* (10), 3325.

111. Camacho, D. H.; Salo, E. V.; Ziller, J. W.; Guan, Z., *Angew. Chem. Int. Edit.* **2004**, *43* (14), 1821.

112. Zhang, D.; Nadres, E. T.; Brookhart, M.; Daugulis, O., *Organometallics* **2013**, *32* (18), 5136.

113. Yuan, J.; Wang, F.; Xu, W.; Mei, T.; Li, J.; Yuan, B.; Song, F.; Jia, Z., *Organometallics* **2013**, *32* (14), 3960.

114. Liu, H.; Zhao, W. Z.; Hao, X. A.; Redshaw, C.; Huang, W.; Sun, W. H., *Organometallics* **2011**, *30* (8), 2418.

115. Rhinehart, J. L.; Mitchell, N. E.; Long, B. K., *ACS Catal.* **2014**, *4* (8), 2501.

116. Yue, E.; Zhang, L.; Xing, Q.; Cao, X. P.; Hao, X.; Redshaw, C.; Sun, W. H., *Dalton Trans.* **2014**, *43* (2), 423.

117. Yue, E.; Xing, Q.; Zhang, L.; Shi, Q.; Cao, X. P.; Wang, L.; Redshaw, C.; Sun, W. H., *Dalton Trans.* **2014**, *43* (8), 3339.

118. Song, K.; Yang, W.; Li, B.; Liu, Q.; Redshaw, C.; Li, Y.; Sun, W. H., *Dalton Trans.* **2013**, *42* (25), 9166.

119. Kong, S.; Song, K.; Liang, T.; Guo, C. Y.; Sun, W. H.; Redshaw, C., *Dalton Trans.* **2013**, *42* (25), 9176.

120. Kong, S.; Guo, C.-Y.; Yang, W.; Wang, L.; Sun, W.-H.; Glaser, R., *J. Organomet. Chem.* **2013**, *725*, 37.

121. Lai, J. J.; Hou, X. H.; Liu, Y. W.; Redshaw, C.; Sun, W. H., *J. Organomet. Chem.* **2012**, *702*, 52.

122. Zhou, Z. H.; Hao, X.; Redshaw, C.; Chen, L. Q.; Sun, W. H., *Catal. Sci. Technol.* **2012**, *2* (7), 1340.

123. Hu, X.; Dai, S.; Chen, C., *Dalton Trans.* **2016**, *45* (4), 1496.

124. Dai, S.; Sui, X.; Chen, C., *Chem. Commun.* **2016**, *52* (58), 9113.

125. Wang, R.; Sui, X.; Pang, W.; Chen, C., *ChemCatChem.* **2016**, *8* (2), 434.

126. Guo, L.; Dai, S.; Chen, C., *Polymers* **2016**, *8* (2), 37.

127. Leibfarth, F. A.; Mattson, K. M.; Fors, B. P.; Collins, H. A.; Hawker, C. J., *Angew. Chem. Int. Edit.* **2013**, *52* (1), 199.

128. Angnes, R. A.; Li, Z.; Correia, C. R.; Hammond, G. B., *Org. Biomol. Chem.* **2015**, *13* (35), 9152.

129. Nicewicz, D. A.; MacMillan, D. W., *Science* **2008**, *322* (5898), 77.

130. Yoon, T. P.; Ischay, M. A.; Du, J., *Nat. Chem.* **2010**, *2* (7), 527.

131. Narayanam, J. M.; Stephenson, C. R., *Chem. Soc. Rev.* **2011**, *40* (1), 102.

132. Tucker, J. W.; Stephenson, C. R., *J. Org. Chem.* **2012**, *77* (4), 1617.

133. Wallentin, C. J.; Nguyen, J. D.; Finkbeiner, P.; Stephenson, C. R., *J. Am. Chem. Soc.* **2012**, *134* (21), 8875.

134. Lu, Z.; Yoon, T. P., *Angew. Chem. Int. Edit.* **2012**, *51* (41), 10329.

135. Corrigan, N.; Shanmugam, S.; Xu, J.; Boyer, C., *Chem. Soc. Rev.* **2016**, *45* (22), 6165.

136. Treat, N. J.; Sprafke, H.; Kramer, J. W.; Clark, P. G.; Barton, B. E.; Read de Alaniz, J.; Fors, B. P.; Hawker, C. J., *J. Am. Chem. Soc.* **2014**, *136* (45), 16096.

137. Dadashi-Silab, S.; Tasdelen, M. A.; Yagci, Y., *J. Polym. Sci., Part A: Polym. Chem.* **2014**, *52* (20), 2878.

138. Nguyen, J. D.; Tucker, J. W.; Konieczynska, M. D.; Stephenson, C. R., *J. Am. Chem. Soc.* **2011**, *133* (12), 4160.

139. Kutahya, C.; Aykac, F. S.; Yilmaz, G.; Yagci, Y., *Polym. Chem.* **2016**, *7* (39), 6094.

140. Pan, X. C.; Lamson, M.; Yan, J. J.; Matyjaszewski, K., *ACS Macro Lett.* **2015**, *4* (2), 192.

141. Miyake, G. M.; Theriot, J. C., *Macromolecules* **2014**, *47* (23), 8255.

142. Fors, B. P.; Hawker, C. J., *Angew. Chem. Int. Edit.* **2012**, *51* (35), 8850.

143. Ryan, M. D.; Pearson, R. M.; French, T. A.; Miyake, G. M., *Macromolecules* **2017**, *50* (12), 4616.

144. Ramsey, B. L.; Pearson, R. M.; Beck, L. R.; Miyake, G. M., *Macromolecules* **2017**, *50* (7), 2668.

145. Theriot, J. C.; Lim, C. H.; Yang, H.; Ryan, M. D.; Musgrave, C. B.; Miyake, G. M., *Science* **2016**, *352* (6289), 1082.

146. Ogawa, K. A.; Goetz, A. E.; Boydston, A. J., *J. Am. Chem. Soc.* **2015**, *137* (4), 1400.

147. Xu, J. T.; Shanmugam, S.; Duong, H. T.; Boyer, C., *Polym. Chem.* **2015**, *6* (31), 5615.

148. Xu, J.; Jung, K.; Atme, A.; Shanmugam, S.; Boyer, C., *J. Am. Chem. Soc.* **2014**, *136* (14), 5508.

149. Fu, C. K.; Xu, J. T.; Tao, L.; Boyer, C., *ACS Macro Lett.* **2014**, *3* (7), 633.

150. Chen, M.; MacLeod, M. J.; Johnson, J. A., *ACS Macro Lett.* **2015**, *4* (5), 566.

151. Allegrezza, M. L.; DeMartini, Z. M.; Kloster, A. J.; Digby, Z. A.; Konkolewicz, D., *Polym. Chem.* **2016**, *7* (43), 6626.

152. Tucker, B. S.; Coughlin, M. L.; Figg, C. A.; Sumerlin, B. S., *ACS Macro Lett.* **2017**, *6* (4), 452.

153. Donovan, B. R.; Ballenas, J. E.; Patton, D. L., *Macromolecules* **2016**, *49* (20), 7667.

154. Kottisch, V.; Michaudel, Q.; Fors, B. P., *J. Am. Chem. Soc.* **2017**, *139* (31), 10665.

155. Michaudel, Q.; Chauvire, T.; Kottisch, V.; Supej, M. J.; Stawiasz, K. J.; Shen, L.; Zipfel, W. R.; Abruna, H. D.; Freed, J. H.; Fors, B. P., *J. Am. Chem. Soc.* **2017**, *139* (43), 15530.

156. Kottisch, V.; Michaudel, Q.; Fors, B. P., *J. Am. Chem. Soc.* **2016**, *138* (48), 15535.

157. Gates, D. P.; Svejda, S. A.; Oñate, E.; Killian, C. M.; Johnson, L. K.; White, P. S.; Brookhart, M., *Macromolecules* **2000**, *33* (7), 2320.

158. Guan, Z., *Chem. Asian. J.* **2010**, *5* (5), 1058.

159. Xu, Y.; Xiang, P.; Ye, Z.; Wang, W.-J., *Macromolecules* **2010**, *43* (19), 8026.

160. McNally, A.; Prier, C. K.; MacMillan, D. W., *Science* **2011**, *334* (6059), 1114.

161. Galland, G. B.; de Souza, R. F.; Mauler, R. S.; Nunes, F. F., *Macromolecules* **1999**, *32* (5), 1620.

162. Galland, G. B.; Quijada, R.; Rojas, R.; Bazan, G.; Komon, Z. J. A., *Macromolecules* **2002**, *35* (2), 339.

163. Cotts, P. M.; Guan, Z.; McCord, E.; McLain, S., *Macromolecules* **2000**, *33* (19), 6945.

164. Hicks, F. A.; Jenkins, J. C.; Brookhart, M., *Organometallics* **2003**, *22* (17), 3533.

165. Wang, X.; Thevenon, A.; Brosmer, J. L.; Yu, I.; Khan, S. I.; Mehrkhodavandi, P.; Diaconescu, P. L., *J. Am. Chem. Soc.* **2014**, *136* (32), 11264.

166. Busico, V.; Cipullo, R.; Friederichs, N.; Ronca, S.; Togrou, M., *Macromolecules* **2003**, *36* (11), 3806.

167. Johnson, L. K.; Killian, C. M.; Brookhart, M., *J. Am. Chem. Soc.* **1995**, *117* (23), 6414.

168. Berman, B., *Bus. Horizons* **2012**, *55* (2), 155.

169. Gill, J. M.; Hart, A. S., *Jala-J Lab Autom* **2016**, *21* (4), 487.

170. Hu, L. G.; Jiang, G. B., *Environ. Sci. Technol.* **2017**, *51* (7), 3597.

171. Hegde, M.; Meenakshisundaram, V.; Chartrain, N.; Sekhar, S.; Tafti, D.; Williams, C. B.; Long, T. E., *Adv. Mater.* **2017**, *29* (31).

172. Bhushan, B.; Caspers, M., *Microsyst. Technol.* **2017**, *23* (4), 1117.

173. Ligon, S. C.; Liska, R.; Stampfl, J.; Gurr, M.; Mulhaupt, R., *Chem. Rev.* **2017**, *117* (15), 10212.

174. Khalimon, A. Y.; Leitao, E. M.; Piers, W. E., *Organometallics* **2012**, *31* (15), 5634.

175. Keitz, B. K.; Grubbs, R. H., *J. Am. Chem. Soc.* **2009**, *131* (6), 2038.

176. Li, R. J.; Nakashima, T.; Kawai, T., *Chem. Commun.* **2017**, *53* (31), 4339.

177. Klikovits, N.; Knaack, P.; Bomze, D.; Krossing, I.; Liska, R., *Polym. Chem.* **2017**, *8* (30), 4414.

178. Devi, R.; Murugavel, S. C., *J. Appl. Polym. Sci.* **2012**, *124* (1), 58.

179. Shirai, M.; Tsunooka, M., *Prog. Polym. Sci.* **1996**, *21* (1), 1.

180. Chen, E. Y.; Marks, T. J., *Chem. Rev.* **2000**, *100* (4), 1391.

181. Moscato, B. M.; Zhu, B.; Landis, C. R., *Organometallics* **2012**, *31*, 2097−2107.

182. Press, K.; Cohen, A.; Goldberg, I.; Venditto, V.; Mazzeo, M.; Kol, M., *Angew. Chem. Int. Edit.* **2011**, *50* (15), 3529.

183. Yeori, A.; Goldberg, I.; Shuster, M.; Kol, M., *J. Am. Chem. Soc.* **2006**, *128* (40), 13062.

184. Busico, V.; Cipullo, R.; Friederichs, N.; Ronca, S.; Talarico, G.; Togrou, M.; Wang, B., *Macromolecules* **2004**, *37* (22), 8201.

185. Cipullo, R.; Busico, V.; Fraldi, N.; Pellecchia, R.; Talarico, G., *Macromolecules* **2009**, *42* (12), 3869.

186. Xie, T.; McAuley, K. B.; Hsu, J. C. C.; Bacon, D. W., *Ind. Eng. Chem. Res.* **1994**, *33* (3), 449.

187. Tannous, K.; Soares, J. B. P., *Macromol. Chem. Phys.* **2002**, *203* (13), 1895.

188. Crivello, J. V.; Jang, M., *J. Photoch. Photobio. A* **2003**, *159* (2), 173.

189. Park, H. J.; Ryu, C. Y.; Crivello, J. V., *J. Polym. Sci., Part A: Polym. Chem.* **2013**, *51* (1), 109.

190. Lalevée, J.; Mokbel, H.; Fouassier, J.-P., *Molecules* **2015**, *20* (4), 7201.

191. Shi, S.; Croutxé-Barghorn, C.; Allonas, X., *Prog. Polym. Sci.* **2017**, *65*, 1.

192. Dadashi-Silab, S.; Doran, S.; Yagci, Y., *Chem. Rev.* **2016**, *116* (17), 10212.

193. Toba, Y.; Saito, M.; Usui, Y., *Macromolecules* **1999**, *32* (10), 3209.

194. Schnabel, W., *Macromol. Rapid. Comm.* **2000**, *21* (10), 628.

195. Crivello, J. V.; Jiang, F., *Chem. Mater.* **2002**, *14* (11), 4858.

196. Phillips, O.; Engler, A.; Schwartz, J. M.; Jiang, J.; Tobin, C.; Guta, Y. A.; Kohl, P. A., *J. Appl. Polym. Sci.* **2019**, *136* (9), 47141.

197. Kavarnos, G. J.; Turro, N. J., *Chem. Rev.* **1986**, *86* (2), 401.

198. Turley, W. D.; Offen, H. W., *J. Phys. Chem-US.* **1984**, *88* (16), 3605.

199. *Radiation Curing in Polymer Science and Technology*. 1 ed.; Springer Netherlands: 1993; Vol. 3, p 563.

200. Desert, X.; Carpentier, J.-F.; Kirillov, E., *Coord. Chem. Rev.* **2019**, *386*, 50.

201. Vatamanu, M.; Boden, B. N.; Baird, M. C., *Macromolecules* **2005**, *38* (24), 9944.

202. Crivello, J. V.; Lam, J. H. W., *J. Polym. Sci., Part A: Polym. Chem.* **1979**, *17* (4), 1059.

203. Wang, T.; Chen, J. W.; Li, Z. Q.; Wan, P. Y., *J. Photoch. Photobio. A* **2007**, *187* (2), 389.

APPENDICES

A.1 Polar Comonomer Incorporation using Cationic Ni α-Diimine Olefin Polymerization Catalysts

A version of this chapter was originally published by Jordan M. Kaiser and Brian K. Long:

Kaiser, J. M., Long, B. K. *Science China Chemistry*, **2019**, *62*, 153-154.

I was responsible for preparation of the manuscript. Dr. Brian Long advised this work and aided in the preparation of the manuscript.

Polyolefins are an indispensable class of materials that have become the most widely produced and utilized polymers today. They are readily synthesized from cheap and abundant monomer feedstocks, such as ethylene and propylene, and are capable of achieving a vast array of thermal and mechanical properties based upon their composition and topology. However, despite their numerous advantages, polyolefins are typically devoid of functional groups which can limit their applicability to many product families, such as coatings, adhesives, and cross-linked polyolefins.

To overcome this issue, researchers typically employ post-polymerization modification techniques to access functionalized polyolefins. These strategies can include functionalization using free radical chemistry, deprotection of incorporated comonomers bearing latent functionality, as well as numerous other methods. Though many of these post-polymerization modification strategies are currently implemented on an industrial

scale, they require additional synthetic steps that incur added reagent and energy consumption costs. In contrast, if functionalized polyolefins could be synthesized via the direct copolymerization of olefins and polar comonomers, multiple advantages may be realized (Figure 1). These could include avoiding additional synthetic steps, more uniform functional group placement, and retention of polymer properties that might otherwise be degraded during post-polymerization modification.

Toward this goal, researchers have turned to the development of group 10 olefin polymerization catalysis capable of copolymerizing simple olefins (ethylene and α-olefins) with polar functionalized vinyl comonomers. These group 10 catalysts generally employ Ni or Pd active metal centers, and are less oxophilic than their early transition metal analogues. Because of this, they are able to tolerate and incorporate polar comonomers more readily. Though Pd- based catalysts generally achieve higher polar comonomer incorporation percentages, they typically exhibit lower activities and/or produce lower molecular weight polymers than their Ni-based analogues.

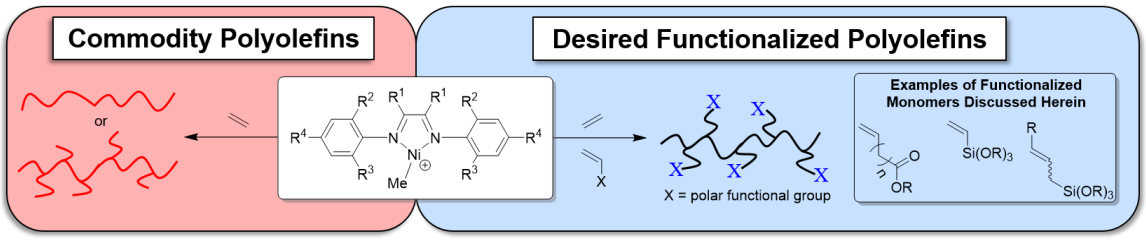

Figure A.1 Current and desired capabilities of cationic, nickel-based olefin polymerization catalysts.

It is for these reasons that the development of Ni-based olefin polymerization catalysts capable of incorporating polar comonomers is of utmost interest to academia and industry alike. Herein, we will describe three recent examples that highlight these efforts.

One of the most frequently targeted classes of polar comonomers are those containing ester functionalities. This is in part due to the vast availability of ester functionalized monomers, as well as their ability to significantly tailor a polyolefin's surface energy and interactions. An example of these efforts was reported by Coates and coworkers who developed a cationic Ni catalyst bearing a bulky dibenzobarrelene-derived α-diimine ligand [1]. This catalyst displayed living ethylene polymerization behavior at room temperature and produced highly linear polyethylene ($T_m \leq 135$ °C) at polymerization temperatures ≤ 20 °C. Furthermore, this unique catalyst was able to incorporate the ester-functionalized comonomer, methyl 10-undecenoate, to yield semi-crystalline copolyethylenes (T_m = 97 – 128 °C) with high molecular weights (M_n = 27 – 105 kg/mol) and modest polar comonomer incorporation percentages (0.3 – 1.0 mol%). This ability to simultaneously produce polar functionalized, semi-crystalline polyethylene represents a unique capability in the area of functionalized polyolefin synthesis using cationic Ni-based catalysts.

A second highly targeted class of polar comonomers are those bearing alkoxysilane moieties. Alkoxysilane functionalized polyethylene is a precursor to cross-linked polyethylene (PEX), which is used in applications such as piping and electrical cable insulation. Currently, these materials are accessed via post-polymerization modification as the direct copolymerization of ethylene and vinyltrialkoxysilane comonomers are often

plagued by undesirable β-silyl elimination. To avoid this, Brookhart, Daugulis, and coworkers recently demonstrated that simple Ni α-diimine catalysts can be used to copolymerize ethylene and vinyltrialkoxysilanes under a variety of conditions [2]. These polymerizations yielded high molecular weight functionalized copolyethylenes ($M_n \leq 173$ kg/mol) with a wide array of branching content (T_m = -29 – 115 °C) and polar comonomer incorporation percentages (0.23 – 10.0 mol%). This range of alkoxysilane incorporation is more than sufficient to generate PEX, which typically only requires ~0.1 – 2.0 mol% alkoxysilane functionalization.

This ability to incorporate alkoxysilane functionalities into polyolefins was further expanded by Chen and coworkers who found that allylic alkoxysilane monomers bearing internal olefins could also be utilized [3]. Therein, they used a Co catalyzed dehydrogenative silylation between 1-octene and various inexpensive alkoxysilane reagents to produce allylic alkoxysilane monomers in high yields (75 – 90%). These polar functionalized monomers were then copolymerized with ethylene using a traditional cationic Ni α-diimine catalyst. The alkoxysilane-functionalized copolyethylenes synthesized were high molecular weight (M_w = 23 – 86 kg/mol) and had moderate branching (70 – 92 branches/1000 carbons) and alkoxysilane incorporation percentages (0.1 – 2.9 mol%). Though these incorporation percentages are lower than those obtained by Brookhart and Daugulis, they are sufficient to produce PEX and are believed to be due to the internal nature of the allylic alkoxysilane's polymerizable olefin. As a result, both the Brookhart/Daugulis and Chen routes to high molecular weight, alkoxysilane-

functionalized polyethylenes represent significant advances in the area of polar functionalized polyolefin synthesis.

In summary, polyolefins are a ubiquitous class of polymers that despite their vast utility, are often limited by their lack of chemical functionality. Though certain functional groups may be installed using post-polymerization modification techniques, their direct synthesis via copolymerization of simple olefinic monomers, such as ethylene and propylene, and polar comonomers is highly desired. Although the reports discussed herein focused on ester and alkoxysilane functionalized polyethylenes, the incorporation of many other chemical functionalities are also of interest. Most importantly, however, these reports encourage current and future scientists that polar functionalized polyolefins may one day be accessible via direct copolymerizations using cationic Ni α-diimine catalysts.

Conflict of interest: The authors declare no conflict of interest.

1 Long BK, Eagan JM, Mulzer M, Coates GW. Angew Chem Int Ed, 2016, 55: 7106-7110

2 Chen Z, Leatherman MD, Daugulis O, Brookhart M. J Am Chem Soc, 2017, 139: 16013-16022

3 Zhou SX, Chen CL. Sci Bull, 2018, 63: 441-445

A.2 Progress Towards Other Light Activating Molecules

A.2.1 Introduction

In Chapter 3, I discussed classical activation methods for dialkyl-ligated olefin polymerization catalysts. These catalysts are effectively activated from Lewis or Brønsted acids. Throughout the chapter, I used a photoacid generator (**I-PAG**) that released a Brønsted acid upon irradiation, ultimately abstracting an alkyl group via protonolysis and activated the catalyst. Another avenue I pursued, but was found to be not as effective, was prompting a photo Lewis acid generator (PhLAG) to release a Lewis acid species for precatalyst activation upon visible light irradiation (Figure A.2).

Arylcylcopentadienyl ferrocenium tetrafluoroborate derivatives have been reported to initiate cationic polymerizations in the presence of visible light.[203] As the complex is excited, the aryl ligand is displaced generating an iron-centered Lewis acid species responsible for instigating monomer polymerization. In my olefin polymerization system, I suspect that this Lewis acid species will activate dialkyl-ligated precatalysts by abstracting an alkyl ligand following a similar mechanism as trityl borate activators, generating active catalyst.[180] Although tetrafluoroborate was not destructive to the cationic polymerizations, it will negatively influence the activity and catalytic lifetime of olefin polymerization catalysts. Instead, napthylcylcopentadienyl ferrocenium tris-(pentafluorophenyl)borate (**VL-PhLAG**) was synthesize according to the literature procedures using the appropriate sodium borate salt.[203]

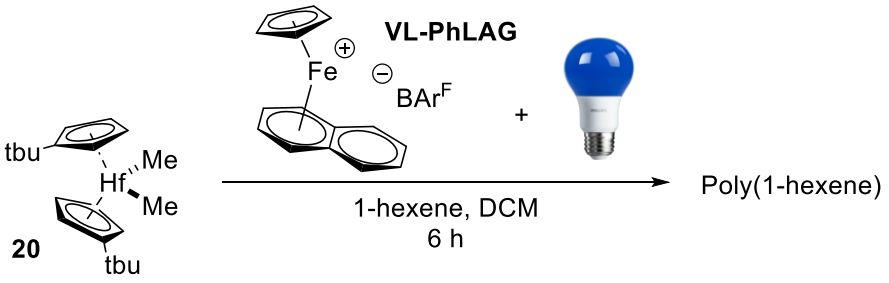

Figure A.2 Polymerization of 1-hexene with precatalyst **20** and **VL-PhLAG** using visible light.

A.2.2 Results and Discussion

Following the synthesis of this PhLAG, I conducted a preliminary 1-hexene polymerization using precatalyst **20**, **VL-PhLAG** in the presence of a 150 W halogen lamp because previous reports use a high-powered white light source. After several hours of irradiation, there was no polymer produced. After further investigation into the energy spectrum of these ferrocenium complexes, I found that these complexes exhibit maximum absorbance in the blue region (~450 nm). This led me to use a 24 W blue LED in place of the halogen light source. I conducted three separate 6-hour polymerizations containing precatalyst **20** and **VL-PhLAG** varying the 24 W blue LED exposure time (1 h, 2 h, and 4 h). After 2 hours of irradiation, I reached maximum catalyst activity to convert 25% of 1-hexene monomer (Figure A.3).

I-PAG and precatalyst **20** lead to 43% monomer conversion when irradiated with 4 W UV light for 15 minutes, which is nearly double this PhLAG method in $^1/_8$ the exposure time and ½ the polymerization time. This led me to assess the polymerization conditions,

where I noticed that the 24 W blue LED produces a lot of heat which has been reported to be detrimental to metallocenes leading to catalyst deactivation/decomposition. Following this observation, I conducted the same 6-hour polymerizations varying in exposure time, except these polymerizations were placed in a room temperature water bath. These temperature-controlled polymerizations displayed improved monomer conversion (Figure A.3). I was pleased to see that the room temperature water bath lead to a significant increase in monomer conversion of 40% after 2 hours of irradiation. It seems that removing the heat released from the light source has restored the activation efficiency to conversions witnessed using photoacid generator systems.

To further confirm the impact that light sources seem to play in this photoinduced activation method, I conducted an ^{1}H NMR experiment tracking the presence of Hf bound methyl protons. As more napthyl groups are displaced from the absorbance of light, an alkyl abstraction will occur, leading to lower integrations at the representative Hf-CH_3 peak. Setting up several vials with deuterated solvent, precatalyst **20** and **VL-PhLAG**, I irradiated the vials to test particular light sources in order to determine their alkyl abstraction capabilities. The three light sources I tested involved the 100 W halogen lamp, 14 W CFL, and 24 W blue LED. Looking at Figure A.4, the halogen lamp performed the worst after not showing a change in the integration after 2.5 hours. This behavior supports our in ability to polymerize 1-hexene with precatalyst **20** and **VL-PhLAG** in the presence of the 100 W halogen lamp. The 14 W CFL showed minimal activation over a 5-hour period, which is expected since both the halogen lamp and CFL emit low concentrations of blue light.

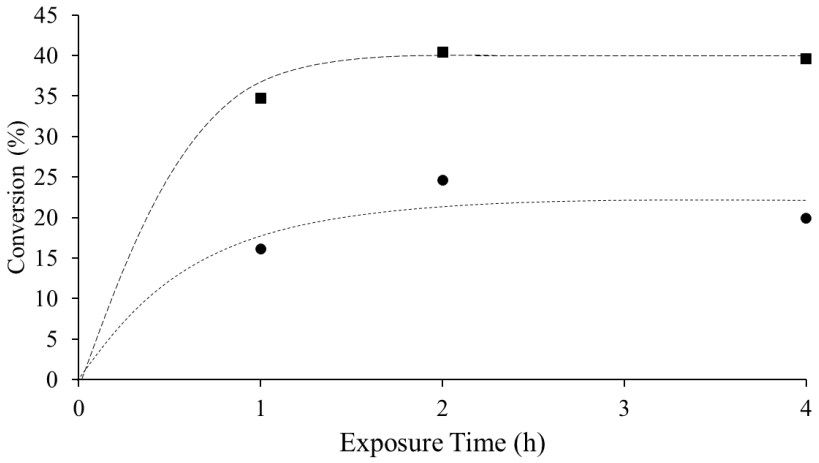

Figure A.3 1-hexene monomer conversion using precatalyst **20** and **VL-PhLAG** as a function of 24 W blue LED exposure time. Polymerizations with no temperature control (●) and polymerizations placed in a room-temperature water bath (■).

The 24 W blue LED shows complete activation after being exposed for 2 hours. These results confirm our exposure time study results presented above. Realizing that a 2-hour irradiation time is excessive and inefficient, I attempted to use two 24 W blue LED lamps to see if doubling the amount of light emitted to the PhLAG could increase the activation rate. Unfortunately, adding another light source has no effect on the activation rate (Figure A.4, ●). This observation was also confirmed by a temperature-controlled 1-hexene polymerization that resulted in 41% monomer conversion with precatalyst 20, VL-PhLAG, and two 24 W blue LED lamps, versus 40% conversion with one lamp.

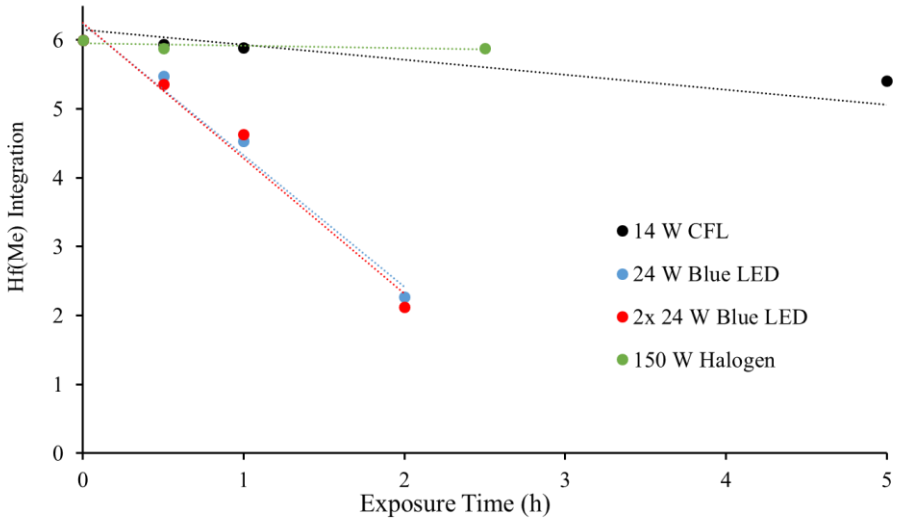

Figure A.4 Monitoring the Hf-CH_3 peak integration of precatalyst **20** as a function of exposure time using ^{1}H NMR spectroscopy.

A.2.3 Conclusion

The purpose behind using molecules that release activating species upon irradiation was to install temporal control over the activation of olefin polymerization catalysts with an external stimulus. This type of external stimulus control has been demonstrated to be a valuable tool to aide in the production of complex 3-D printed materials (e.g. SLA and DLP). Till my reports within this dissertation (Chapter 3), light-stimulated activation of olefin polymerization catalysts has not been possible. In this appendix section, I attempted to use a PhLAG, instead of a PAG, to implement external stimulus control of the precatalyst activation process. Using VL-PhLAG to activate precatalyst 20 in a room temperature water bath upon exposure with a 24 W blue LED, 40% of monomer conversion was reached. Precatalyst 20 was successfully activated by this ferrocenium Lewis acid species

produced upon irradiation, but it required 2 hours of light exposure. Due to the inability to access a high-powered light source in order to reduce the excessive exposure time required, I did not conduct any further studies with this PhLAG.

A.2.4 Experimental

A.1.1.1 General Methods and Materials

All reactions were performed under an inert nitrogen atmosphere using an MBraun UniLab glovebox or using standard Schlenk techniques, unless otherwise noted. All solvents were dried using an Innovative Technologies PureSolv Solvent Purification System and degassed via three freeze-pump-thaw cycles. Precatalyst **20** was purchased from Strem Chemicals Inc. and used as received. **VL-PhLAG** was prepared according to literature.# Quantitative NMR analysis was obtained using a Varian 500 MHz NMR and spectra are referenced relative to their residual solvent signal. Precatalyst **20** = 10 μmol, **VL-PhLAG** = 15 μmol, C_6D_6 = 2 mL.

A.1.1.2 General 1-hexene Polymerization Conditions

Under an inert atmosphere and shielded from ambient light, a quartz flask was charged with precatalyst **20** (10 μmol), **VL-PhLAG** (15 μmol), 1-hexene (1 mL), dichloromethane (3 mL), and a magnetic stir bar. To initiate the polymerization, the reaction flask was irradiated using a 24 W blue LED lamp operating at 450 nm for a pre-determined time. Following irradiation, the reaction was stirred continuously until the total desired reaction time was reached. All polymerizations were quenched, and polymer

precipitated, by the addition of MeOH (10 mL). The polymer was collected and dried to constant weight in vacuo.

A.3 Supporting Information for Chapter 3

A.3.1 Gel Permeation Chromatography

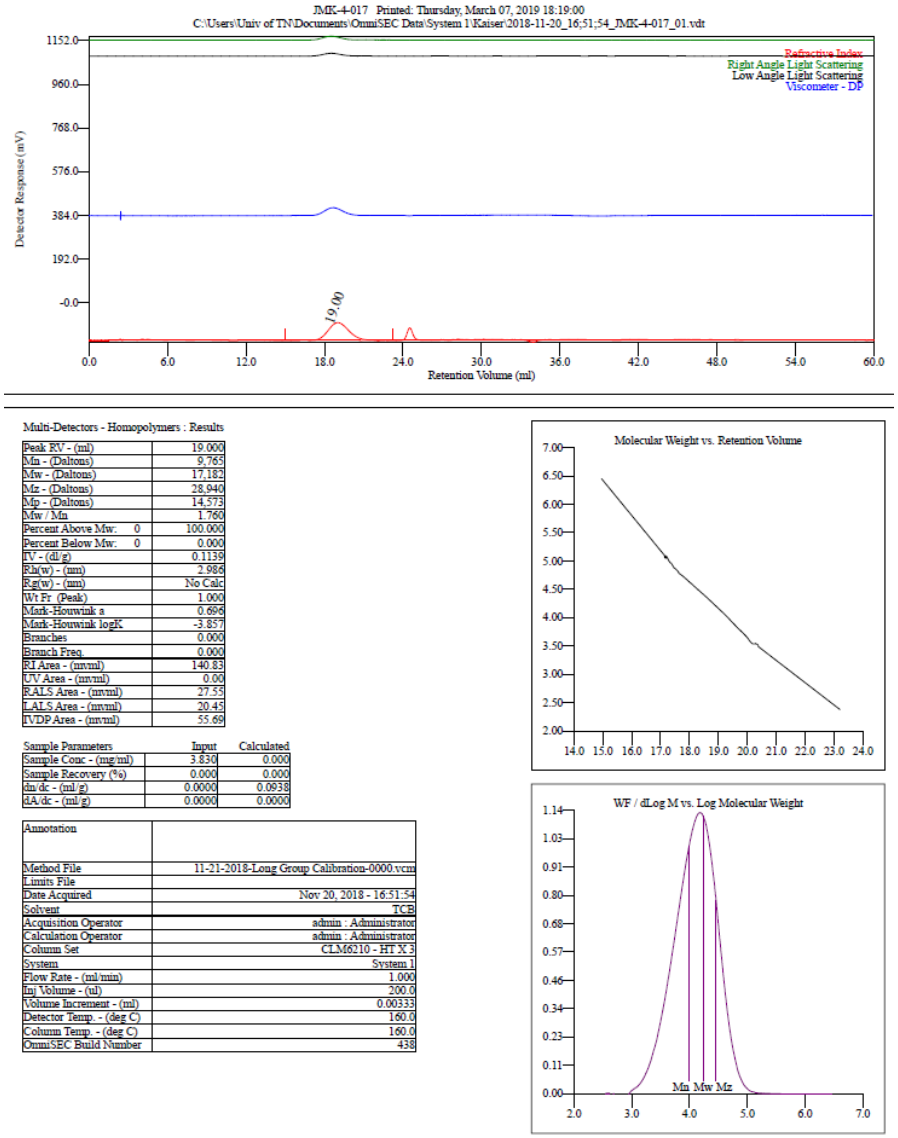

Peak RV - (ml)	19.000
Mn - (Daltons)	9,765
Mw - (Daltons)	17,182
Mz - (Daltons)	28,940
Mp - (Daltons)	14,573
Mw / Mn	1.760
Percent Above Mw: 0	100.000
Percent Below Mw: 0	0.000
IV - (dl/g)	0.1139
Rh(w) - (nm)	2.986
Rg(w) - (nm)	No Calc
Wt Fr (Peak)	1.000
Mark-Houwink a	0.696
Mark-Houwink logK	-3.857
Branches	0.000
Branch Freq	0.000
RI Area - (mvml)	140.83
UV Area - (mvml)	0.00
RALS Area - (mvml)	27.55
LALS Area - (mvml)	20.45
IVDP Area - (mvml)	55.68

Sample Parameters	Input	Calculated
Sample Conc - (mg/ml)	3.830	0.000
Sample Recovery (%)	0.000	0.000
dn/dc - (ml/g)	0.0000	0.0938
dA/dc - (ml/g)	0.0000	0.0000

Annotation	
Method File	11-21-2018-Long Group Calibration-0000.vcm
Limits File	
Date Acquired	Nov 20, 2018 - 16:51:54
Solvent	TCB
Acquisition Operator	admin : Administrator
Calculation Operator	admin : Administrator
Column Set	CLM6210 - HT X 3
System	System 1
Flow Rate - (ml/min)	1.000
Inj Volume - (ul)	200.0
Volume Increment - (ml)	0.00333
Detector Temp. - (deg C)	160.0
Column Temp. - (deg C)	160.0
OmniSEC Build Number	438

Figure A.5 GPC of poly(1-hexene). (Table 3.1, entry 1)

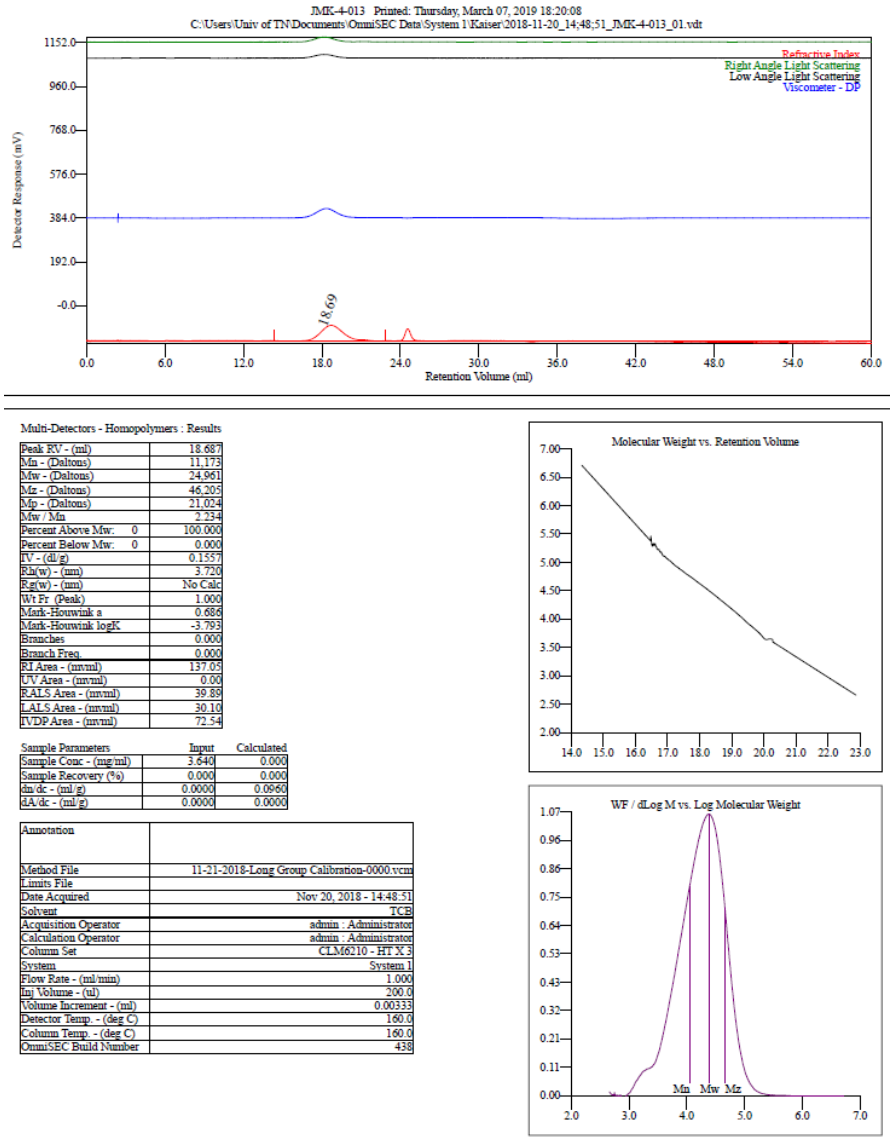

Peak RV - (ml)	18.687
Mn - (Daltons)	11,173
Mw - (Daltons)	24,961
Mz - (Daltons)	46,205
Mp - (Daltons)	21,024
Mw / Mn	2.234
Percent Above Mw: 0	100.000
Percent Below Mw: 0	0.000
IV - (dl/g)	0.1557
Rh(w) - (nm)	3.720
Rg(w) - (nm)	No Calc
Wt Fr (Peak)	1.000
Mark-Houwink a	0.686
Mark-Houwink logK	-3.793
Branches	0.000
Branch Freq.	0.000
RI Area - (mvml)	137.05
UV Area - (mvml)	0.00
RALS Area - (mvml)	39.89
LALS Area - (mvml)	30.10
IVDP Area - (mvml)	72.54

Sample Parameters	Input	Calculated
Sample Conc - (mg/ml)	3.640	0.000
Sample Recovery (%)	0.000	0.000
dn/dc - (ml/g)	0.0000	0.0960
dA/dc - (ml/g)	0.0000	0.0000

Annotation	
Method File	11-21-2018-Long Group Calibration-0000.vcm
Limits File	
Date Acquired	Nov 20, 2018 - 14:48:51
Solvent	TCB
Acquisition Operator	admin : Administrator
Calculation Operator	admin : Administrator
Column Set	CLM6210 - HT X 3
System	System 1
Flow Rate - (ml/min)	1.000
Inj Volume - (ul)	200.0
Volume Increment - (ml)	0.00333
Detector Temp. - (deg C)	160.0
Column Temp. - (deg C)	160.0
OmniSEC Build Number	438

Figure A.6 GPC of poly(1-hexene). (Table 3.1, entry 2)

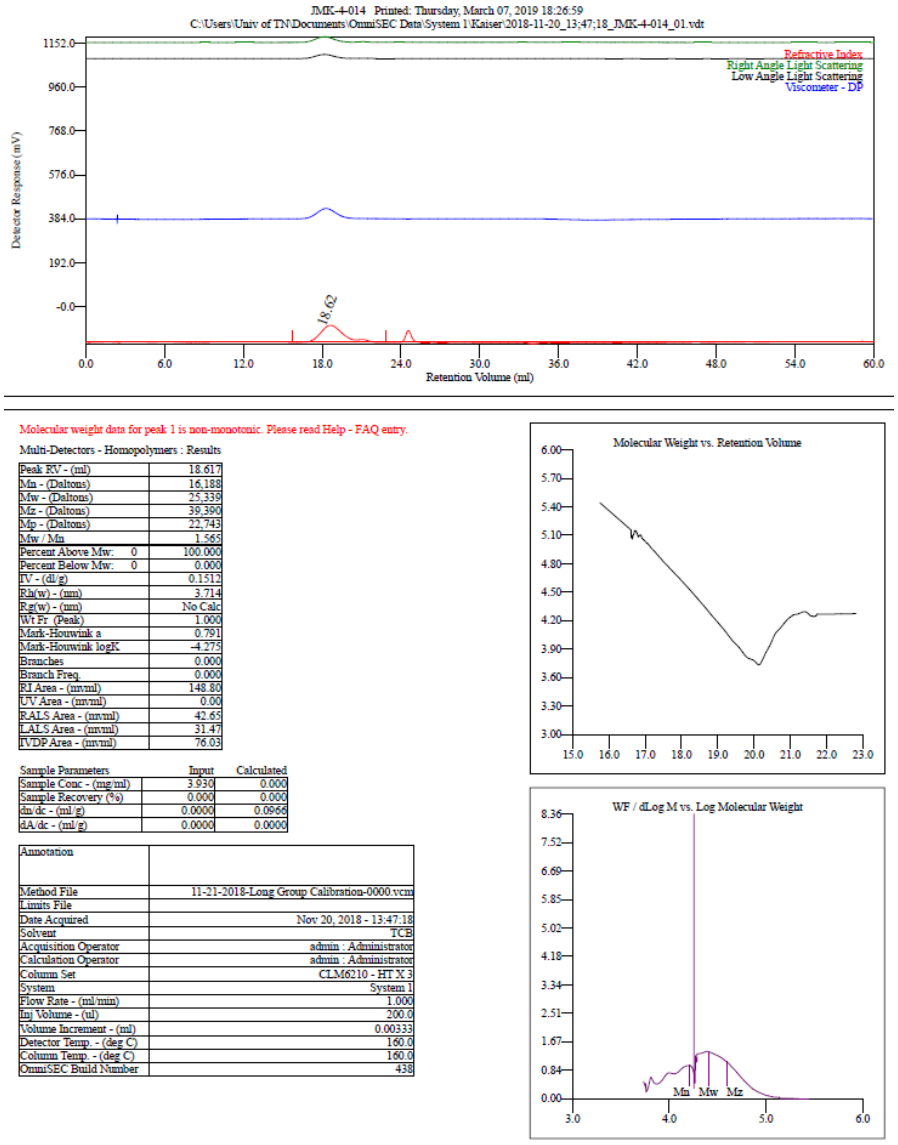

Peak RV - (ml)	18.617
Mn - (Daltons)	16,188
Mw - (Daltons)	25,339
Mz - (Daltons)	39,390
Mp - (Daltons)	22,743
Mw / Mn	1.565
Percent Above Mw: 0	100.000
Percent Below Mw: 0	0.000
IV - (dl/g)	0.1512
Rh(w) - (nm)	3.714
Rg(w) - (nm)	No Calc
Wt Fr (Peak)	1.000
Mark-Houwink a	0.791
Mark-Houwink logK	-4.275
Branches	0.000
Branch Freq.	0.000
RI Area - (mvml)	148.80
UV Area - (mvml)	0.00
RALS Area - (mvml)	42.65
LALS Area - (mvml)	31.47
IVDP Area - (mvml)	76.03

Sample Parameters	Input	Calculated
Sample Conc - (mg/ml)	3.930	0.000
Sample Recovery (%)	0.000	0.000
dn/dc - (ml/g)	0.0000	0.0966
dA/dc - (ml/g)	0.0000	0.0000

Annotation	
Method File	11-21-2018-Long Group Calibration-0000.vcm
Limits File	
Date Acquired	Nov 20, 2018 - 13:47:18
Solvent	TCB
Acquisition Operator	admin : Administrator
Calculation Operator	admin : Administrator
Column Set	CLM6210 - HT X 3
System	System 1
Flow Rate - (ml/min)	1.000
Inj Volume - (ul)	200.0
Volume Increment - (ml)	0.00333
Detector Temp. - (deg C)	160.0
Column Temp. - (deg C)	160.0
OmniSEC Build Number	438

Figure A.7 GPC of poly(1-hexene). (Table 3.1, entry 3)

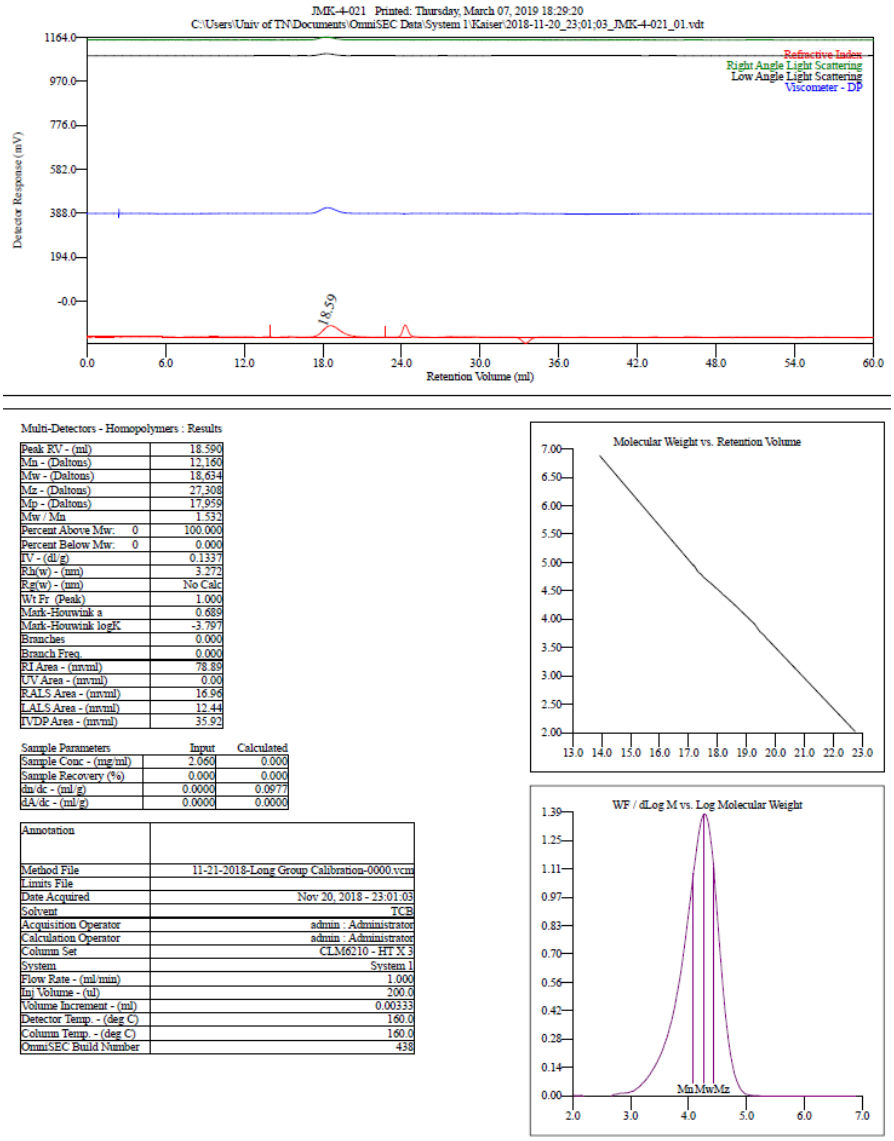

Figure A.8 GPC of poly(1-hexene). (Table 3.1, entry 4)

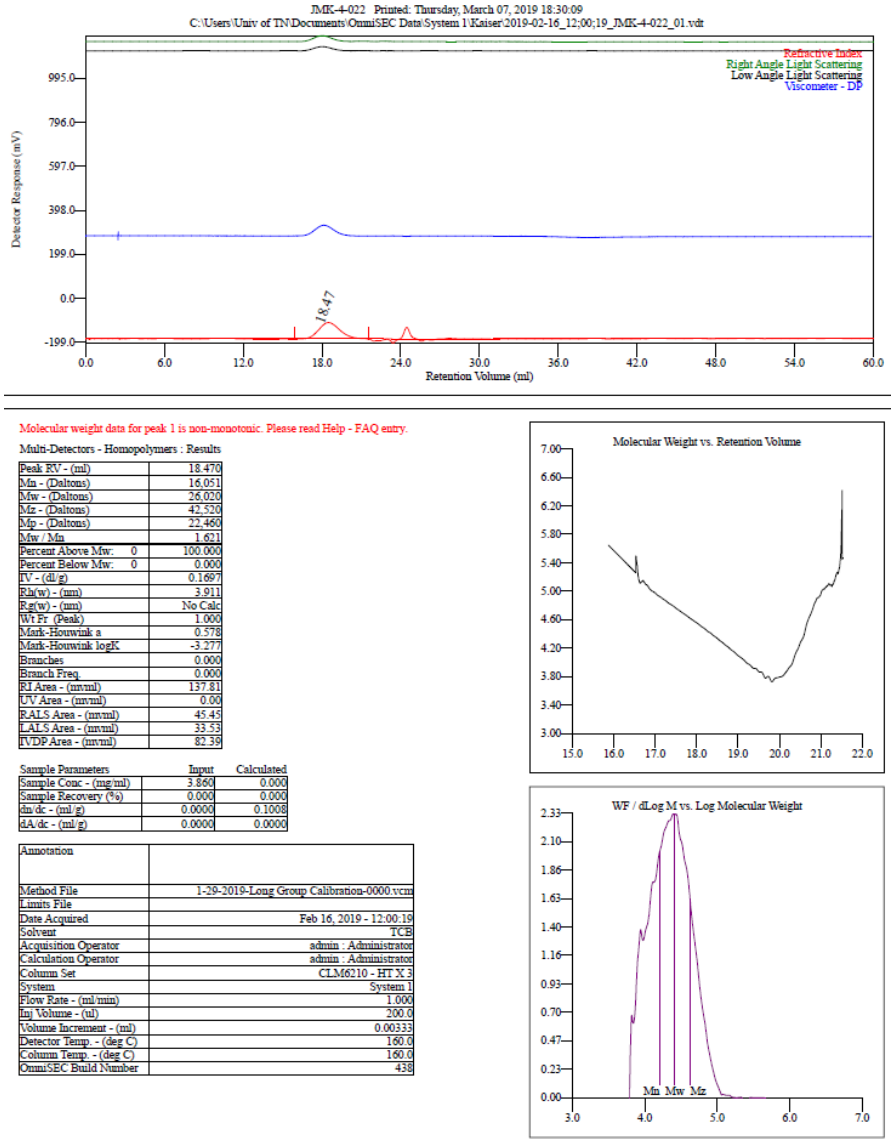

Peak RV - (ml)	18.470
Mn - (Daltons)	16,051
Mw - (Daltons)	26,020
Mz - (Daltons)	42,520
Mp - (Daltons)	22,460
Mw / Mn	1.621
Percent Above Mw: 0	100.000
Percent Below Mw: 0	0.000
IV - (dl/g)	0.1697
Rh(w) - (nm)	3.911
Rg(w) - (nm)	No Calc
Wt Fr (Peak)	1.000
Mark-Houwink a	0.578
Mark-Houwink logK	-3.277
Branches	0.000
Branch Freq.	0.000
RI Area - (mvml)	137.81
UV Area - (mvml)	0.00
RALS Area - (mvml)	45.45
LALS Area - (mvml)	33.53
IVDP Area - (mvml)	82.39

Sample Parameters	Input	Calculated
Sample Conc - (mg/ml)	3.860	0.000
Sample Recovery (%)	0.000	0.000
dn/dc - (ml/g)	0.0000	0.1008
dA/dc - (ml/g)	0.0000	0.0000

Annotation	
Method File	1-29-2019-Long Group Calibration-0000.vcm
Limits File	
Date Acquired	Feb 16, 2019 - 12:00:19
Solvent	TCB
Acquisition Operator	admin : Administrator
Calculation Operator	admin : Administrator
Column Set	CLM6210 - HT X 3
System	System 1
Flow Rate - (ml/min)	1.000
Inj Volume - (ul)	200.0
Volume Increment - (ml)	0.00333
Detector Temp. - (deg C)	160.0
Column Temp. - (deg C)	160.0
OmniSEC Build Number	438

Figure A.9 GPC of poly(1-hexene). (Table 3.1, entry 5)

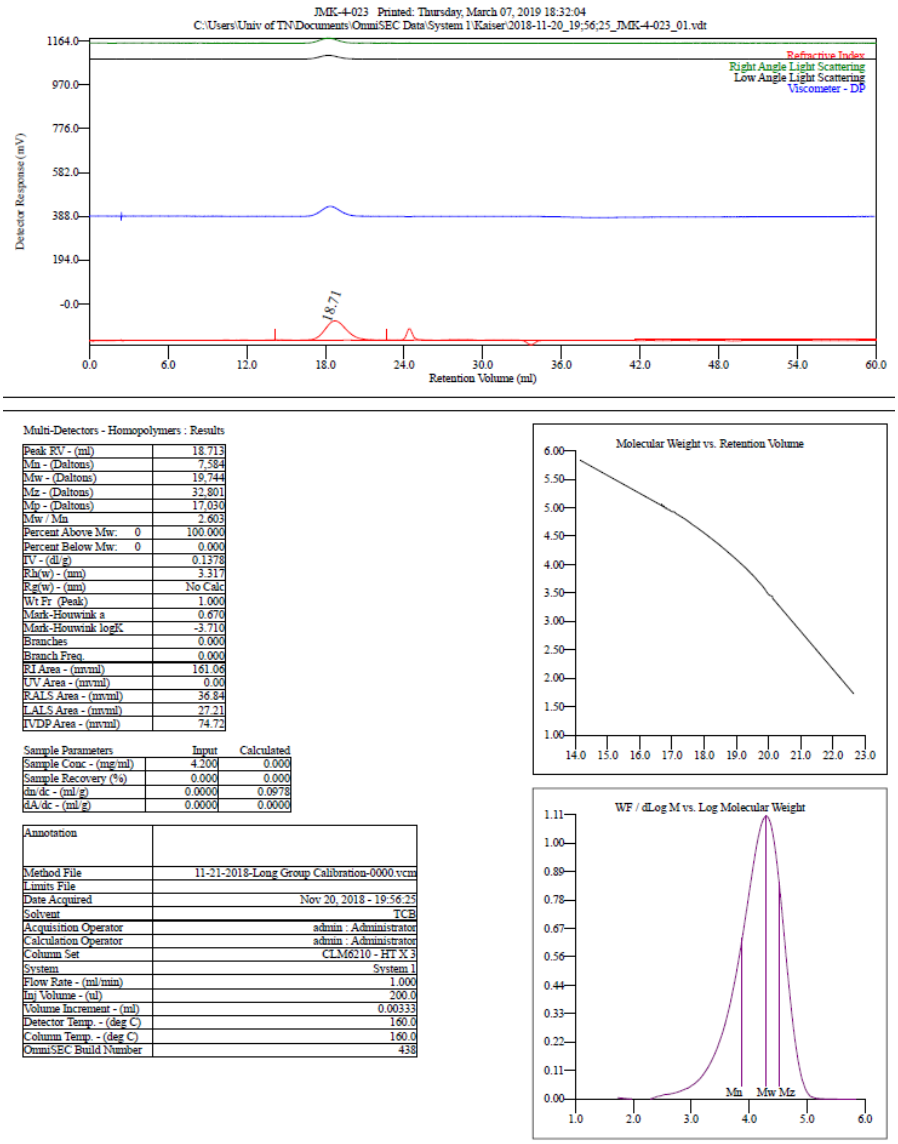

Peak RV - (ml)	18.713
Mn - (Daltons)	7,584
Mw - (Daltons)	19,744
Mz - (Daltons)	32,801
Mp - (Daltons)	17,030
Mw / Mn	2.603
Percent Above Mw: 0	100.000
Percent Below Mw: 0	0.000
IV - (dl/g)	0.1378
Rh(w) - (nm)	3.317
Rg(w) - (nm)	No Calc
Wt Fr (Peak)	1.000
Mark-Houwink a	0.670
Mark-Houwink logK	-3.710
Branches	0.000
Branch Freq.	0.000
RI Area - (mv/ml)	161.06
UV Area - (mv/ml)	0.00
RALS Area - (mv/ml)	36.84
LALS Area - (mv/ml)	27.21
IVDP Area - (mv/ml)	74.72

Sample Parameters	Input	Calculated
Sample Conc - (mg/ml)	4.200	0.000
Sample Recovery (%)	0.000	0.000
dn/dc - (ml/g)	0.0000	0.0978
dA/dc - (ml/g)	0.0000	0.0000

Annotation	
Method File	11-21-2018-Long Group Calibration-0000.vcm
Limits File	
Date Acquired	Nov 20, 2018 - 19:56:25
Solvent	TCB
Acquisition Operator	admin : Administrator
Calculation Operator	admin : Administrator
Column Set	CLM6210 - HT X 3
System	System 1
Flow Rate - (ml/min)	1.000
Inj Volume - (ul)	200.0
Volume Increment - (ml)	0.00333
Detector Temp. - (deg C)	160.0
Column Temp. - (deg C)	160.0
OmniSEC Build Number	438

Figure A.10 GPC of poly(1-hexene). (Table 3.1, entry 6)

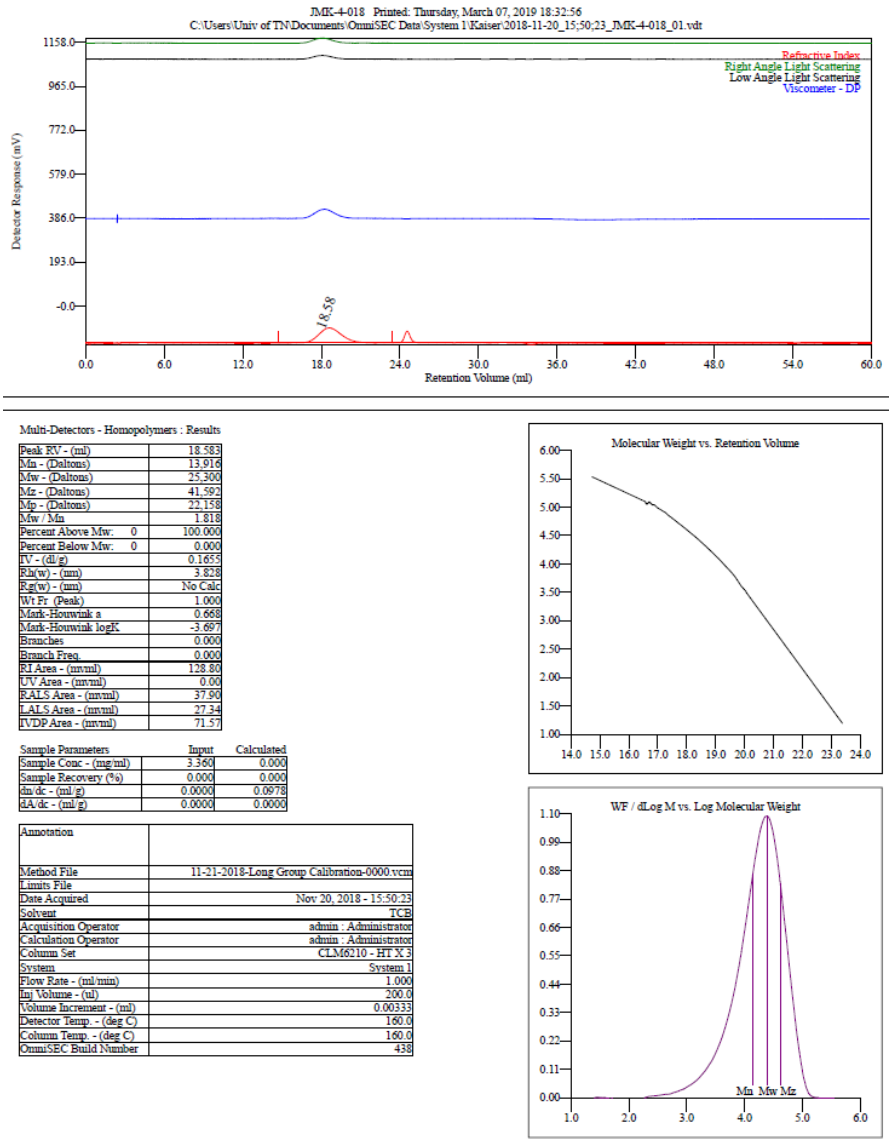

Peak RV - (ml)	18.583
Mn - (Daltons)	13,916
Mw - (Daltons)	25,300
Mz - (Daltons)	41,592
Mp - (Daltons)	22,158
Mw / Mn	1.818
Percent Above Mw: 0	100.000
Percent Below Mw: 0	0.000
IV - (dl/g)	0.1655
Rh(w) - (nm)	3.828
Rg(w) - (nm)	No Calc
Wt Fr (Peak)	1.000
Mark-Houwink a	0.668
Mark-Houwink logK	-3.697
Branches	0.000
Branch Freq.	0.000
RI Area - (mvml)	128.80
UV Area - (mvml)	0.00
RALS Area - (mvml)	37.90
LALS Area - (mvml)	27.34
IVDP Area - (mvml)	71.57

Sample Parameters	Input	Calculated
Sample Conc - (mg/ml)	3.360	0.000
Sample Recovery (%)	0.000	0.000
dn/dc - (ml/g)	0.0000	0.0978
dA/dc - (ml/g)	0.0000	0.0000

Annotation	
Method File	11-21-2018-Long Group Calibration-0000.vcm
Limits File	
Date Acquired	Nov 20, 2018 - 15:50:23
Solvent	TCB
Acquisition Operator	admin : Administrator
Calculation Operator	admin : Administrator
Column Set	CLM6210 - HT X 3
System	System 1
Flow Rate - (ml/min)	1.000
Inj Volume - (ul)	200.0
Volume Increment - (ml)	0.00333
Detector Temp. - (deg C)	160.0
Column Temp. - (deg C)	160.0
OmniSEC Build Number	438

Figure A.11 GPC of poly(1-hexene). (Table 3.1, entry 7)

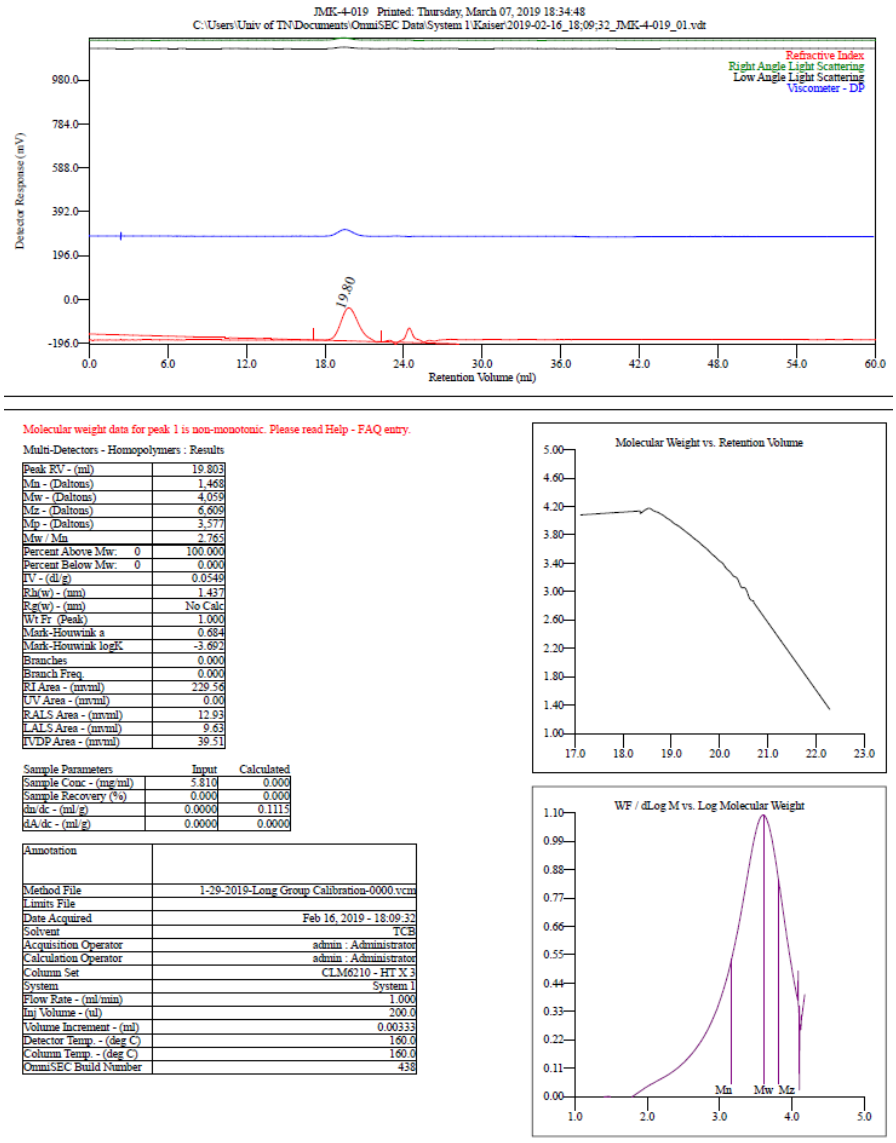

Figure A.12 GPC of poly(1-hexene). (Table 3.2, entry 1)

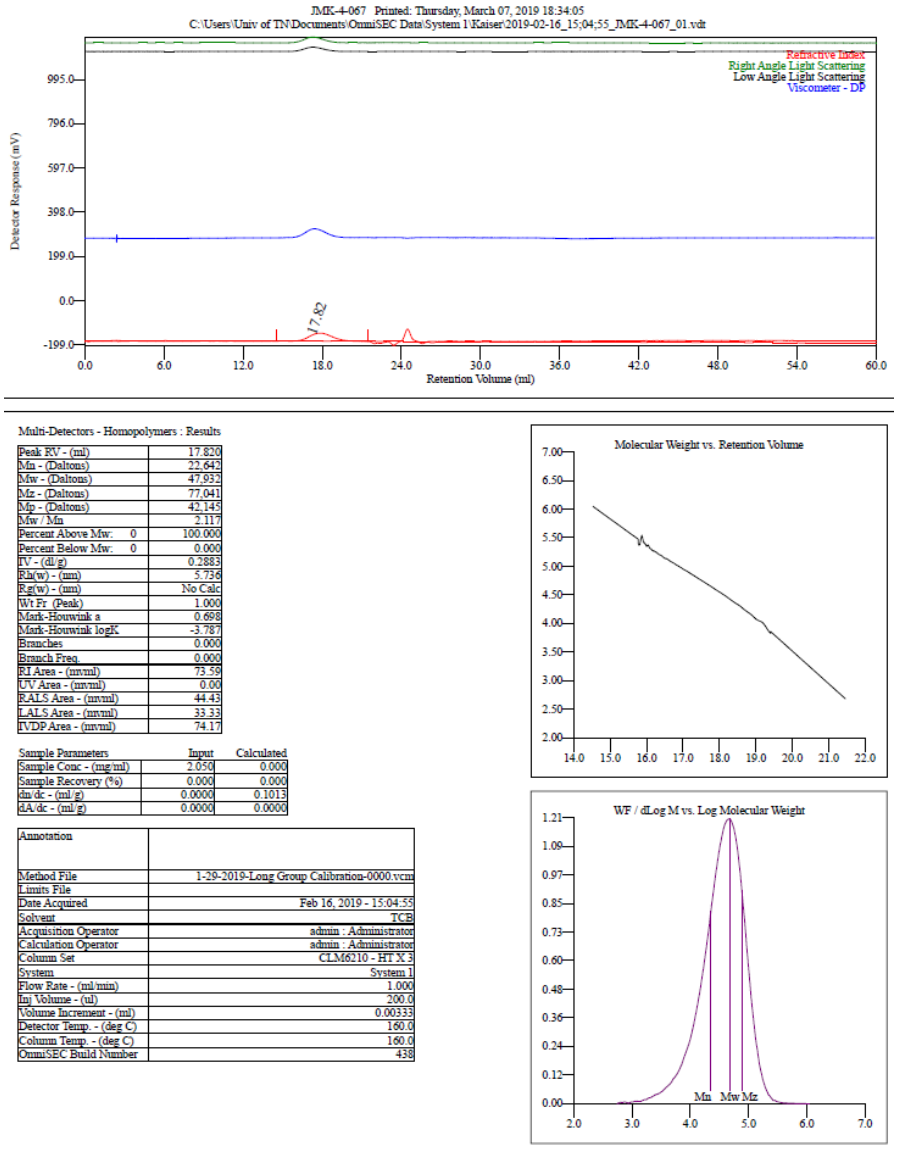

Figure A.13 GPC of poly(1-hexene). (Table 3.2, entry 2)

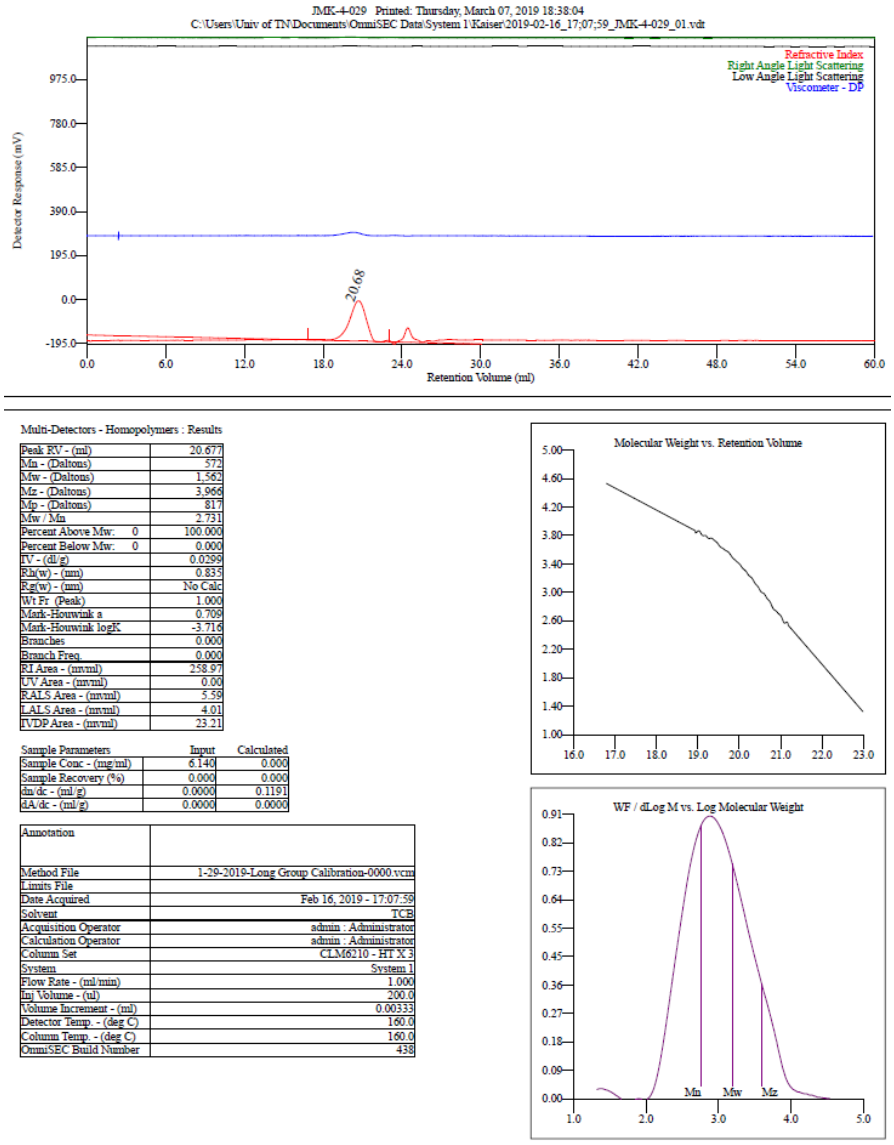

Figure A.14 GPC of poly(1-hexene). (Table 3.2, entry 3)

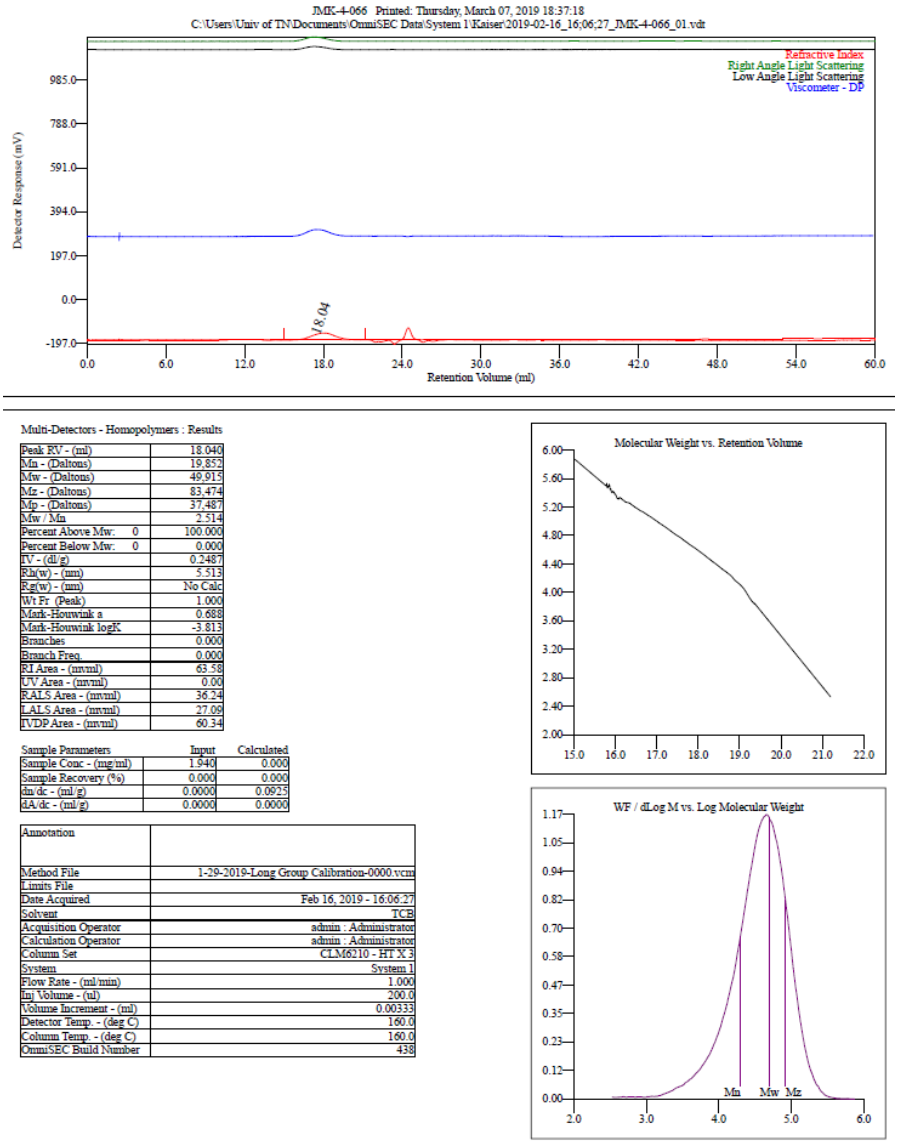

Figure A.15 GPC of poly(1-hexene). (Table 3.2, entry 4)

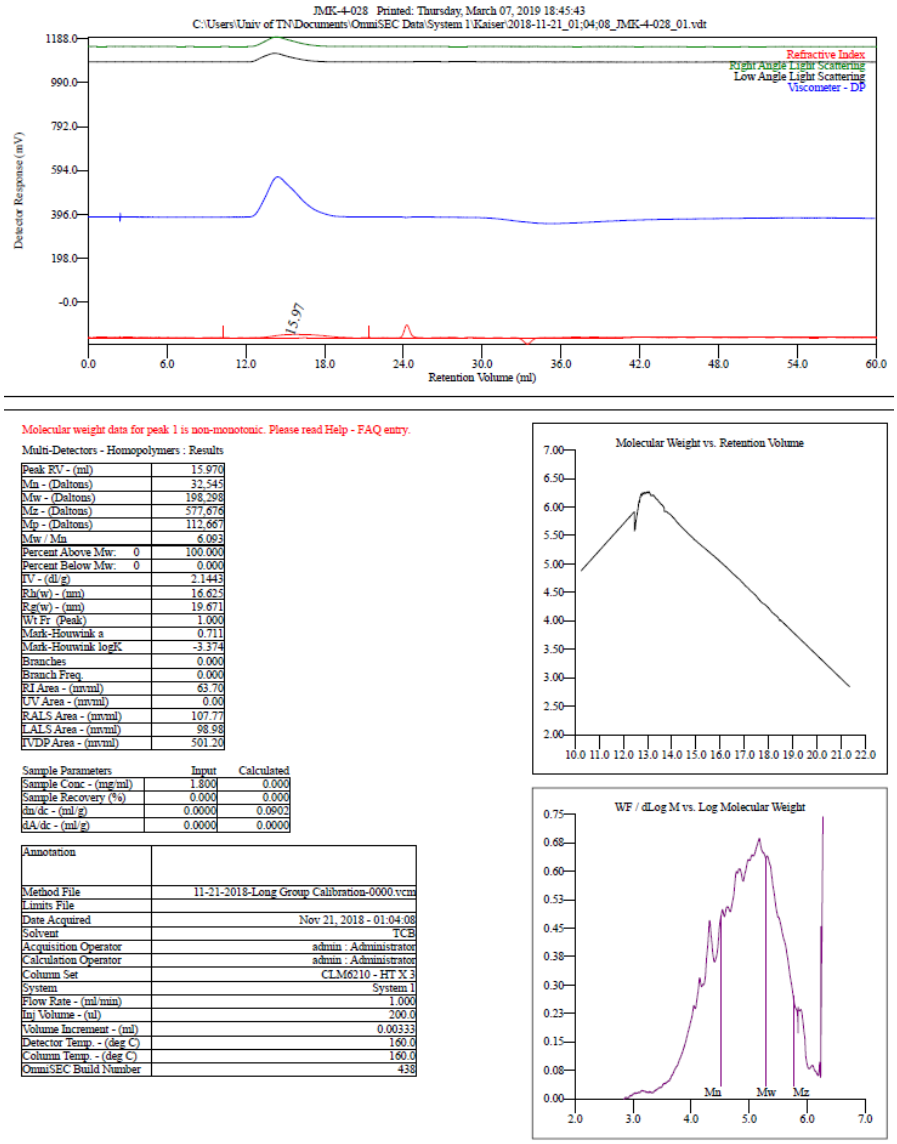

Figure A.16 GPC of polyethylene. (Table 3.3, entry 1)

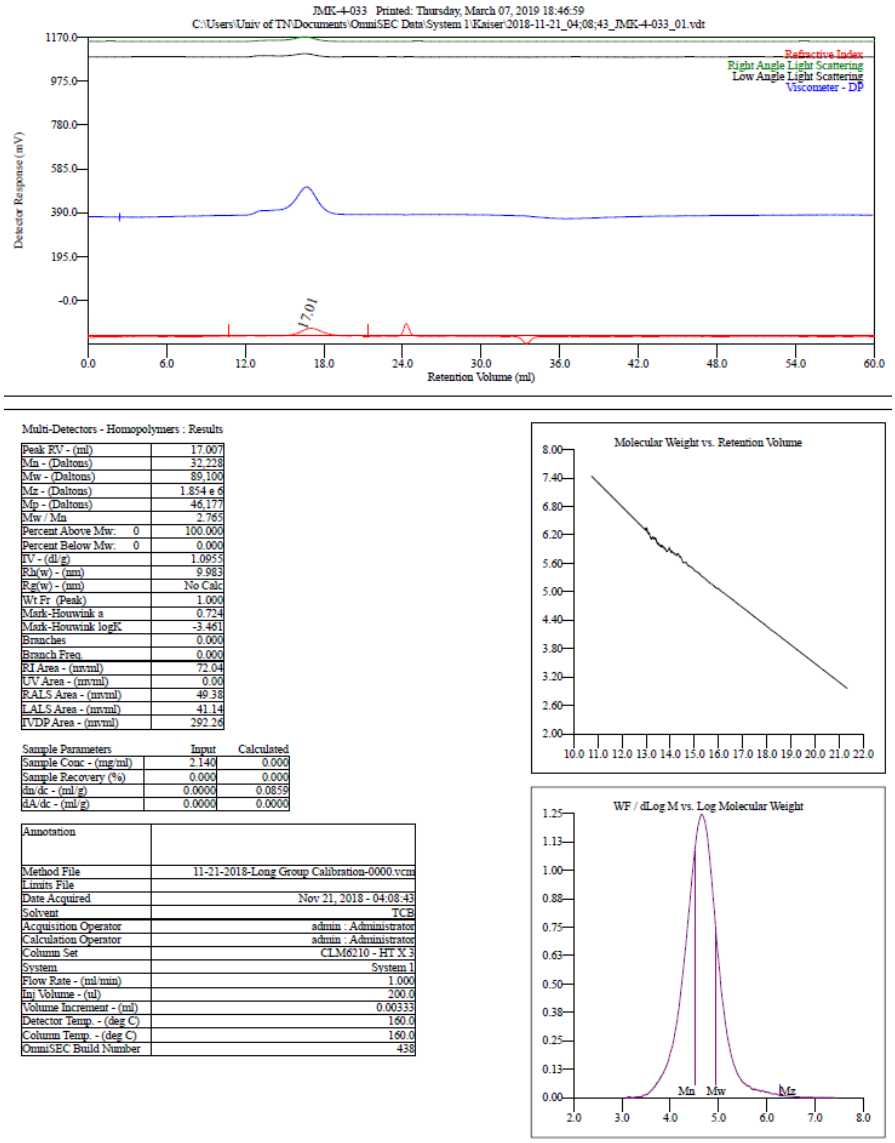

Peak RV - (ml)	17.007
Mn - (Daltons)	32,228
Mw - (Daltons)	89,100
Mz - (Daltons)	1.854 e 6
Mp - (Daltons)	46,177
Mw / Mn	2.765
Percent Above Mw: 0	100.000
Percent Below Mw: 0	0.000
IV - (dl/g)	1.0955
Rh(w) - (nm)	9.983
Rg(w) - (nm)	No Calc
Wt Fr (Peak)	1.000
Mark-Houwink a	0.724
Mark-Houwink logK	-3.461
Branches	0.000
Branch Freq	0.000
RI Area - (mvml)	72.04
UV Area - (mvml)	0.00
RALS Area - (mvml)	40.38
LALS Area - (mvml)	41.14
IVDP Area - (mvml)	292.26

Sample Parameters	Input	Calculated
Sample Conc - (mg/ml)	2.140	0.000
Sample Recovery (%)	0.000	0.000
dn/dc - (ml/g)	0.0000	0.0859
dA/dc - (ml/g)	0.0000	0.0000

Annotation	
Method File	11-21-2018-Long Group Calibration-0000.vcm
Limits File	
Date Acquired	Nov 21, 2018 - 04:08:43
Solvent	TCB
Acquisition Operator	admin : Administrator
Calculation Operator	admin : Administrator
Column Set	CLM6210 - HT X 3
System	System 1
Flow Rate - (ml/min)	1.000
Inj Volume - (ul)	200.0
Volume Increment - (ml)	0.00333
Detector Temp. - (deg C)	160.0
Column Temp. - (deg C)	160.0
OmniSEC Build Number	438

Figure A.17 GPC of polyethylene. (Table 3.3, entry 2)

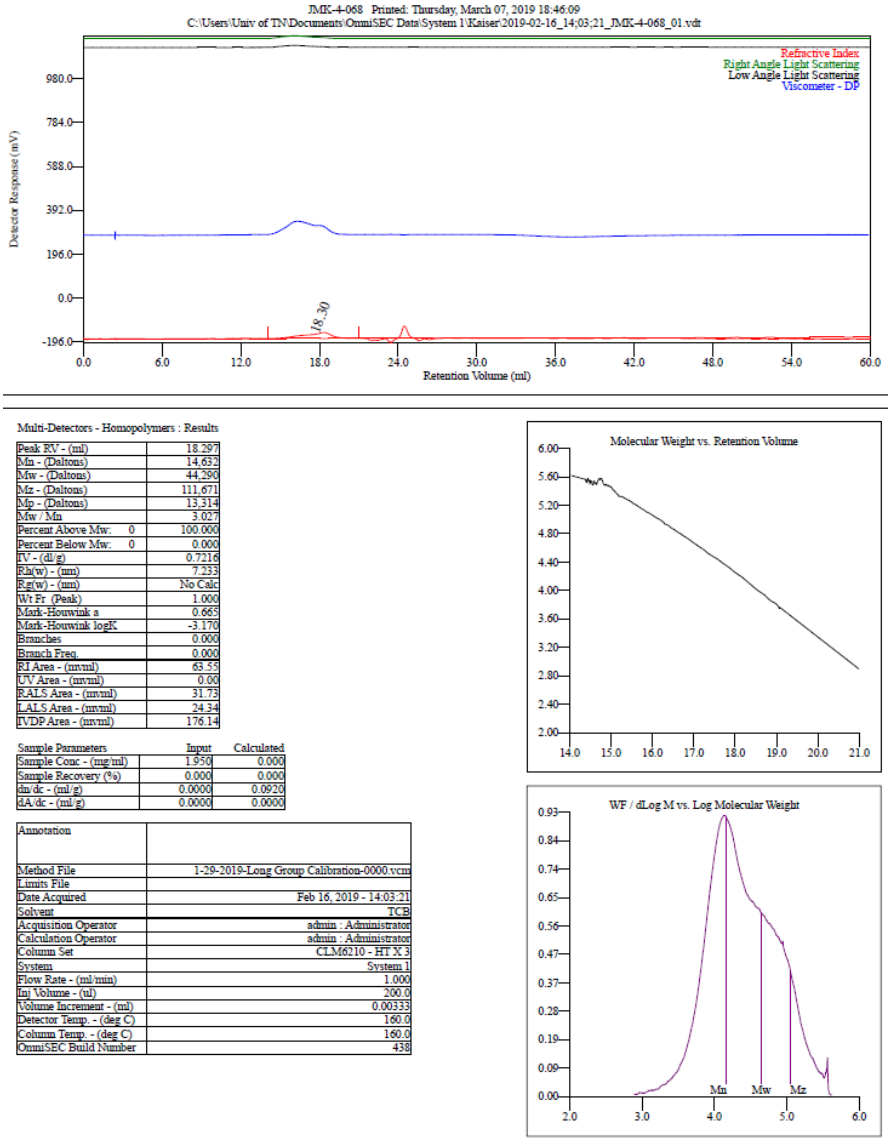

Figure A.18 GPC of polyethylene. (Table 3.3, entry 3)

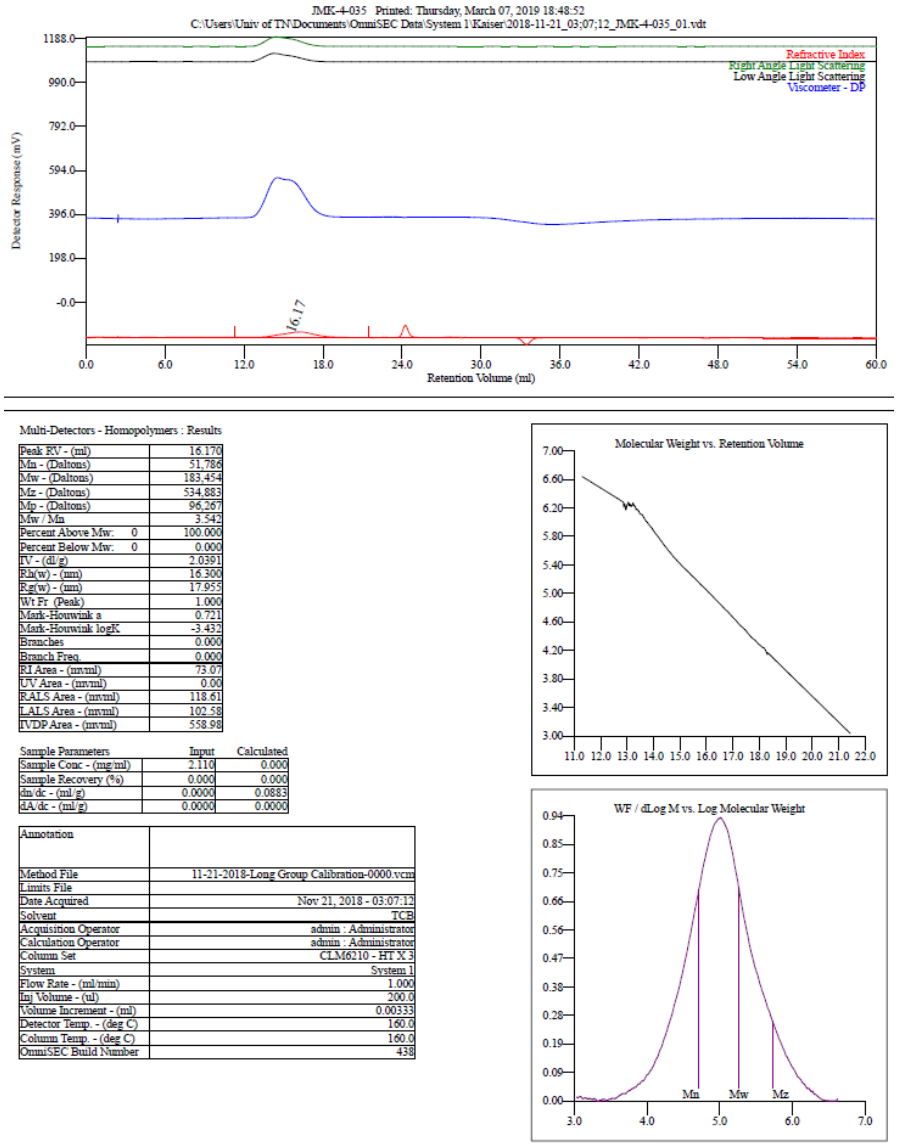

Peak RV - (ml)	16.170
Mn - (Daltons)	51,786
Mw - (Daltons)	183,454
Mz - (Daltons)	534,883
Mp - (Daltons)	96,267
Mw / Mn	3.542
Percent Above Mw: 0	100.000
Percent Below Mw: 0	0.000
IV - (dl/g)	2.0391
Rh(w) - (nm)	16.300
Rg(w) - (nm)	17.955
Wt Fr (Peak)	1.000
Mark-Houwink a	0.721
Mark-Houwink logK	-3.432
Branches	0.000
Branch Freq.	0.000
RI Area - (mvml)	73.07
UV Area - (mvml)	0.00
RALS Area - (mvml)	118.61
LALS Area - (mvml)	102.58
IVDP Area - (mvml)	558.98

Sample Parameters	Input	Calculated
Sample Conc - (mg/ml)	2.110	0.000
Sample Recovery (%)	0.000	0.000
dn/dc - (ml/g)	0.0000	0.0883
dA/dc - (ml/g)	0.0000	0.0000

Annotation	
Method File	11-21-2018-Long Group Calibration-0000.vcm
Limits File	
Date Acquired	Nov 21, 2018 - 03:07:12
Solvent	TCB
Acquisition Operator	admin : Administrator
Calculation Operator	admin : Administrator
Column Set	CLM6210 - HT X 3
System	System 1
Flow Rate - (ml/min)	1.000
Inj Volume - (ul)	200.0
Volume Increment - (ml)	0.00333
Detector Temp. - (deg C)	160.0
Column Temp. - (deg C)	160.0
OmniSEC Build Number	438

Figure A.19 GPC of polyethylene. (Table 3.3, entry 7)

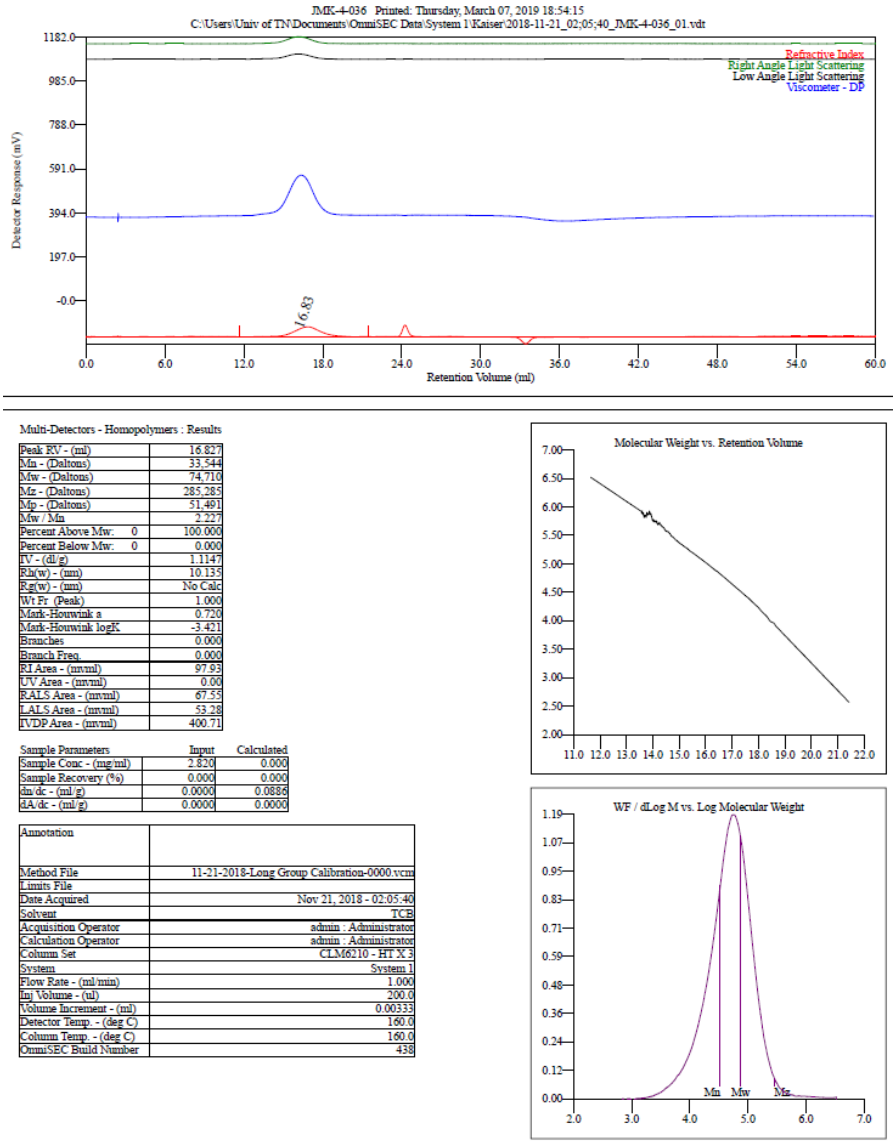

Peak RV - (ml)	16.827
Mn - (Daltons)	33,544
Mw - (Daltons)	74,710
Mz - (Daltons)	285,285
Mp - (Daltons)	51,491
Mw / Mn	2.227
Percent Above Mw: 0	100.000
Percent Below Mw: 0	0.000
IV - (dl/g)	1.1147
Rh(w) - (nm)	10.135
Rg(w) - (nm)	No Calc
Wt Fr (Peak)	1.000
Mark-Houwink a	0.720
Mark-Houwink logK	-3.421
Branches	0.000
Branch Freq.	0.000
RI Area - (mvml)	97.93
UV Area - (mvml)	0.00
RALS Area - (mvml)	67.55
LALS Area - (mvml)	53.28
IVDP Area - (mvml)	400.71

Sample Parameters	Input	Calculated
Sample Conc - (mg/ml)	2.820	0.000
Sample Recovery (%)	0.000	0.000
dn/dc - (ml/g)	0.0000	0.0886
dA/dc - (ml/g)	0.0000	0.0000

Annotation	
Method File	11-21-2018-Long Group Calibration-0000.vcm
Limits File	
Date Acquired	Nov 21, 2018 - 02:05:40
Solvent	TCB
Acquisition Operator	admin : Administrator
Calculation Operator	admin : Administrator
Column Set	CLM6210 - HT X 3
System	System 1
Flow Rate - (ml/min)	1.000
Inj Volume - (ul)	200.0
Volume Increment - (ml)	0.00333
Detector Temp. - (deg C)	160.0
Column Temp. - (deg C)	160.0
OmniSEC Build Number	438

Figure A.20 GPC of polyethylene. (Table 3.3, entry 8)

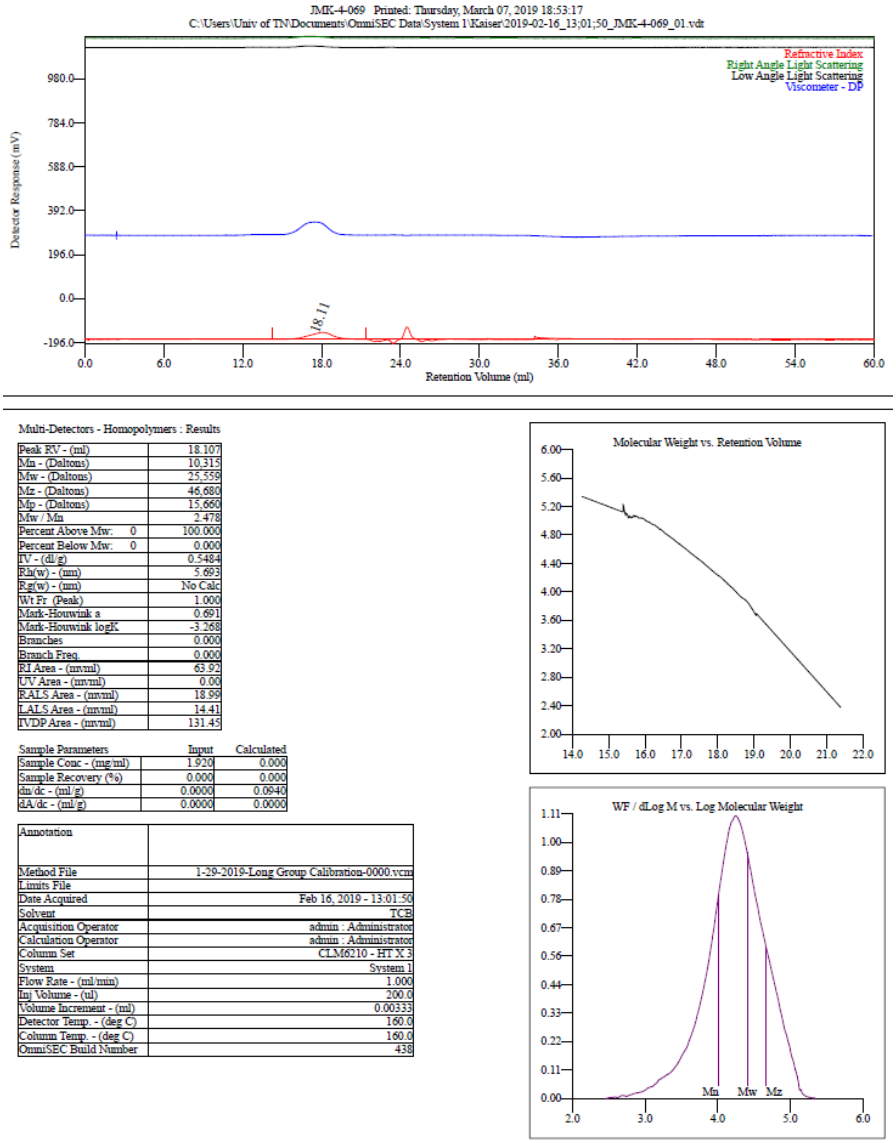

Figure A.21 GPC of polyethylene. (Table 3.3, entry 9)

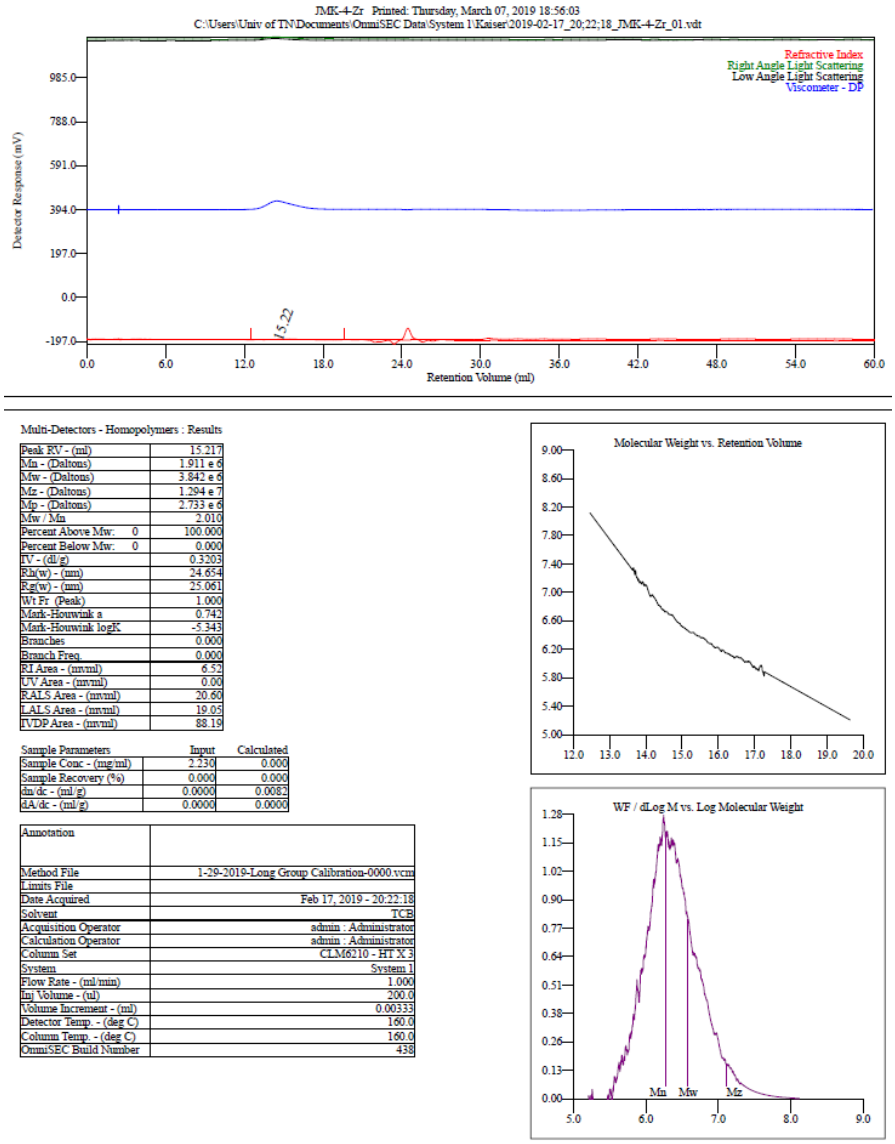

Figure A.22 GPC of polyethylene. (Table 3.4, entry 1)

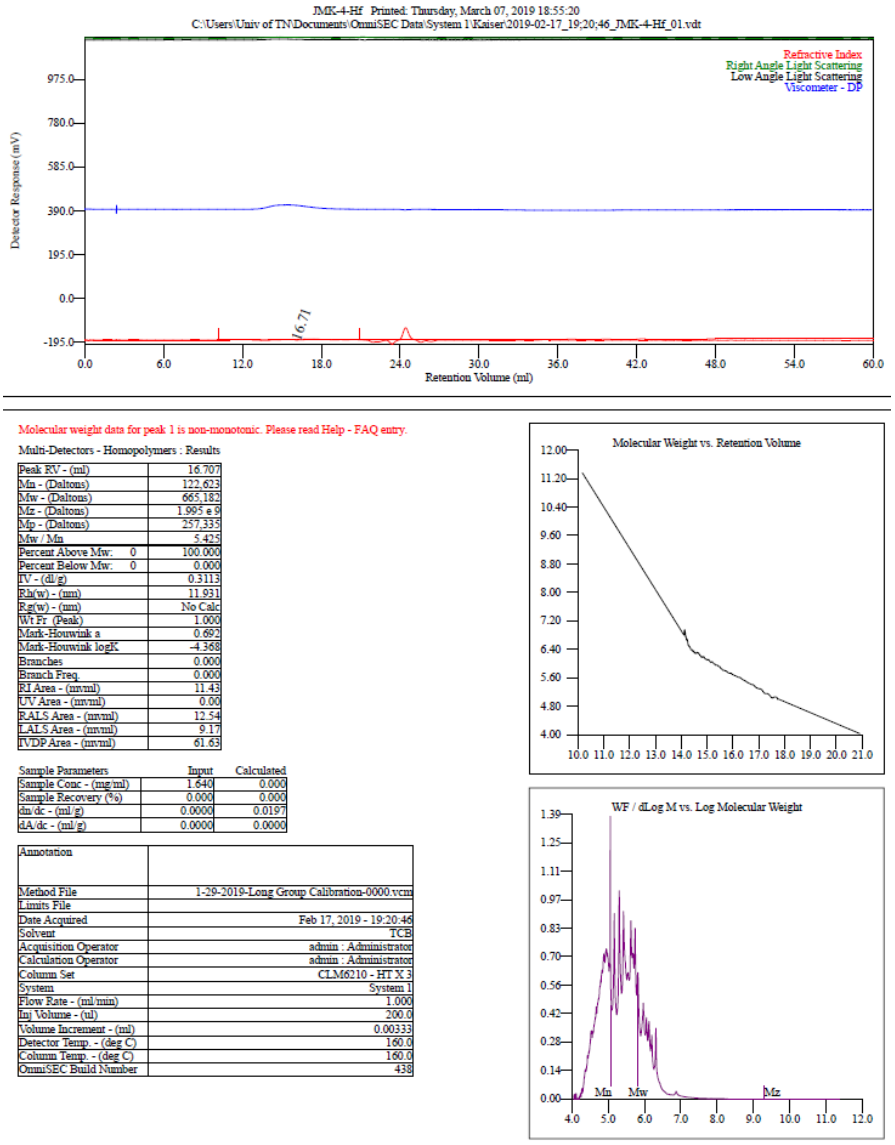

Figure A.23 GPC of polyethylene. (Table 3.4, entry 2)

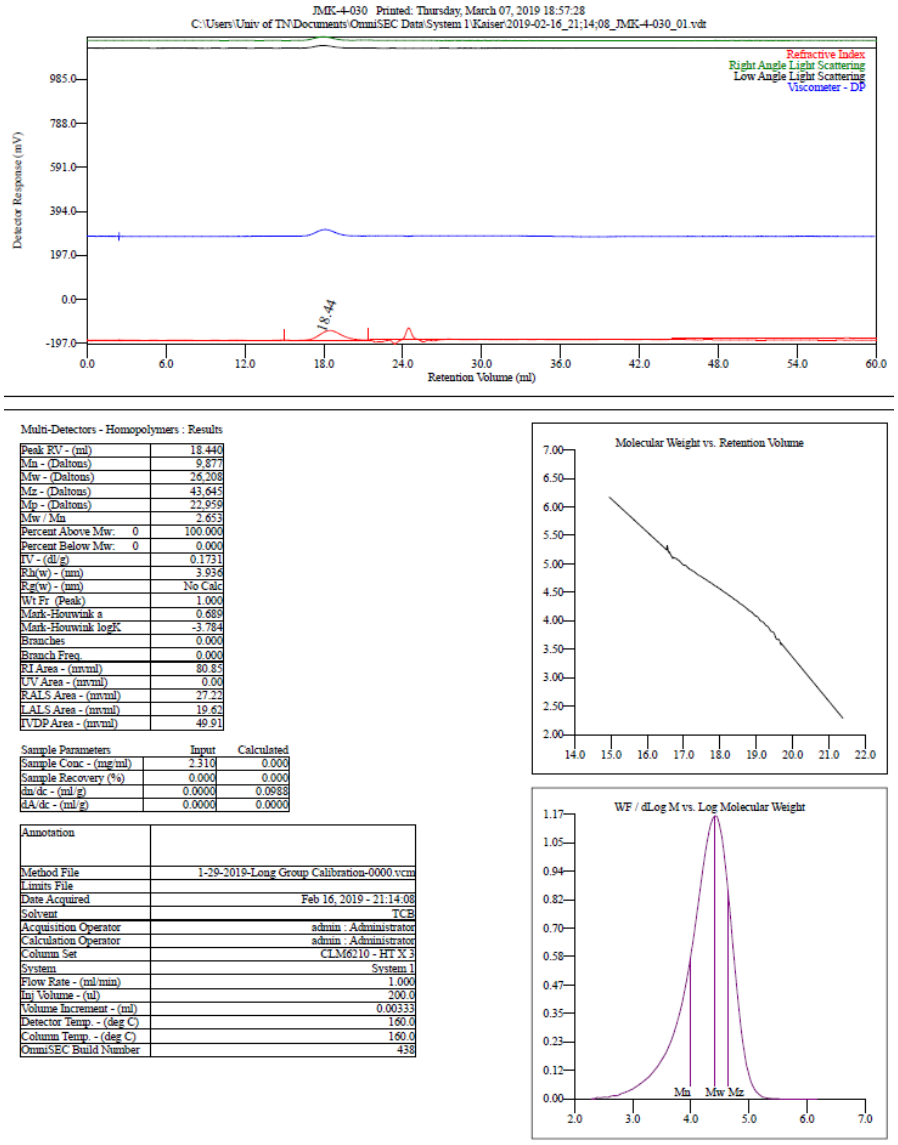

Figure A.24 GPC of poly(1-hexene). (Table 3.5, entry 2)

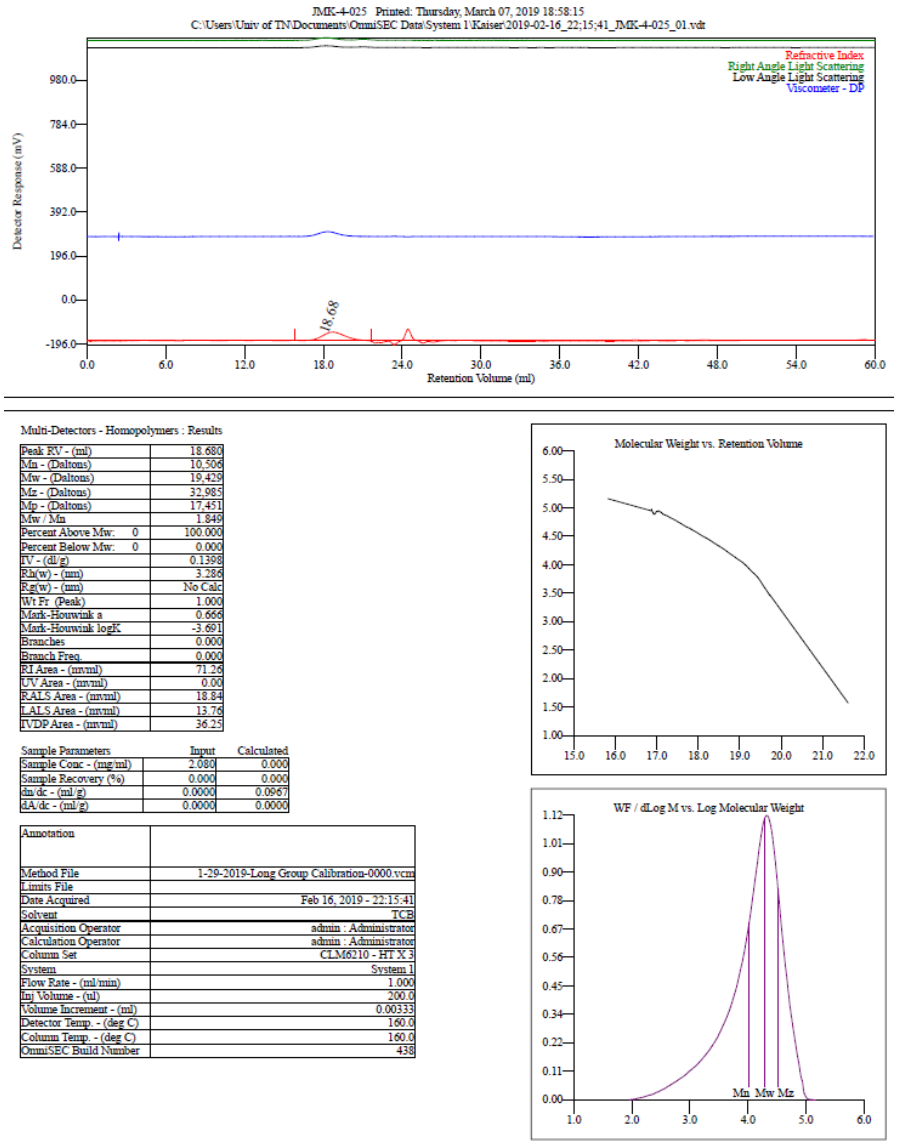

Figure A.25 GPC of poly(1-hexene). (Table 3.5, entry 3)

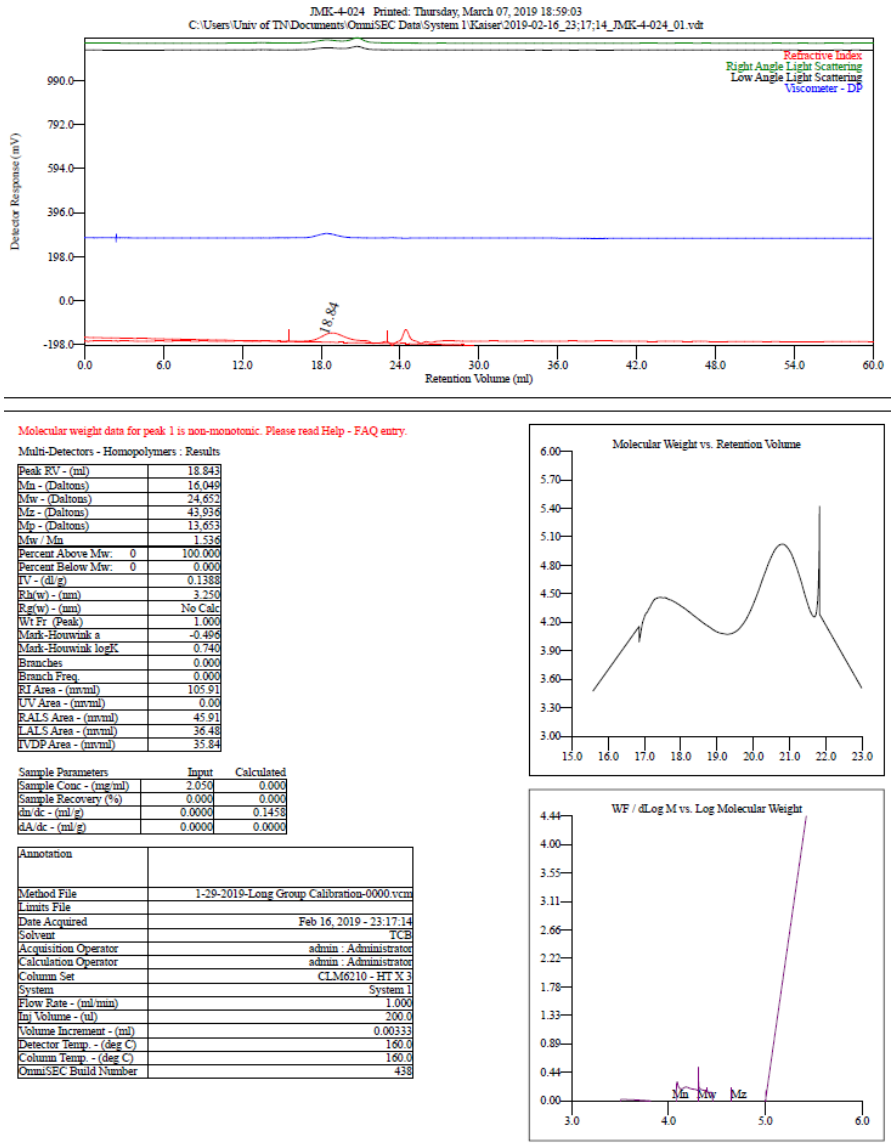

Figure A.26 GPC of poly(1-hexene). (Table 3.5, entry 4)

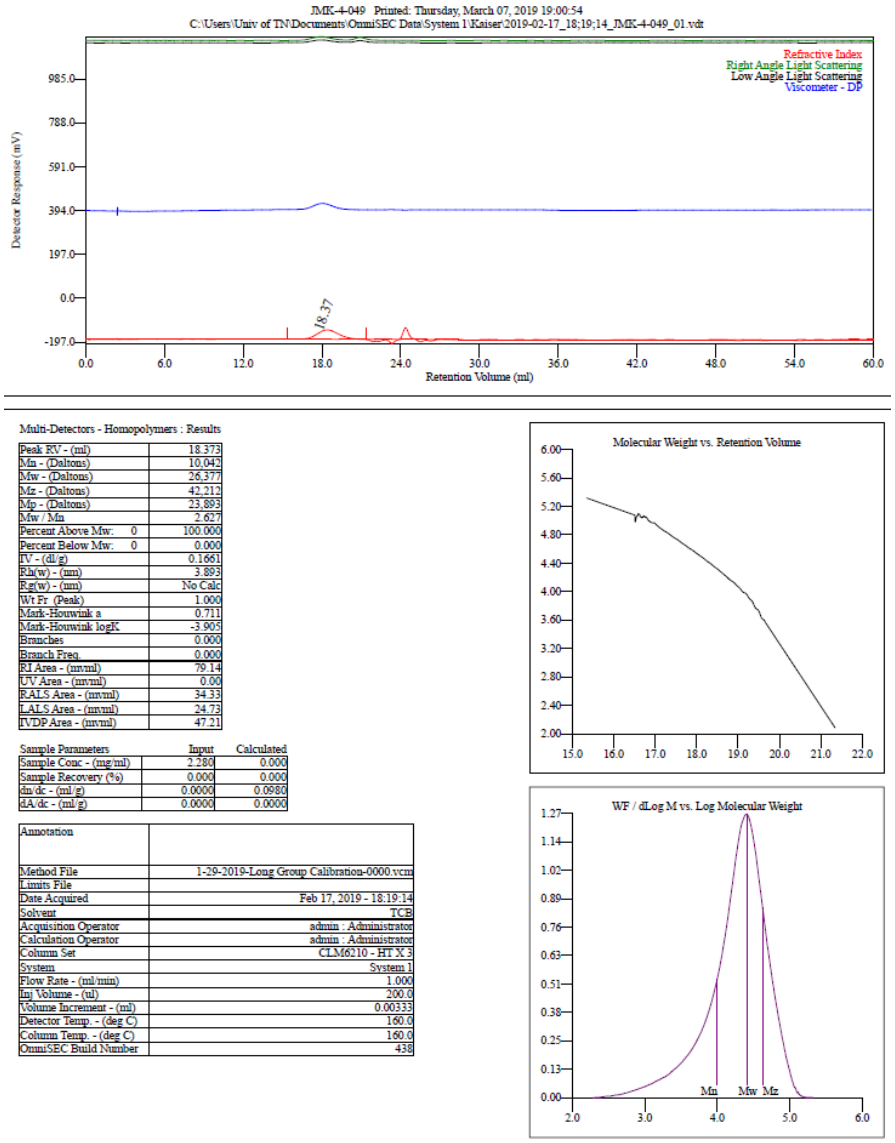

Figure A.27 GPC of poly(1-hexene). (Table 3.5, entry 5)

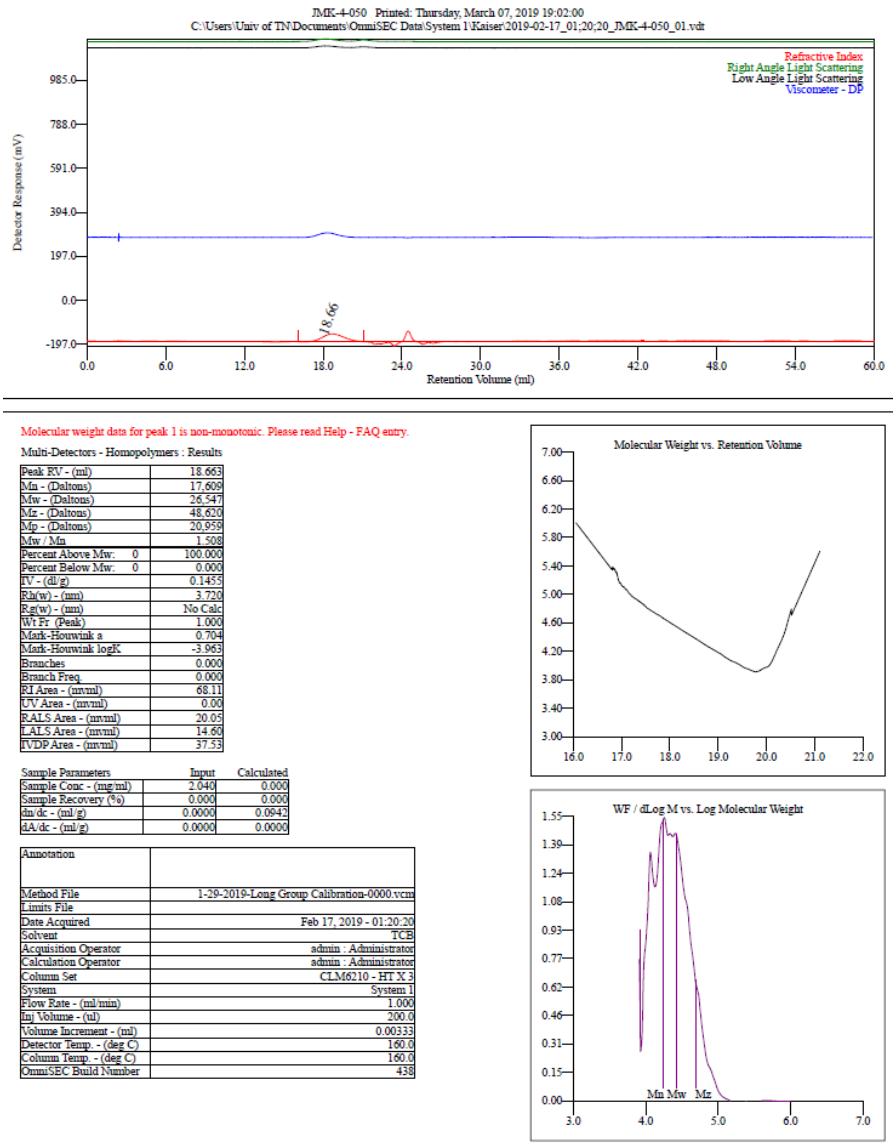

Figure A.28 GPC of poly(1-hexene) (Table 3.5, entry 6)

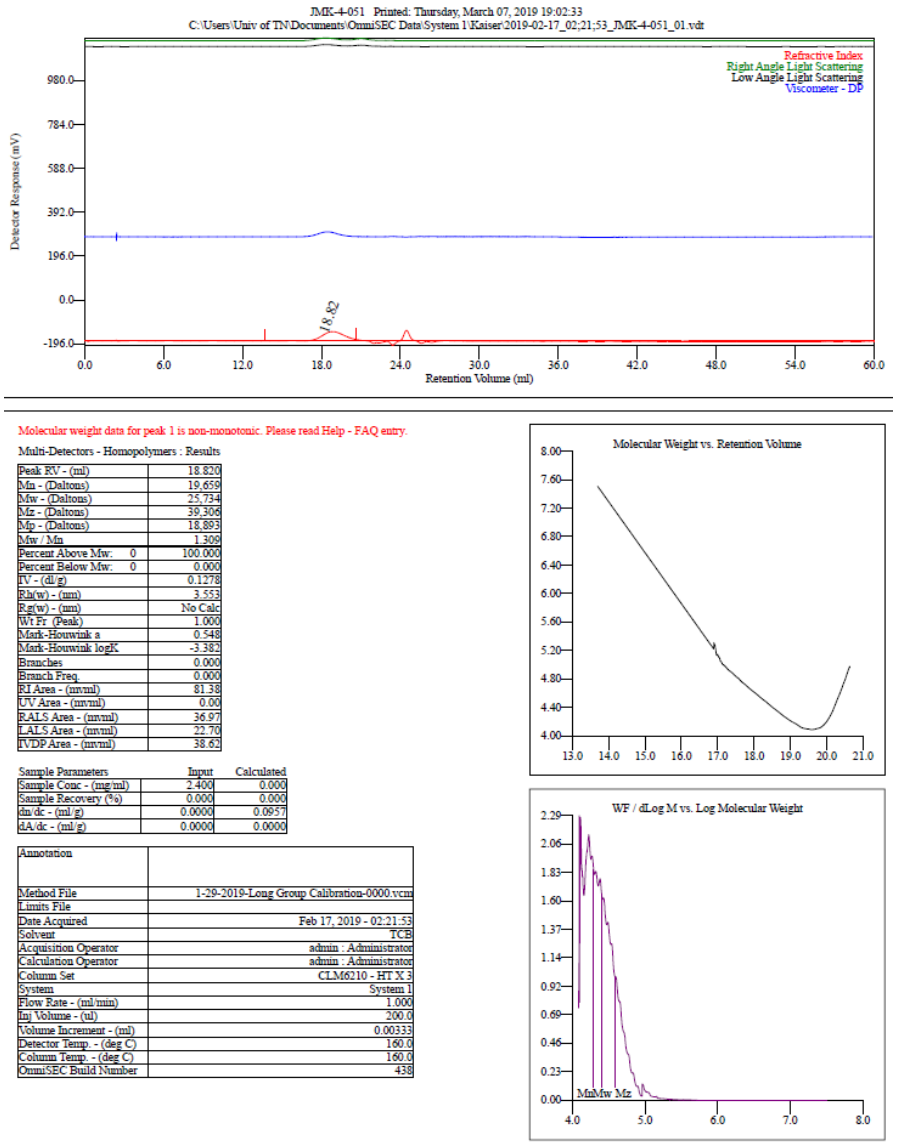

Figure A.29 GPC of poly(1-hexene). (Table 3.5, entry 7)

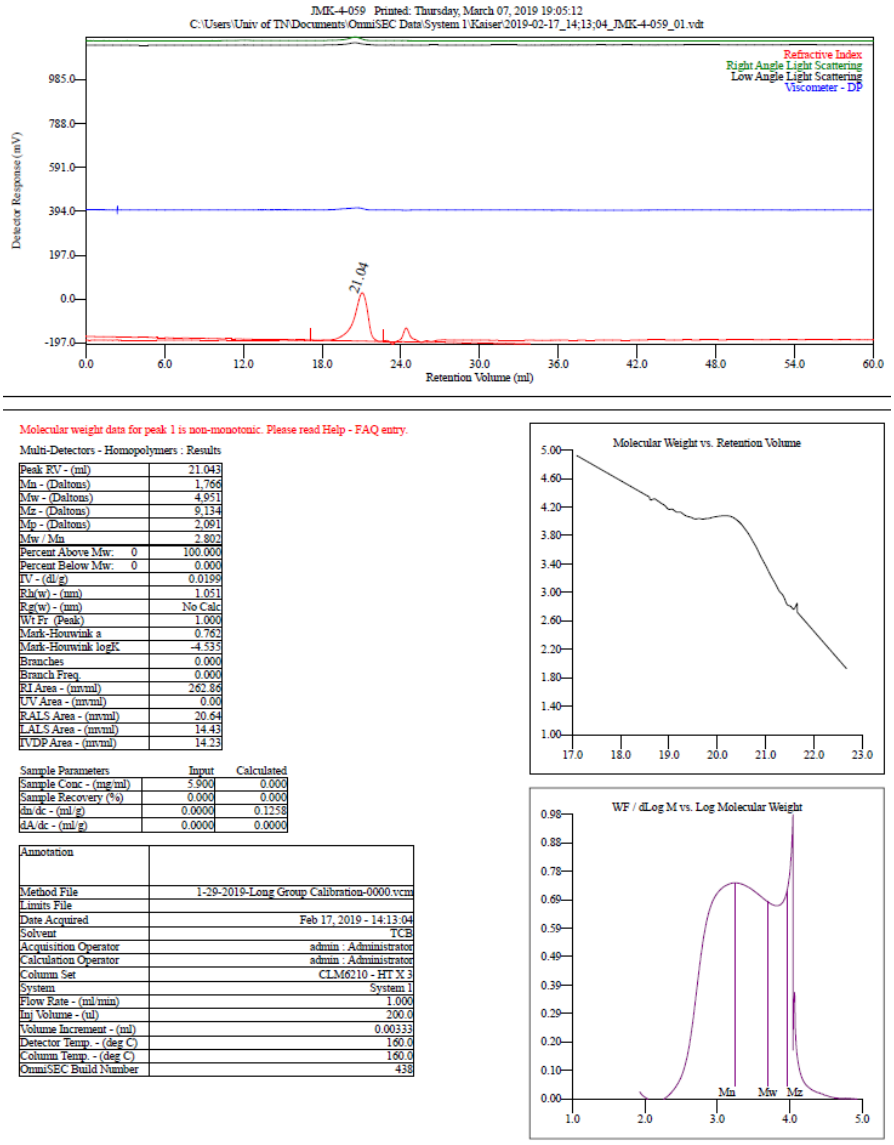

Figure A.30 GPC of poly(1-hexene). (Table 3.6, entry 3)

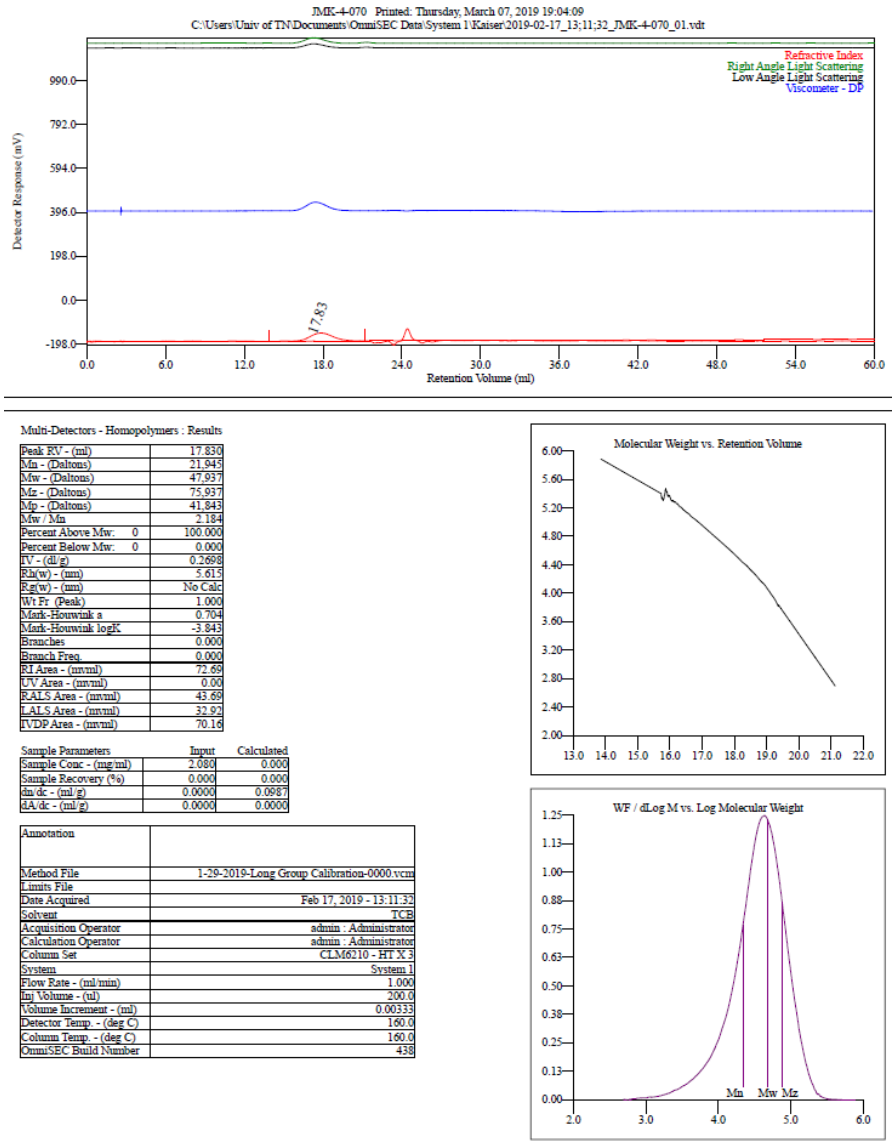

Figure A.31 GPC of poly(1-hexene). (Table 3.6, entry 4)

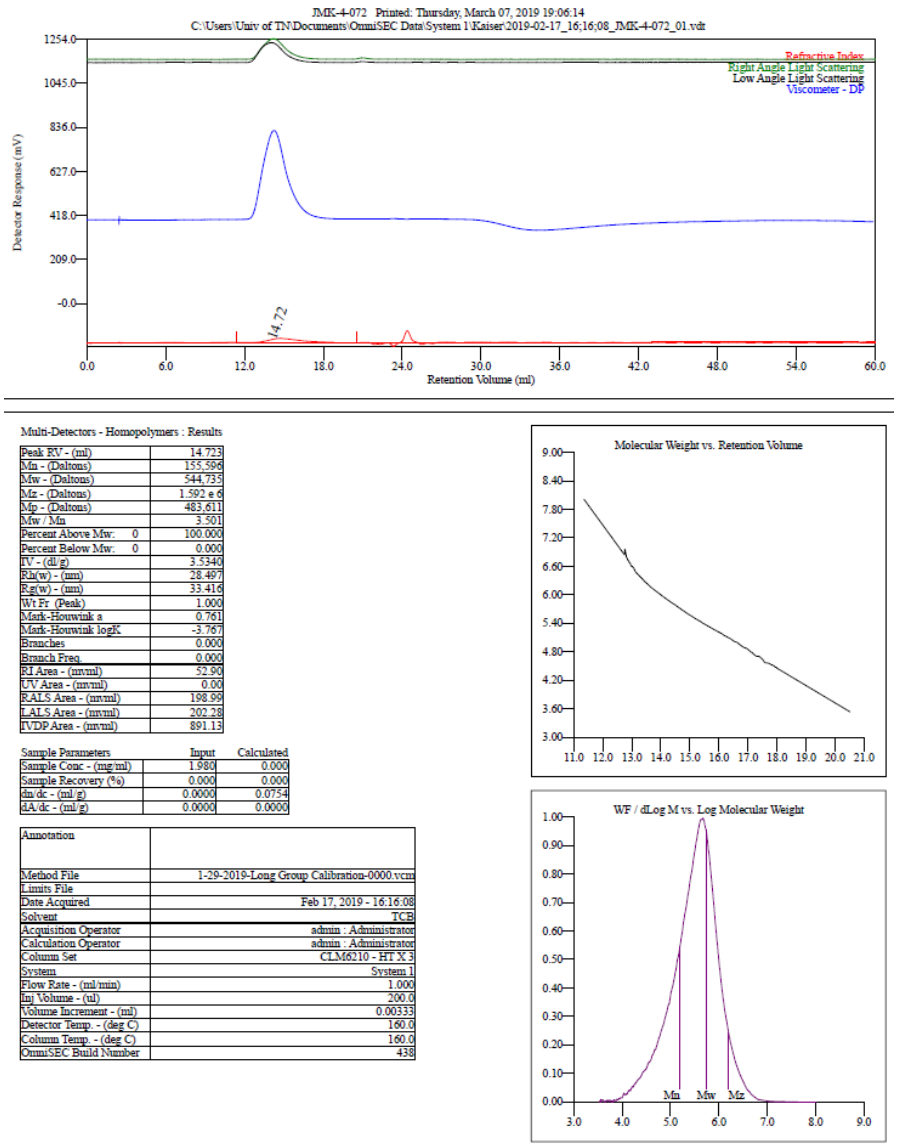

Figure A.32 GPC of polyethylene. (Table 3.7, entry 4)

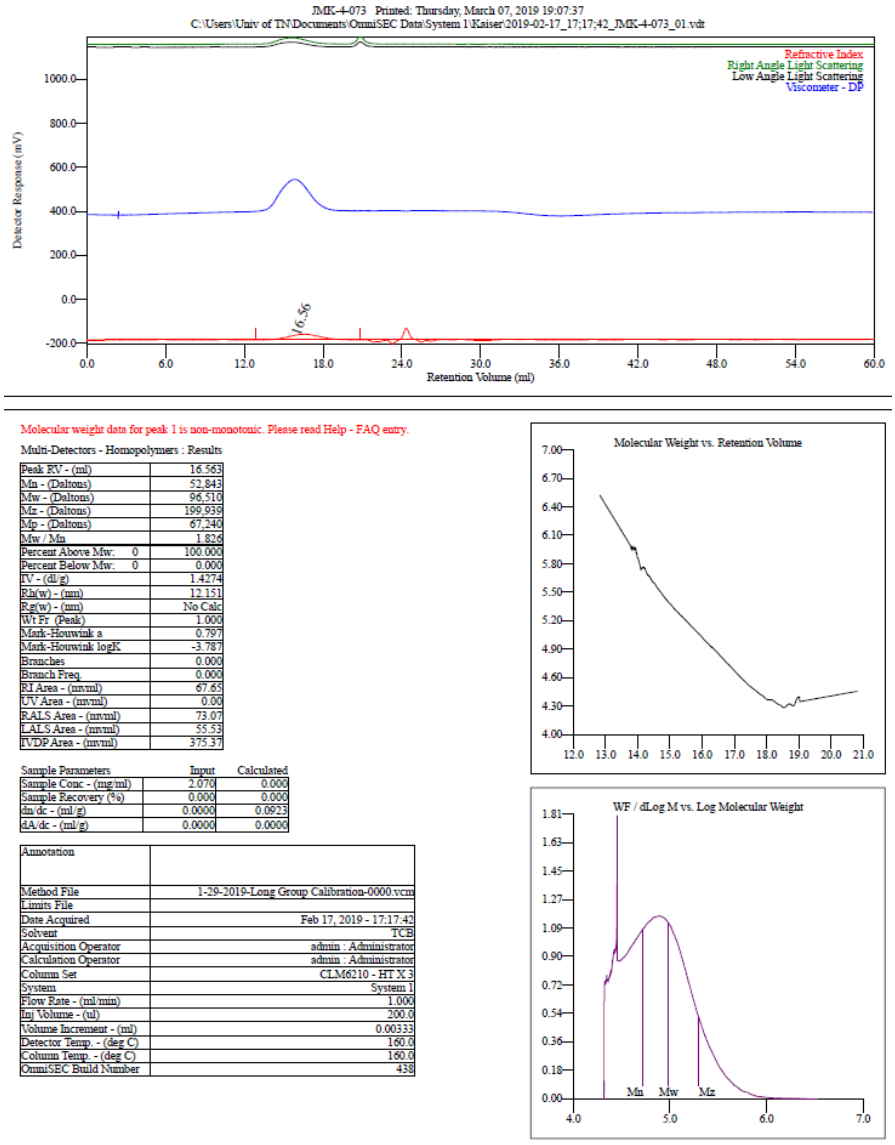

Figure A.33 GPC of polyethylene. (Table 3.7, entry 5)

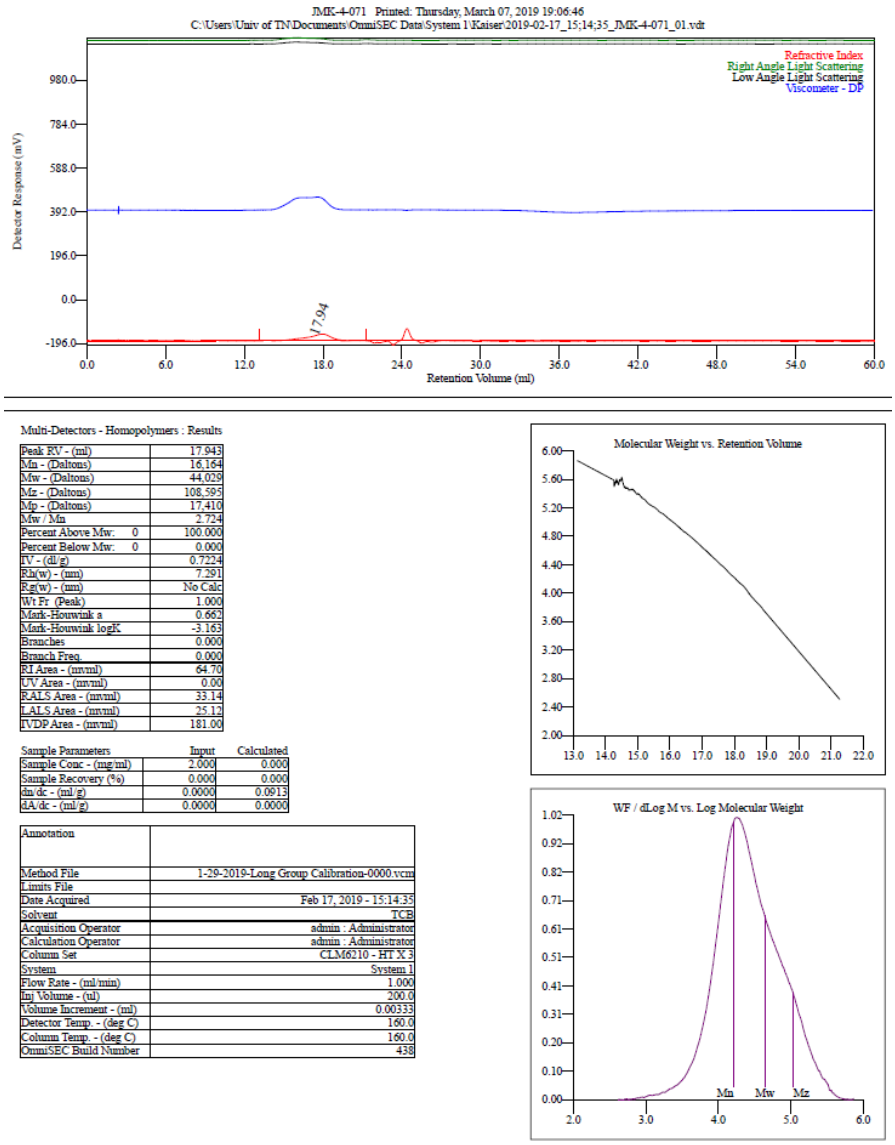

Figure A.34 GPC of polyethylene. (Table 3.7, entry of 6)

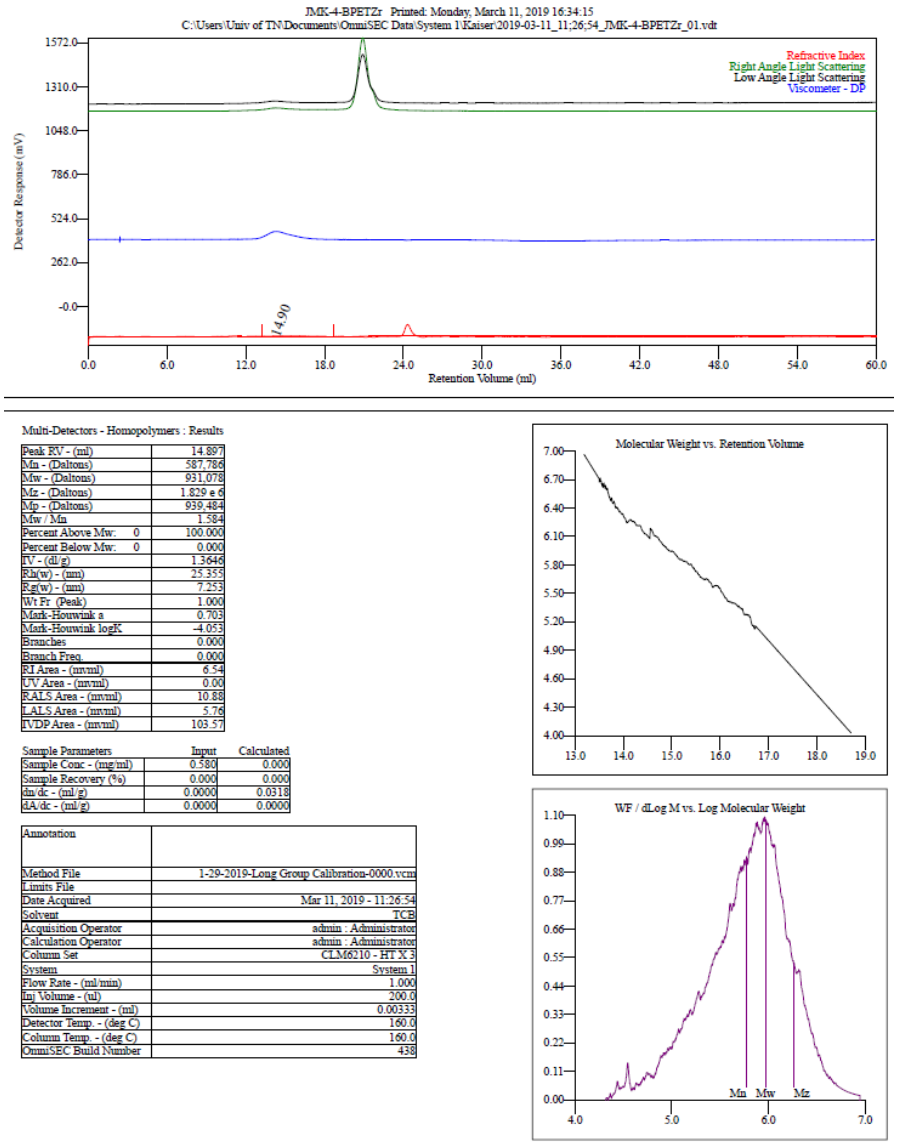

Figure A.35 GPC of polyethylene. (Table 3.8, entry 1)

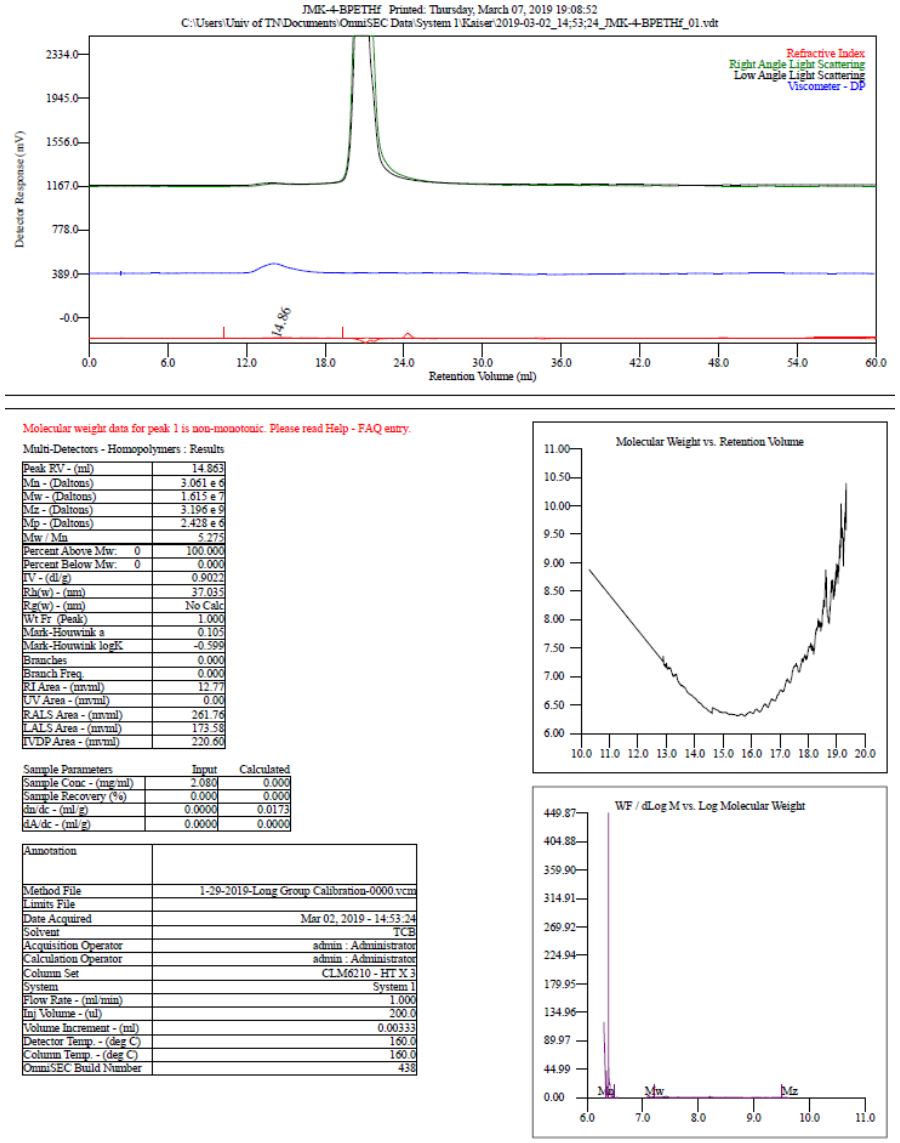

Peak RV - (ml)	14.863
Mn - (Daltons)	3.061 e 6
Mw - (Daltons)	1.615 e 7
Mz - (Daltons)	3.196 e 9
Mp - (Daltons)	2.428 e 6
Mw / Mn	5.275
Percent Above Mw: 0	100.000
Percent Below Mw: 0	0.000
IV - (dl/g)	0.9022
Rh(w) - (nm)	37.035
Rg(w) - (nm)	No Calc
Wt Fr (Peak)	1.000
Mark-Houwink a	0.105
Mark-Houwink logK	-0.599
Branches	0.000
Branch Freq.	0.000
RI Area - (mvml)	12.77
UV Area - (mvml)	0.00
RALS Area - (mvml)	261.76
LALS Area - (mvml)	173.58
IVDP Area - (mvml)	220.60

Sample Parameters	Input	Calculated
Sample Conc - (mg/ml)	2.080	0.000
Sample Recovery (%)	0.000	0.000
dn/dc - (ml/g)	0.0000	0.0173
dA/dc - (ml/g)	0.0000	0.0000

Annotation	
Method File	1-29-2019-Long Group Calibration-0000.vcm
Limits File	
Date Acquired	Mar 02, 2019 - 14:53:24
Solvent	TCB
Acquisition Operator	admin : Administrator
Calculation Operator	admin : Administrator
Column Set	CLM6210 - HT X 3
System	System 1
Flow Rate - (ml/min)	1.000
Inj Volume - (ul)	200.0
Volume Increment - (ml)	0.00333
Detector Temp. - (deg C)	160.0
Column Temp. - (deg C)	160.0
OmniSEC Build Number	438

Figure A.36 GPC of polyethylene. (Table 3.8, entry 2)

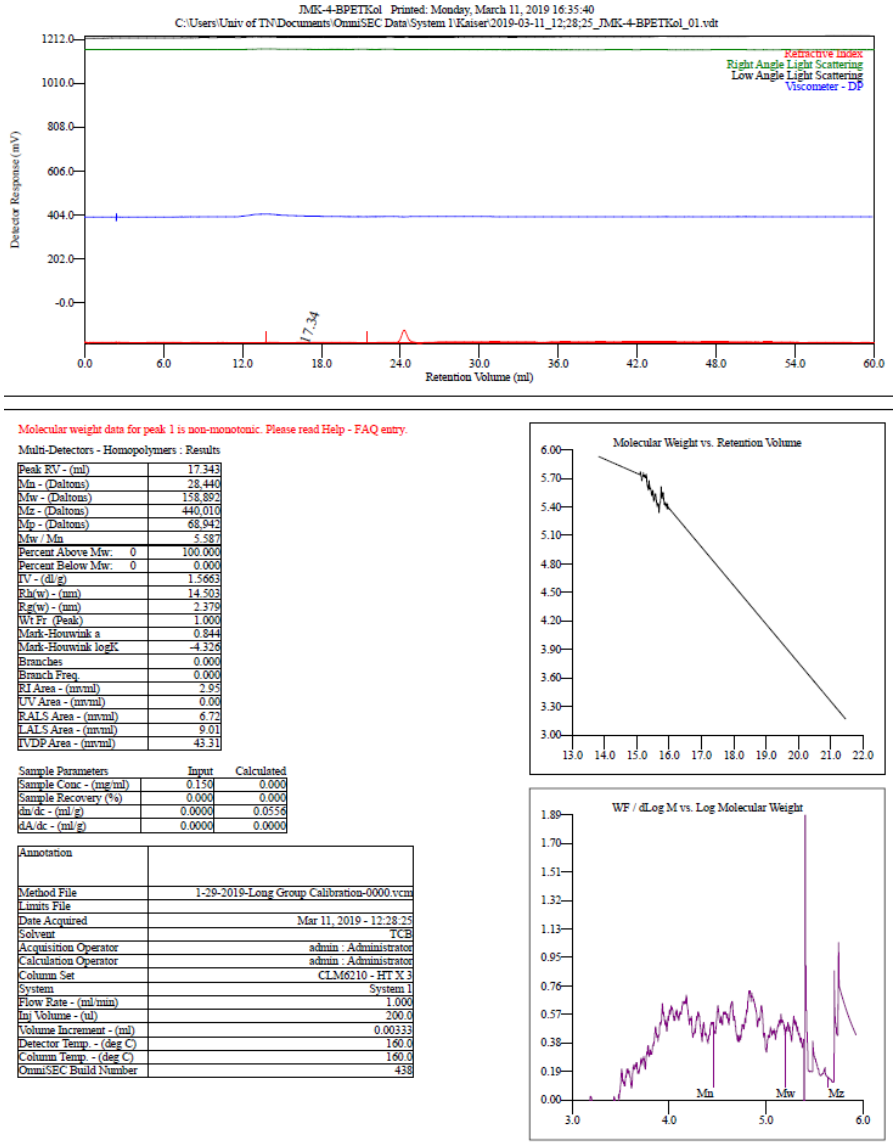

Peak RV - (ml)	17.343
Mn - (Daltons)	28,440
Mw - (Daltons)	158,892
Mz - (Daltons)	440,010
Mp - (Daltons)	68,942
Mw / Mn	5.587
Percent Above Mw: 0	100.000
Percent Below Mw: 0	0.000
IV - (dl/g)	1.5663
Rh(w) - (nm)	14.503
Rg(w) - (nm)	2.379
Wt Fr (Peak)	1.000
Mark-Houwink a	0.844
Mark-Houwink logK	-4.326
Branches	0.000
Branch Freq.	0.000
RI Area - (mvml)	2.95
UV Area - (mvml)	0.00
RALS Area - (mvml)	6.72
LALS Area - (mvml)	9.01
IVDP Area - (mvml)	43.31

Sample Parameters	Input	Calculated
Sample Conc - (mg/ml)	0.150	0.000
Sample Recovery (%)	0.000	0.000
dn/dc - (ml/g)	0.0000	0.0556
dA/dc - (ml/g)	0.0000	0.0000

Annotation	
Method File	1-29-2019-Long Group Calibration-0000.vcm
Limits File	
Date Acquired	Mar 11, 2019 - 12:28:25
Solvent	TCB
Acquisition Operator	admin : Administrator
Calculation Operator	admin : Administrator
Column Set	CLM6210 - HT X 3
System	System 1
Flow Rate - (ml/min)	1.000
Inj Volume - (ul)	200.0
Volume Increment - (ml)	0.00333
Detector Temp. - (deg C)	160.0
Column Temp. - (deg C)	160.0
OmniSEC Build Number	438

Figure A.37 GPC of polyethylene. (Table 3.8, entry 3)

VITA

Jordan Michael Kaiser was born and raised in Hanover Park, Illinois. In 2010, he graduated from Glenbard North High School and then attended Lewis University in the fall. Jordan graduated from Lewis University in the spring of 2014 with a B.S. in Chemical Physics. After graduation, he attended The University of Tennessee-Knoxville in the fall to pursue a graduate degree in chemistry. At Tennessee, Jordan studied under the guidance of Dr. Brian K. Long where he published several manuscripts, attended national and regional conferences, and earned multiple awards for his accomplishments, including ACS-POLY Excellence in Polymer Research Award, ACS-ETS Graduate Fellowship, and College of Arts and Sciences Dissertation Fellowship. Aside from his graduate work, Jordan devoted time to several extracurricular activities. Within the chemistry department, Jordan held numerous positions in the Association of Chemistry Graduate Students such as President, Graduate Student Senate Representative, Recruitment Chair, Social Chair, and Secretary. Outside his department, he was a member of the Travel Awards Committee, Graduate Student Advisory Committee, and Graduate and Professional Student Professional Development Committee. In his free time, Jordan played on and coached the men's club volleyball team, as well as volunteered with Leader For Readers teaching elementary students how to read.